Doctoral Thesis

Functional roles of alpha oscillations in visual perception and their neuroanatomical basis
（視覚情報処理におけるアルファ波の機能的役割とその解剖学的基盤）

Sorato Minami
Nanobiology Laboratories (Prof. Yanagida),
Graduate School of Frontier Biosciences, Osaka University

March 2019

Abstract

Introduction: Neural oscillations at around 10 Hz, called alpha oscillations, appear most saliently among all neural oscillations especially during the rest. In recent years, correlation between characteristics of alpha oscillations such as power/frequency/phase and various perceptual phenomena has been established. However, there has not been conclusive evidence about the causal contribution of alpha oscillations to visual perception. In this dissertation, I first focused on a phenomenon called motion-induced spatial conflict where illusory visual vibrations are experienced at around 10 Hz. To prove a causal link between the alpha oscillation and the illusory jitter perception, I utilized inter- and intra-individual variations and manipulations of the intrinsic alpha frequency. Second, I focused on the neuroanatomical basis of inter-individual differences in the alpha power and frequency, which is known to be correlated with several visual phenomena. To study the relationship between microstructural properties of white matter tracts connecting visual areas and alpha oscillations, I utilized both diffusion-weighted imaging (DWI) and quantitative MRI (qMRI).
Purpose/Methods: In the first part, to verify whether the alpha oscillation contributes to the illusory jitter perception, I investigated whether perceived frequency of illusory jitter is correlated with inter/intra-individual variability in the intrinsic alpha frequency. I also invented a method to manipulate alpha frequency, which was enabled by amplitude modulated transcranial alternating current stimulation (AM-tACS). The illusory jitter frequency was estimated by the constant method, while the alpha frequency was measured by magnetoencephalography (MEG). Furthermore, I performed the source analysis on MEG during the observation of illusory jitter. In the second part, to investigate the relationship between the amplitude and frequency of alpha oscillations and microstructural properties of the major white matter tracts connecting visual areas and, I measured MEG during rest, DWI and qMRI for the same participants.
Results/Discussion: There was a strong correlation between alpha frequency during rest and illusory jitter frequency across participants. Also, small fluctuation of alpha frequency within participant was correlated with the illusory jitter frequency. In addition, when the frequency of the alpha oscillation was increased or decreased by amplitude modulated-tACS, the illusory jitter frequency also changed reflecting the change in the alpha frequency. From these experiments, I found that the illusory jitter directly mirrors the intrinsic alpha frequency. Furthermore, the phase synchronization of alpha oscillations was found to be increased between IPL and IT, which are located in the dorsal and ventral areas respectively. Illusory jitter may arise from the cyclic correction of the dissociation between positional representation in dorsal and ventral visual pathways. In the second part, the power and frequency of alpha oscillations were found to be significantly correlated with the tissue structural properties in optic radiation (OR), which connects LGN and V1. The results suggest that alpha oscillations may originate from the interaction between LGN and V1. In conclusion, I elucidated a functional role of alpha oscillations in visual processing and neuroanatomical substrate characterizing alpha oscillations.

CONTENTS

1 General introduction

In this dissertation, I first study the functional role of alpha oscillations in visual processing (Chapter 2). Then, I study the neuroanatomical basis determining the characteristics of alpha oscillations (Chapter 3). The outline of this dissertation is as follows.

In 1.1, I will explain previous studies related to this thesis. As the introduction for the Chapter 2, I will first review literature on the relationship between alpha oscillations and visual processing. I will specifically describe an illusory jitter called motion-induced spatial conflict, which is used in the main experiments (Chapter 2) of this dissertation. As the introduction for the Chapter 3, I will also introduce previous studies on the relationship between vision and microstructural properties of white matter tracts using diffusion magnetic resonance imaging (dMRI). In 1.2, I will explain brain imaging techniques used in the present study, which include magnetoencephalography (MEG), diffusion magnetic resonance imaging (dMRI), and quantitative MRI (qMRI). In 1.3, I will explain transcranial current stimulation techniques, which was used to manipulate neural oscillations. Amplitude-modulated current stimulation will also be introduced. In 1.4, I will present the purpose of this research.

In 2, I will study the relationship between alpha oscillations and visual perception to elucidate the functional role of alpha oscillations in visual processing.

In 3, I will study the relationship between alpha oscillations and microstructural properties in the visual white matter to elucidate the neuroanatomical basis of the inter-individual differences in alpha oscillations.

In 4 I will give a general discussion based on these experimental results.

1.1 Background for this study

1.1.1 The relationship between alpha oscillations and visual processing

In our brain, rhythmic synchronization phenomena are formed by enormous neural activities. The neural oscillations are labeled by each frequency band, such as alpha (8–13 Hz), beta (13–30 Hz), and gamma (30–100 Hz) band. These neural oscillations are widespread across cortical areas and their functional roles have been investigated for a long time. Their functional roles can be feature binding [1], neuronal communication [2, 3], and memory [1, 4]. Among these neural oscillations, the most salient signal among these neural oscillations is called the alpha oscillation.

Although alpha oscillations were originally thought to reflect idling state of the brain, accumulating evidences suggesting that alpha oscillations are correlated with various types of visual perception. For example, when attention of participants is directed to the object in the left visual field, alpha oscillations are dominantly suppressed in the right hemisphere. On the other hand, alpha oscillations remain strong in the left hemisphere. This result suggests that alpha oscillations are suppressed in the brain region associated with processing of the object information in which spatial attention is directed to objects, whereas the alpha increase may reflect inhibition on processing of the non-salient object information [5].

There are also several studies that discovered the correlation between the phase of alpha oscillations and visual perception. In Matthewson's study [6], the experiment using meta-contrast stimuli was performed. A target stimulus was shown to the participants only for a moment and a mask stimulus was presented immediately thereafter. By separating the electroencephalogram (EEG) data into detected and non-detected target trials, it was found that the detection of the target stimulus depends on the phase of alpha oscillations at the timing of the target stimulus. The target tends to be perceived when the phase of the alpha oscillations is a trough at the time of presenting the target stimulus, and unperceived when alpha phase is the peak.

The phase of alpha oscillations also affects the interaction of multiple sensory processing between distant regions. Several studies have shown the involvement of inter-regional alpha phase synchronization in visual perception. Siegel and colleagues [3] showed that the alpha coherence between middle temporal (MT) area processing object movement, and intraparietal sulcus (IPS) in the dorsal visual pathway is modulated by visual attention. Moreover, Driel's study showed that the strength of alpha phase synchrony between auditory and visual regions depended on cross-modal attention [7]. These results suggest that attention selectively routes sensory information through the cortical hierarchy or cross-modal network by dynamically altering alpha coherence between neuronal groups across distant cortical areas.

As well as the amplitude and phase of alpha oscillations, the relationship between the peak frequency of alpha oscillations and visual perception has also been studied. In the study by Haegens [8], the amplitude of the alpha oscillations during the N-back task decreased as compared to the resting state. On the other hand, PAF significantly increased from rest to 0-back, and from rest/0-back to 2-back. This study suggests that the degree of load in

information processing correlates with the state of the alpha oscillations. In a research by Sokoliuk [9], it is known that the frequency of blinking illusion called Wagon Wheel illusion roughly matches with the frequency of alpha oscillations, which is about 9.1 Hz on average. In addition, the amplitude of the alpha oscillation changes at the occipital region during illusory perception, and the frequency of the alpha component with the largest change rate correlates strongly with the alpha frequency at the rest. Therefore, there is a possibility that the frequency of this illusion directly reflects the frequency of the alpha oscillation. Also, in a research by Samaha [10], they used an illusion called two-flash fusion in which the flash originally presented twice is only perceived once. The interstimulus interval (ISI) at which two light flashes could be discriminated from a single flash is known as the two-flash fusion threshold. The threshold became lower when participant's alpha frequency was higher. Furthermore, the threshold of two-flash fusion was correlated with the frequency of alpha oscillations measured both at the resting eye-closed condition and immediately before the stimulus presentation. From these results, Samaha and colleagues suggested that participants with high alpha frequencies, ie narrow trough phases, may be able to accommodate narrower interval two-flash stimuli and vice versa.

As well as the involvement of alpha oscillations in visual perception, alpha oscillations are also associated with various types of the neural activities related to visual processing. For example, in the study by Scheeringa, a simultaneous measurement of functional magnetic resonance imaging (fMRI) and EEG was performed [11]. The Blood Oxgenation Level Dependent (BOLD) signal fluctuates according to the phase of the alpha oscillations at the visual onset. As is the case with the dependence of BOLD signal on alpha phase, the firing rate of the neuron group on the visual information processing is associated with alpha oscillations. Haegens and colleagues showed that the firing rate was highest at the trough of the alpha cycle in prefrontal regions [12]. Based on recent findings that alpha oscillations inhibit the excitability of postsynaptic cells in the local neuronal network, suppress network interactions, and consequently conform to the level of visual attention, Bonnefond and colleagues have recently proposed a hypothesis that the alpha phase synchronization has the top-down effect on local neural networks in visual information processing [13].

1.1.2 Modulation of alpha oscillations by external stimulation and its effect on human visual perception

As described in 1.1.1, although the correlation between alpha oscillations and visual information processing has been reported in many previous studies, it is not yet clear whether the alpha oscillations are causally involved in visual processing. One approach to clarify this problem is to modulate the alpha oscillations by an external stimulation, and observe the influence of the change in alpha oscillations on visual perception. Previous studies have established some methods such as presenting a cue stimulus or a cyclic sensory stimulus, transcranial magnetic stimulation (TMS), transcranial direct current stimulation (tDCS), and transcranial alternating current stimulation (tACS).

One example is modulating the alpha oscillations by visual stimulus. This method has an advantage that it is possible to observe neural oscillations during external stimulation because the visual stimulus generates no artifacts derived from the external stimulation, unlike TMS and current stimulation. In the research on the discrimination task using Gabor patches [14], participants were provided with cues whose color were predictive of the timing of visual target onset. In such a case, the phase of alpha oscillations before target onset was modulated toward each participant's optimal phase for stimulus discrimination, which improved the discrimination accuracy. A method to more directly modulate alpha oscillations is to use a periodic visual pattern around 10 Hz, which tunes the phase of the alpha oscillation into the phase of the visual stimulus. For example, in a study by Spaak [15], alpha oscillations are phase-locked by the cyclic visual stimulus pattern in the same frequency as the intrinsic alpha oscillation, and the target stimulus was randomly presented after the stimulus pattern. The correct rate of the discrimination task varied depending on the phase difference between the target stimulus and the cyclic stimulus pattern. This study suggests that not only the phase of the intrinsic alpha oscillations [6] but also the phase of the entrained alpha oscillations affects visual perception.

Transcranial magnetic stimulation (TMS), which generates a weak current in the brain by changing a magnetic field, can also be used to modulate alpha oscillations. Previous studies have indicated that TMS targeted at the frontal, parietal, and occipital cortices increases in occipital alpha rhythm power [16, 17], although the underlying mechanism is unclear. A study using rhythmic TMS (rTMS) at the alpha frequency has reported that the intrinsic alpha oscillation was phase-locked to the phase of rTMS and the alpha power was enhanced at the

parietal area [18]. Based on these findings, recent studies have investigated the effects of rTMS at the alpha frequency on the performance of visual tasks [17, 19]. For example, when a near-threshold dot was presented in the left or right visual field during rTMS at the alpha frequency in the left or right hemisphere, the visibility of the target ipsilateral to the rTMS was increased [19]. It is believed that reducing cortical excitability by rTMS leads to the excitation of the other hemisphere, which results in the ipsilateral enhancement of visual attention. However, the direct relationship between the modulation of the intrinsic alpha oscillations by rTMS and the task performance has not been reported because of the huge artifact from TMS. In a study using TMS [20], the authors discovered that the amplitude of alpha oscillations induced by TMS tends to decrease during visual attention, which was also found for intrinsic alpha oscillations. This result suggests that alpha oscillations induced by TMS may reflect similar physiological mechanism as intrinsic alpha oscillations.

As mentioned above, studies on modulation of intrinsic alpha oscillations have been conducted by various approaches. Among them, transcranial alternating current stimulation (tACS) has recently attracted attention as a method to effectively change neural activity and visual perception (see Section 1.2 for details). For example, a recent EEG study utilized sound-induced double-flash illusion [21]. In this illusion, a single flash is perceived as two flashes when it is accompanied by two beeps. It was confirmed that the threshold interval of the beep that can produce the illusion correlates with the frequency of the alpha oscillations for each participant. In addition, the authors showed the threshold interval of the beep changes by the tACS at the frequency of peak alpha frequency (PAF) ± 2 Hz. These findings suggest that alpha oscillations determine the temporal window for interactions between audio and visual regions. In this way, the modulation of neural activity due to electrical stimulation is considered to be an effective method for verifying the relationship between alpha oscillations and visual perception. However, even if electrical stimulation results in the change in perception, there is no guarantee that the alpha oscillations are modulated as predicted. Considering this problem, in order to discuss the causal relation between alpha oscillations and visual perception, I established a technique combining the amplitude-modulated tACS (AM-tACS) and a noise reduction technique (tSSS), which enables us to measure neural activities during current stimulation. With this technique, I investigated the relationship between the alpha oscillation and visual perception during current stimulation (section 2.3).

1.1.3 Motion-Induced Spatial Conflict

The illusory phenomena such as flickering wheel illusion [9], two-flash fusion [10], and sound-induced double-flash illusion [21] as described above are candidates for the visual perceptual phenomenon exhibiting a strong correlation. Furthermore, there is another illusion in which the frequency of the alpha oscillation may be directly reflected in the visual perception. Here, I focus on an illusory jitter termed the motion-induced spatial conflict [22, 23] which can be visual vibrations perceived at the same frequency as the intrinsic alpha oscillations. The perceived jitter frequency of this illusion may match the intrinsic peak alpha frequency (PAF) and varies depending on its inter- and intra-participant variations.

In the motion-induced spatial conflict, moving borders defined by color contrast and those defined by luminance contrast are placed in close proximity. Because of the influence of motion on spatial coding, the motion of the color contrast is thought to be perceived more slowly than that of the luminance contrast. As a result, the positional delay of the green bar is thought to be shaken back by intracerebral correction, which seems to be jittering.

The flickering wheel illusion [9] is a phenomenon in which illusory flicker is perceived at around the similar frequency as the motion induced spatial conflict. This illusion is a phenomenon that the center of the wheel stimulus with the luminance boundary blinks at about 10 Hz while watching the fixation point. As a phenomenon related to the illusory jitter used in this research, there is a phenomenon called a motion standstill on a color lattice [24]. The phenomenon is that the bar moving at a constant speed is perceived to be stationary when isoluminant red and green bars are alternately arranged and the arrangement is continuously switched at about 4 Hz. This phenomenon is similar to the illusory jitter in that an isoluminant color grid is perceived later than a physical movement. However, this phenomenon is caused not by comparing isoluminant color boundary and luminant boundary but from only isoluminant color boundary or black-white luminant boundary, so these phenomena will be caused by different mechanisms.

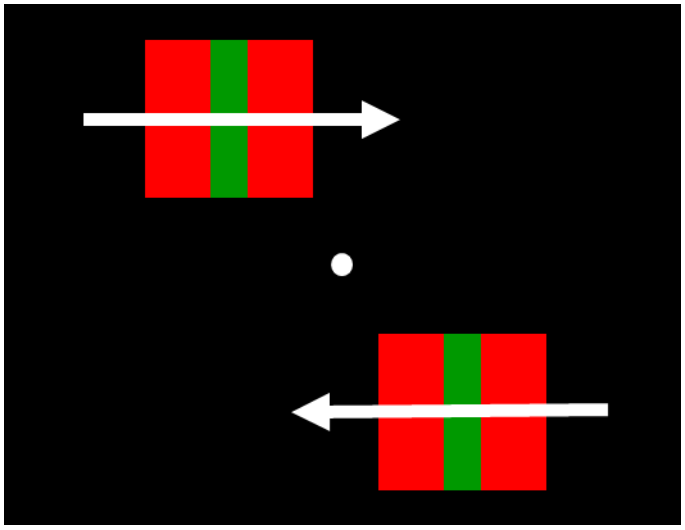

Figure 1.1：Motion-induced spatial conflict

In a previous research [25], they measured the perceived frequency of this illusory jitter by presenting the illusory jitter (target stimulus) and a physical jitter (matching stimulus). The frequency of the matching stimulus was adjusted by pressing buttons until it was perceived to be at the same frequency as the illusory jitter. As a result, the frequency of the illusory jitter was found to be around 10 Hz under. Furthermore, in the power spectrum of MEG signals during the observation of the illusory jitter, the amplitude of alpha oscillations increased relative to the condition without illusory jitter. The interesting point of this finding is that the frequency of illusory jitter matched the frequency of neural activity increasing during illusory jitter perception, suggesting a link between alpha oscillations and illusory jitter.

A previous study suggested a correlation between alpha power and illusory jitter. However, as shown in Figure 1.2, the neural activity at the illusory jitter perception is thought to be either the cause of the illusory jitter perception or the result from the illusory jitter perception. Therefore, it is still unclear whether the increase in power of alpha oscillations is involved in the generation of illusory jitter perception, or it is an epiphenomenon of the illusory jitter perception. Next, I propose the functional hypothesis of the alpha oscillation that the alpha oscillation is involved in the generation of the illusory jitter perception.

Figure 1.2：The relationship between alpha oscillations and illusory jitter

1.1.4 Microstructural properties and visual perception

Alpha oscillations in the human brain are tightly related to several types of visual perception. As described above, although recent studies have suggested functional roles of alpha oscillations in visual perception, neuroanatomical substrates for determining the characteristics of alpha oscillation are not well understood. One of the reasons why this problem has not been verified experimentally is that conventional neuroanatomical methods such as a chemical tract tracing [26] are invasive and only applicable to investigate fiber pathways in post-mortem animal brains. Therefore, direct comparison with neural oscillations in living animals has been difficult. Recent advancement of non-invasive neuroimaging methods, such as diffusion-weighted magnetic resonance imaging (dMRI) and quantitative magnetic resonance imaging (qMRI), have opened an avenue to investigate the relationship between structural properties of fiber pathways and properties of the human alpha oscillation measured by MEG or EEG. Here, I utilized a method to quantify the white matter property by measuring dMRI and qMRI (see 1.2 for details), which can non-invasively measure microstructural property of living human brain. These methods enable us to study the neuroanatomical basis of the characteristics of alpha oscillation.

A few previous studies using dMRI have investigated the relationship between the tissue microstructure of white matter and perceptual ability. Thiebaut de Schotten and colleagues utilized a line bisection test in which participants were instructed to write rounds at the center of the line segment on the paper. Even in a healthy person, a small left deviation of the round position is observed in this test, which is known as the pseudoneglect effect. By comparing the dMRI data with the performance obtained from the line bisection test, it was found that the tendency of pseudoneglect effect was correlated with the lateralization of tract volume of the second branch of the superior longitudinal fasciculus (SLF Ⅱ). Recently, a study comparing stereoacuity and structural neuroimaging (dMRI and qMRI) data has suggested that

the individual variability in human stereoacuity is related to macromolecular tissue volume (MTV, see section 1.1.3**)** in the vertical occipital fasciculus (VOF) connecting the dorsal and ventral visual pathways.

These studies suggest that the tissue properties of white matter connecting visual regions may be related with the characteristics of inter-regional information transmission, which is reflected by the individual differences in visual function. In addition to the relationship between dMRI and perception, previous studies examined the relationship between dMRI and MEG. A study by Hindriks examined whether alpha amplitude measured by MEG correlates with measurements on fiber pathways by performing tractography on dMRI data and counting a number of streamlines connecting between the brain regions defined by the Automated Anatomical Labeling (AAL) atlas [27]. As a result, the amplitude of the occipital alpha oscillations correlated with the streamline count on estimated fiber pathways between primary visual cortex and other visual areas. However, other lines of studies pointed out limitations in streamline counting approach to quantify structural connectivity. This is because it significantly depends on the geometric factor of fiber pathways (length and curvature) [28, 29] and estimated connectivity is not symmetric (i.e. estimated connectivity from area A to B significantly differ from that from B to A) [30]. Thus, it is not fully clear whether observed correlation between alpha amplitude and structural connectivity reflect tissue properties of fiber pathways or geometric configuration of fiber pathways.

Alternative approach to measure properties of white matter pathways is termed tractometry. This approach first identified major white matter tracts known to exist by analyzing dMRI data with constraints from prior anatomical knowledge [31, 32] and then evaluate microstructural measurement obtained from dMRI and qMRI data along those tracts [33, 34, 35]. This approach enables us to precisely test specific hypotheses about the relationship between alpha oscillations and specific microstructural measurements along a specific white matter tract, with removing the influence of fiber length and curvature. The most promising candidate for characterizing the intrinsic alpha oscillation is optic radiation (OR), which is connecting LGN and V1. A previous study [36] has reported that alpha current generators appear to be in layer 4C receiving the input from LGN and layer 6 projecting back to LGN. This finding suggested that the intrinsic occipital alpha oscillations are generated from the consequence of thalamocortical interaction between LGN and V1.

There is another problem that has not been clarified in previous studies. Although the study by Hindriks and colleagues suggested that the connection strength between primary visual cortex and other visual areas characterizes the occipital alpha power, the involvement of the visual areas in the alpha frequency which is another primal characteristic of the intrinsic alpha oscillation has not been shown. As well as the alpha power, there are a lot of previous studies about the relationship between the frequency of occipital alpha oscillations and visual processing [8-10, 27]. Therefore, it is also necessary to investigate the relationship between the alpha frequency and white matter tracts connecting to visual areas.

In order to address the above-mentioned problems, I investigated whether the tissue properties of the OR relate to the power and frequency of the occipital alpha oscillations (Chapter 3). To compare the characteristics of alpha oscillations with the microstructural properties of visual white matter tracts, I utilize inter-individual variations in alpha oscillations and microstructural properties. By combining the measurements of magnetoencephalography (MEG) during the resting state, dMRI, and qMRI, I quantified the characteristics of occipital alpha oscillations and microstructural property of several visual white matter tracts.

1.2 Measurement and analysis methods

In this chapter, I will explain several techniques to non-invasively measure neural activities and the brain structures. I will also explain methods to analyze the measured data.

1.2.1 Magnetoencephalography (MEG)

Magnetoencephalography (MEG) [37] is used for neural activity measurement in Chapter 2, 3 in this study. The features of MEG measurement will be briefly described below. When the brain is active, a weak current flows in the nerve cell, and a magnetic field is generated around it. This change in magnetic field can be measured using a very sensitive magnetic sensor called SQUID (Superconducting Quantum Interference Device) [38]. The time-space signal of the measured magnetic field is called the magnetoencephalogram (MEG). MEG is used not only for clinical diagnosis for epilepsy but also for studying sensory functions such as vision and audition higher brain functions such as language and calculation. MEG has high temporal resolution, and can capture magnetic field fluctuation in milliseconds order. This is one of the biggest advantages compared with functional MRI (fMRI) [39], which has a

temporal resolution of seconds order. Therefore, MEG is suitable for detecting rapid changes in neural activity with respect to a time-varying stimulus.

Electroencephalography (EEG) [40] is another method for measuring neural activities with high temporal resolution. EEG is sensitive to extra-cellular currents generated by postsynaptic potentials. On the other hand, MEG is sensitive to intra-cellular currents associated with their synaptic potentials. Since EEG is sensitive to radial components of a current source in a spherical volume conductor, EEG mainly detects activity in the cortical gyri. On the other hand, MEG mainly detects activity originating in sulci because MEG is most sensitive to its tangential components. Since electric potentials transmitted through various tissues having different electrical conductivities such as cerebrospinal fluid, skull and scalp are measured, the electric activity of the local brain area is weakened, which leads to the low spatial resolution. In that respect, the magnetic permeability of the above-mentioned tissue is almost equal to that of air, so the spatial resolution is high in the case of MEG and the signal source can be estimated with higher accuracy than EEG. In summary, MEG is a brain imaging technique with relatively high spatial and very high temporal resolutions, which is advantageous for the measurement of neural oscillations.

Bandlimiting and signal-averaging

Bandlimiting and signal-averaging are fundamental signal processing methods to improve the SNR (signal to noise ratio). In general, the signals outside the bandwidth of 1 Hz to 100 Hz in the frequency domain are excluded by a filter. Especially in this study, because I focused on the functional role of alpha oscillations, cyclic neural activities at 8 - 13 Hz, we mainly adapted 40 Hz low-pass filter as preprocessing for measured MEG data. However, even after removing the noise due to the band-limitation, the SNR is insufficient for the single trial data and it is difficult to extract the brain magnetic field reaction. Therefore, the signal-averaging method is used together to further reduce the noise. Signal-averaging is a widely used method especially for MEG signal processing with an aim to extract the evoked response. Signal-averaging of data based on the assumption that the noise is independent for each trial and the brain magnetic field signal is invariant in all trials in which the response to the same stimulus is repeatedly measured under the same condition for n trials, the noise dispersion σ can be reduced by σ^2/n. Therefore, the SNR is improved by $\sqrt{n}$ times. In fact, however, the neural activities of participants are not constant for each trial due to the influence

of repetitive presentation of stimuli. In order to avoid long-term measurement by repetitive presentation, the development of data analysis method with few trials is desired.

Independent component analysis (ICA)

In this study, independent component analysis (ICA) [41] was used for the noise removal as preprocessing in Chapter 2, 3. ICA is a kind of Blind Source Separation (BBS) that can separate unknown multivariate signals of mixing process into original signals before mixing.

When there are the n sensor signals measured by the MEG, then the data of the i th is defined as $x_i(t)$, the vector in which all the sensor signals are arranged is expressed as Equation 1 - 1.

$$x(t) = (x_1(t), x_2(t), ..., x_n(t))^T, (t = 1,2,...,l) \qquad 1-1$$

Here, t represents a time as each discrete value. l is the total number of time data. An unknown m-dimensional original signal is expressed as Equation 1 - 2. The original signal is an individual magnetic field change generated from each stimulus, which is assumed to be mixed in the MEG data.

$$s(t) = (s_1(t), s_2(t), ..., s_m(t))^T, (t = 1,2,...,l) \qquad 1-2$$

At this time, using the $n \times m$ mixing matrix A of the measurement signal $x(t)$ and the original signal $s(t)$, I assume the relationship of Equation 1 - 3.

$$x(t) = As(t) \qquad 1-3$$

In this way, ICA is a method of estimating an unknown original signal $s(t)$ by obtaining an unknown mixing matrix A from observed data $x(t)$. If W is the inverse matrix of A, it becomes possible to obtain the original signal as shown in Equation 1 - 4 by using the component w_{ij} of W.

$$s_i(t) = \sum_j w_{ij} x_j \qquad 1-4$$

Here, since the original signal $s(t)$ and the mixing matrix A are unknown, a unique solution cannot be obtained. Therefore, in the ICA, the five hypotheses, "the components are independent from each other", "the distribution of the independent components basically follows a non-normal distribution", "the dimension of the independent component data is the same as or smaller than the dimension of the measured data", "mixing matrix is immutable regardless of time", "$rank(A)$ of mixing matrix must be full rank " are set for finding a solution..

SSS (the Signal Space Separation method)

The Signal Space Separation method (SSS) [42] is a method for separating internal signals and external signals in the conceptual diagram at MEG measurement shown in Figure 1.1. The blue line in Figure 1.3 covers the whole brain space, but the red line covers the entire brain and sensor space. Here, the blue and red spheres have the same center point. In the model of Figure 1.1, neural activity occurs in the blue sphere. Here, this space is referred to as "inner area". On the other hand, all the MEG sensors are included in the space between the blue and red spheres, and this space is referred to as "intermediate area" or "sensor area". Further, the outside of the red sphere where the interference electromagnetic noise is generated is referred to as an "outside region".

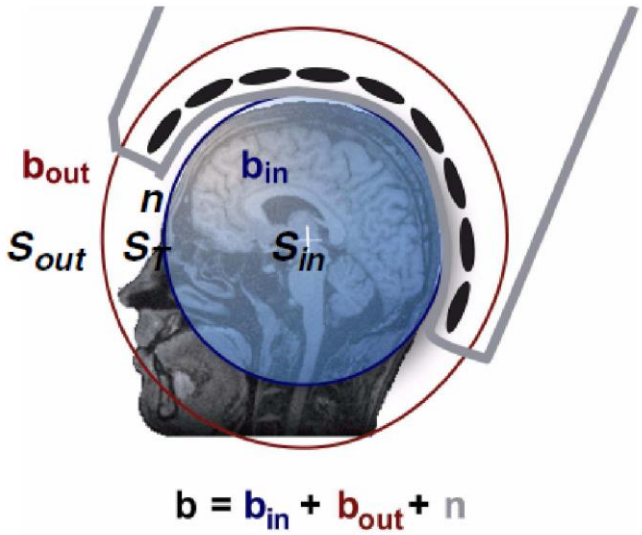

Figure 1.3：Conceptual diagram of spatial segmentation on the signal reconstruction by SSS

As is widely known, the magnetic field B of the sensor area can be written as a quasi-static Maxwell's equation as follows.

$$\nabla \times B = \mu_0 J, \qquad \nabla \cdot B = 0 \qquad 1-5$$

Here, μ_0 represents vacuum permeability. The sensor of the MEG system obtains $\nabla \times B = 0$ because the current density becomes $J = 0$ when the source volume is not present. This curl-free magnetic field B can thus be expressed as the gradient of the scalar potential.

$$B = -\mu_0 \nabla \Phi \qquad 1-6$$

Considering Equations 1 - 6, Φ must satisfy Laplace equation $\nabla^2 \Phi = 0$. In the spherical coordinate (r, θ, φ), the solution of the Laplace equation can be expanded by a spherical harmonic function as follows.

$$\begin{aligned} \Phi(r,\theta,\varphi) &= \sum_{l=0}^{\infty} \sum_{m=-l}^{l} \frac{1}{r^{l+1}} \alpha_l^m \mathrm{Y}_l^m(\theta,\varphi) + \sum_{l=0}^{\infty} \sum_{m=-l}^{l} r^l \beta_l^m \mathrm{Y}_l^m(\theta,\varphi) \\ &= \Phi_{in} + \Phi_{out} \end{aligned} \qquad 1-7$$

Here, $\mathrm{Y}_l^m(\theta,\varphi)$ is a spherical harmonic function.

Substituting Equations 1 - 7 into Equations 1 - 6, the magnetic field can be expressed as follows.

$$\begin{aligned} B(r,\theta,\varphi) &= -\mu_0 \sum_{l=0}^{\infty} \sum_{m=-l}^{l} \alpha_l^m \nabla \left(\frac{\mathrm{Y}_l^m(\theta,\varphi)}{r^{l+1}} \right) - \mu_0 \sum_{l=0}^{\infty} \sum_{m=-l}^{l} \beta_l^m \nabla \left(r^l \mathrm{Y}_l^m(\theta,\varphi) \right) \\ &= B_{in} + B_{out} \end{aligned} \qquad 1-8$$

Since l is an infinite number, the number from the inside and outside also becomes infinite, and this expansion formula reconstructs the magnetic field accurately. In practice, however, since the magnetic field B is mostly described by a finite number l, internal and external derived numbers such as coefficients can be expressed in matrix form.

In the spherical harmonic coordinate standard, the MEG data B can be expressed as follows.

$$B = x_{in}S_{in} + x_{out}S_{out} \qquad 1-9$$

Here, S_{in} and S_{out} are matrices containing the gradient of the spherical harmonics on Equations 1 - 8, and x_{in} and x_{out} are matrices containing coefficients α_l^m and β_l^m. Expressions 1 - 9 can be omitted as follows.

$$B = \begin{bmatrix} x_{in} & x_{out} \end{bmatrix} \begin{bmatrix} S_{in} \\ S_{out} \end{bmatrix} = XS \qquad 1-10$$

Here, S derived from the SSS can be divided into subspaces S_{in} and S_{out}, each associated with an internal biomagnetic field signal and an external interference signal. x_{in} and x_{out} indicate internal and external derived coefficients.

From Equations 1 - 10, the coefficients x_{in} and x_{out} can be calculated from the pseudo inverse matrix S as follows.

$$\begin{bmatrix} \hat{x}_{in} & \hat{x}_{out} \end{bmatrix} = S^{\dagger}B = \left(S^T S\right)^{-1} S^T B \qquad 1-11$$

By using the internally derived S_{in} and the calculated coefficient $\hat{x}_{in}$, only the estimated biomagnetic field can be reconstructed as follows.

$$B_{in} = \hat{x}_{in}S_{in} \qquad 1-12$$

tSSS (the temporally extended signal space separation method)

The temporally extended signal space separation method (tSSS) [43] is an extension of the Maxwell filter described in the previous section to the time dimension. Since the result of tSSS does not depend on preconditions and user's experience, it is considered that noise can be removed more efficiently.

In tSSS, firstly, B_{in} and B_{out} which are spatially reconstructed for each sensor and each sample are subtracted from measurement data $B(t)$.

$$b_s(t) = b(t) - (b_{in}(t) + b_{out}(t)) \qquad 1-13$$

Data b_{in} and b_{out} are convolved with $n \times m$ matrix B_{in} and B_{out}. Here, m is a sensor and n is a sample. The singular value decomposition is as follows.

$$B_{in} = U_{in} S_{in} V_{in}^T \qquad S_{in} = diag(\sigma_k^{in})$$
$$B_s = U_s S_s V_s^T \qquad S_s = diag(\sigma_k^s)$$
$$where \quad k = 1, ..., m \qquad 1-14$$

The V_{in} and V_s columns span the waveform $b_{in}(t)$ and $b_s(t)$, and the subspace intersections between the waveforms can be estimated by QR special position decomposition.

$$V_{in} = Q_{in} R_{in} \; ; V_s = Q_s R_s \qquad 1-15$$

Here, $Q^T Q = I_m$ and $R \in \Re^{m \times m}$ are satisfied. The $m \times m$ matrix C is constructed from the $n \times m$ matrix Q_{in} and Q_s as follows.

$$C = Q_{in}^T Q_s \qquad 1-16$$

When special position decomposition is used, it becomes as follows.

$$C = Y S_C Z^T \qquad 1-17$$

Here, the diagonal matrix S_C contains the singular value σ_k of the matrix C. This singular value defines the principal angle θ_k of the two subspaces: $\cos(\theta_k) = \sigma_k$. The intersection of the subspace contains the waveform corresponding to $\sigma_k^C = 1$. The upper limit value of subspace correlation on MaxFilter is set to 0.90 in this study. If the p value exceeds the upper limit of the correlation, this program will have a projection operator $(I - LL^T)$. Here, $L(n \times p)$ contains the crossing waveform (the first p column of matrix $Q_S Z$). These waveforms are finally projected as follows.

$$\hat{b}_{in} = (I - LL^T) b_{in} \qquad 1-18$$

By the above operation, only the estimated biomagnetic field can be reconstructed.

Mapping by isomagnetic curves and source reconstruction

The MEG system used in this study has 360 sensors that cover the entire head of participants. By visualizing the channel data with a topographic map, it is possible to roughly identify the area related to the task, such as motor cortex and visual cortex. However, this area estimation depends greatly on the position of the head in the MEG helmet and the anatomical structure of the head.

In order to specify more detailed signal sources of MEG signals, researchers usually estimate the position of the electric activity from the magnetic field. In such case, it is required to solve the inverse problem for the source localization. In general, because the number of source configurations is much greater than the number of MEG sensors, there are no unique solutions to the inverse problem, even in the absence of noise. Although there is no unique solution, several methods using models based on prior knowledge of brain activity have been developed. The simplest approach is the equivalent current dipole estimation. This method assumes that the measured MEG signals are explained by one or a few current dipoles, and calculate the dipole parameters (the position and moment of the signal source) that minimize the square error between the measured magnetic field and theoretical value of the magnetic field generated from the assumed current dipoles.

A single dipole estimation method is a model assuming single current dipole with maximum amplitude, which can be applied in the case where a single magnetic field signal source (localized neural activity) is assumed from physiological knowledge and the measured magnetic field shows bipolar distribution. This technique has been applied for a long time to estimate sensory-evoked magnetic fields including visually-evoked and somatosensory-evoked magnetic fields. However, single dipole is inadequate for modeling complex brain activities arising from multiple signal sources. In order to obtain an appropriate solution, a model including accurate knowledge about neural activity is essential. However, it is generally very difficult to decide the number of dipoles.

To deal with more complicated signal patterns, a method called beamformer is used. The beamformer is constructing a spatial filter to estimate the contribution of a single brain position to the measured field. A spatial filter is calculated by minimizing the source power or variance in a certain time width at the lattice point, and the current value is estimated. Beamformer has several approaches using different calculation algorithms, such as Minimum-Norm Estimates (MNE) [44], Low Resolution Brain Electromagnetic Tomography

(LORETA) [45], Linearly Constrained Minimum Variance Method (LCMV) [46], Dynamic Imaging of Coherent Sources (DICS) [47], and so on. The DICS used in this study (Experiment 2.4) is an algorithm which uses a spatial filter to localize coherent brain regions and provides the time courses of neural activity. This method allows investigation of the inter-regional interactions in a specific frequency band by imaging power and coherence estimates within the human brain.

1.2.2 Diffusion-weighted magnetic resonance imaging (dMRI)

Diffusion-weighted magnetic resonance imaging (dMRI) is a method to measure the magnitude and orientation of diffusion of water molecules [48, 49]. Since diffusion of water molecules in white matter is restricted by fiber tracts, water molecules preferentially diffuse toward parallel direction to fiber orientation. Therefore, dMRI measurements provide fiber orientation distribution in each white matter voxel, based on anisotropy of water diffusion restricted by fiber tracts.

Analysis on dMRI data in individual voxel provides useful information to infer white matter microstructure. For example, one could calculate fractional anisotropy [50] in each white matter voxel by quantifying a degree of diffusion anisotropy in dMRI measurements. Alternatively, one could also calculate Orientation Dispersion Index (ODI) [51], which aims to quantify spatial configuration of the neurite structures. dMRI-based microstructural measurements, such as FA and ODI, have been often used to evaluate inter-subject differences in white matter microstructure [52-54].

In addition to the microstructural measurements, analysis on dMRI data provides a position and trajectory of white matter tracts, by using tractography [49, 55-57]. Tractography is a method to track orientation of dMRI signal, and generate candidates of white matter connections. In a common practice, tractography is often restricted by anatomical prior information to reduce false positive estimates [31, 32, 58]. For example, one could use anatomical knowledge on connection between lateral geniculate nucleus (LGN) and primary visual cortex (V1) to restrict tractography, in order to estimate the optic radiation in a consistent manner with post-mortem anatomical studies [59].

By combining microstructural measurements and tractography, we could quantify microstructural measurements along white matter tracts of interest. Since dMRI measurements can be performed from living human brains, this approach open the avenue for studying the

relationship between specific white matter tracts and development [60, 33], aging [34], diseases [61, 62], and perceptual function [63-65].

In this dissertation, I used a dMRI index proposed in the previous studies, called Orientation Dispersion Index (ODI). It is thought that ODI indicates the spatial configuration of the neurite structures [51, 66, 67].

1.2.3 quantitative magnetic resonance imaging (qMRI)

T1-weighted image has been often used to measure tissue properties. However, it is difficult to compare an intensity of T1-weighted image across brain areas and subjects, since image intensity significantly affected by inhomogeneity of the measurements [68]. In order to solve this problem, a technique called quantitative MRI (qMRI) has been developed to quantify neuroanatomical images [34, 69].

Sereno and colleagues combines proton-density weighted image and T1-weighted image, and then measures the nonuniformity of radiofrequency field (B1), so that more quantitative MRI index was calculated [69]. Mezer and colleagues combined the Spin-echo Inversion Recovery (SEIR) method which is less affected by the bias and the high resolution scan (Spoiled gradient echo method), to measure high resolution quantitative MRI data. Their measurements provide quantification of the volume of non-proton macromolecules (Macromolecular Tissue Volume; MTV).

These measurements from qMRI have been proven to be highly reproducible [34] and also be correlated with histological measurements on myelin [70]. Furthermore, by combining with dMRI-based tractography, we could measure qMRI measurements along white matter tracts in order evaluate white matter disorder [34] and aging [52]. In this dissertation, I used MTV to measure microstructural properties of white matter tracts.

1.2.4 Current stimulation

There are mainly two types of non-invasive brain stimulation methods, magnetic stimulation and electrical stimulation. In magnetic stimulation such as transcranial magnetic stimulation (TMS) [71], neuronal axons are directly stimulated by pulsed magnetic field change, whereas transcranial direct current stimulation (tDCS) [72] changing the membrane potential of neurons affects firing rate. Although the current used in tDCS is about 1 mA, which is very weak, it has been shown that permeation of current through the scalp can cause long-term change in neural activity. It is thought that tDCS changes the excitability of the targeted brain region depending on the polarity of the electrode and its effect lasts from several minutes to

several days after the end of stimulation. Stimulation by the anode side may temporarily enhances the excitability of the site under stimulation and improve the cognitive function. On the other hand, stimulation by the cathode side suppresses the excitability of neurons. From such effects, the possibility of application such as the rehabilitation effect on patients with stroke and the effect of improving cognitive ability in healthy participants is beginning to be studied.

Transcranial Alternating Current Stimulation (tACS) [73] is a transformation method of tDCS, which has been demonstrated to be effective in recent years, to AC stimulation. Previous studies have demonstrated that it is possible to change neural activity sufficiently by flowing tDCS with about 1 mA for 5 - 10 minutes [72]. Therefore, also in tACS, it is expected that a biophysical meaningful current reaches the cerebral cortex and weakly influence the membrane potential of nerve cells. One of the features of tACS not found in tDCS is a frequency-dependent effect in the brain. It is expected that the neural oscillation is amplified by the current stimulation causing resonance phenomena when giving tACS close in frequency to the periodical activity in the brain. Based on these characteristics, tACS is considered to be suitable for changing neural activity having specific periodicity such as alpha oscillation. In addition, a certain effect is expected also for visual perception having periodicity like the illusory jitter used in this study.

A problem in handling tACS is that tACS itself causes artifacts in measured signals. Since tACS current is overwhelmingly larger than neural oscillations, the observation of neural oscillations is difficult during current stimulation. For this reason, the assumption that tACS entrains the neural oscillations in a specific frequency has not been demonstrated by actually observing changes in neural activity. Previous studies have evaluated the effect of tACS on neural oscillations from observing some sustained effect after giving tACS. For example, it has been reported that the amplitude of the alpha oscillation remains to be increased after the occipital area is stimulated for about 10 minutes in the alpha band (8 - 13 Hz). In addition, when tACS in the delta band (0.5 - 4 Hz) is given during sleep, it is observed that the phase-locked EEG persists even after the current stimulation [74].

As described above, since the current noise is too large in the conventional tACS, it is difficult to measure the electroencephalogram during the electrical stimulation. Therefore, in this research, in order to reduce the current noise, we adopted a method of amplitude modulation of high frequency tACS.

In recent years, Witkowski and colleagues succeeded in measuring MEG data that does not include current-derived noise by using an alternating current stimulus whose amplitude is modulated in the high frequency [75]. For example, the amplitude of the tACS with 2 mA having a carrier frequency of 220 Hz is modulated so that the modulation frequency is 11 Hz. This method enables us to observe the neural activity at around target frequency band during the current stimulation (see 2.3 Method).

1.3 The purpose of this thesis

From the above background, I will describe the purpose of this research. The aim of this research is to essentially understand the characteristics of the alpha oscillation. To that end, I investigate alpha oscillation from two viewpoints and comprehensively discuss the findings. In particular, I think it is vital to investigate both visual functional role and neuroanatomical substrate of alpha oscillations. Based on this motivation, I mainly conducted two experiments. First, to examine the role of alpha oscillation in visual perceptual information processing, I conduct the experiments combining human psychophysical experiments and electroencephalogram measurements, and examine the relationship between the characteristics of alpha oscillations and illusory jitter perception (chapter 2). Next, in order to investigate the involvement of the fundamental characteristics such as the power and frequency of alpha oscillations in the microstructural properties of the white matter tracts, I performed dMRI measurement and compared it with the MEG data at the rest (chapter 3).

2 The relationship between alpha oscillations and illusory jitter

2.1 Effects of inter-individual variation in resting state PAF on jitter frequency

2.1.1 Methods

Participants

Twelve (3 females; age range: 22–53 yr) participants (all males; age range: 22–53 yr) took part in the experiments 1. All participants gave their written informed consent to participate and had normal or corrected-to-normal vision. The ethics committee of the National Institute of Information and Communications Technology (NICT) approved all experimental procedures.

MEG measurement

MEG measurement was conducted in a magnetically shielded room, using a 360-channel whole head MEG system (Neuromag® 360, Elekta) composed of 204 planar gradiometers, 102 magnetometers, and 54 axial gradiometers. A sampling frequency of magnetic signals was at 1000 Hz. Two hundred planar gradiometer channels were used for the analysis as they have relatively high signal-to-noise ratios. The planar gradiometers consist of two coils measuring spatial derivatives of magnetic fields along the surface. Pairs of planar gradiometers were located at 102 positions and measure the derivatives in orthogonal directions (x and y). First, I performed a Fast Fourier Transforms (FFT) analysis for each planar gradiometer and summed the power of the two gradient components at the same location, termed combined channels. I then plotted a topographic map and selected channels whose amplitude were maximum. In this experiment, artifacts generated from blinks or heart beats were removed by independent component analysis (ICA); bandpass filtering between 1 and 40 Hz was then applied before FFT analysis.

Apparatus and visual stimuli

Visual stimuli were presented on a translucent screen in a magnetically shielded room by using an LCD projector (PT-DZ680, Panasonic). The span of projector was 34.8 × 26.1 deg of the visual angle (800 × 600 resolution) and refresh rate was a 60 Hz.

To estimate the perceived frequency of an illusory jitter, a visual stimulus for illusory jitter was presented in the upper visual field. Simultaneously, a visual stimulus for physical jitter was presented in the lower visual field. For both visual stimuli of illusory and physical

jitter, a vertical bar [0.5 × 2.9 deg (W × H)] at the center of a red square [2.9 × 2.9 deg (W × H)] moved across a black background at the speed of 5.1 deg/s (Figure 2.1.2A). The center of the red square was located 3.6 deg above or below a fixation point. The luminance of a green bar for the illusory jitter was isoluminant with the surrounding red square, whereas that of a bar for the physical jitter was black. The black bar physically moved sinusoidally in horizontal directions to mimic an illusory jitter. At the first phase of the experiment, I adjusted the green luminance for the illusory jitter [CIE 1931: x = 0.36, y = 0.61, luminance = 19.2–25.9 cd/m^2] to be perceptually isoluminant with red [CIE 1931: x = 0.66, y = 0.34, luminance = 21.8 cd/m^2] using a flicker method [76] on each participant. All visual stimuli were made using Psychtoolbox 3 [77] that runs on Matlab.

Procedure for experiment 1

To investigate the effects of inter-individual variation in resting state PAF on jitter frequency, I compared the perceived jitter frequency of each individual participant with resting state PAF. To estimate PAF, I measured MEG data in the resting condition in a session which is separate from the illusory jitter frequency measurement. Participants were instructed to open and close their eyes for 30 s in response to a sound cue in a dark room, which was repeated 6 times. Therefore, I obtained MEG data for total 3 min in the eyes-open and -closed resting conditions.

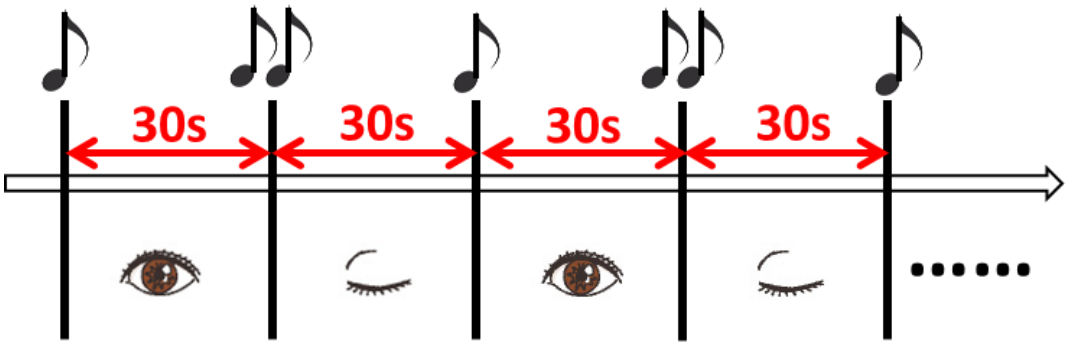

Figure 2.1.1：Time course of the MEG measurement in the resting condition

To estimate perceived jitter frequency (Figure 2.1.2B), I conducted the psychophysical experiment whose trial composed of a 2-s stimulus presentation period and a 2-s response period. Participants were instructed to judge whether a physical jitter, presented in the lower visual field, was faster than an illusory jitter, presented in the upper visual field, by pushing one of two buttons. The frequency of the physical jitter was selected randomly from seven levels

(5.5, 6.7, 7.5, 8.6, 10.0, 12.0, and 15 Hz). In total, twenty trials were repeated for each frequency of the physical jitter.

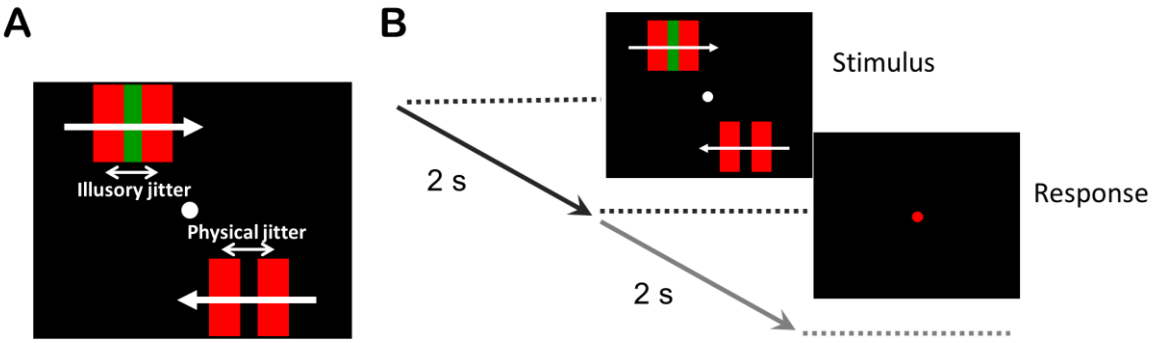

Figure 2.1.2: Visual stimuli for estimation of illusory jitter frequency

Analysis

I analyzed MEG data by using FieldTrip toolbox [78] running on Matlab. Data throughout the manuscript are presented by mean ± SEM. Details of n for each experiment indicate the number of participants. A significant *p*-value was 0.05.

I first applied FFT analysis on MEG data within 10-s time windows (10,000 time-points) shifted by 1 s and averaged 126 spectra (21 spectra per each 30-s period). I then selected 5 combined channels (10 planar gradiometers) which had the largest alpha amplitude for each participant. From these, I defined the peak alpha frequency (PAF) and the peak alpha power (PAP) from the frequency of the maximum power in the alpha band (8–13 Hz). As a control, I also estimated the peak beta frequency. Linear regression was applied to fit a linear model to the log-transformed spectrum in the beta range (13–30 Hz) [8]. The fitted linear trend (1/f component) was subtracted from the spectrum because of the smaller peaks in the beta range. I then defined the peak beta frequency (PBF) and power (PBP) from the frequency which had the maximum power in the beta band (15–25 Hz). The value of the PBP was estimated using the original spectrum before subtracting the linear trend was used. I estimated the beta frequency/power only during the eyes-closed resting condition because the beta peak did not clearly appear during the eyes-open resting condition for a few participants.

For the psychophysical data, I plotted the response rate as a function of physical jitter frequency and fitted a cumulative Gaussian function for each participant. The frequency of perceived illusory jitter was defined as the frequency corresponding to a 50% response rate.

Finally, I calculated the correlations between the perceived jitter frequency and the peak

alpha/beta amplitude/frequency (n = 12).

2.1.2 Results

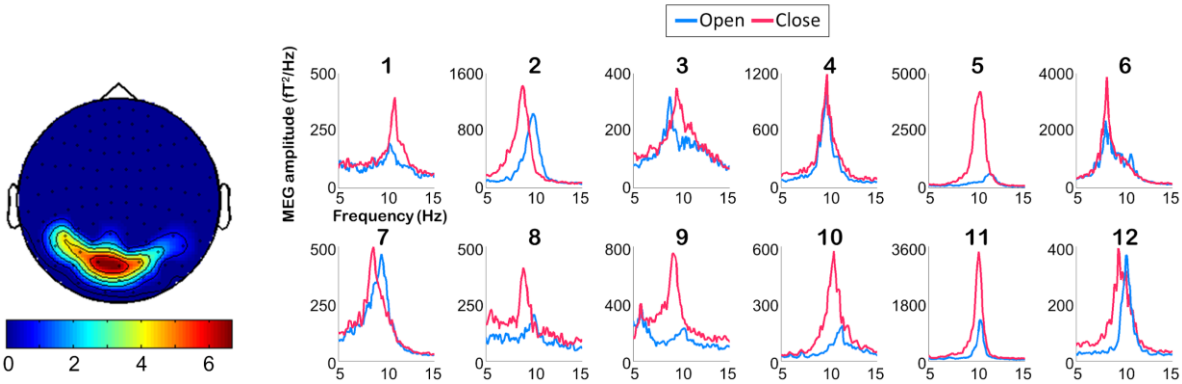

Figure 2.1.3: The distribution map of selected gradiometer channels and power spectra of all participants

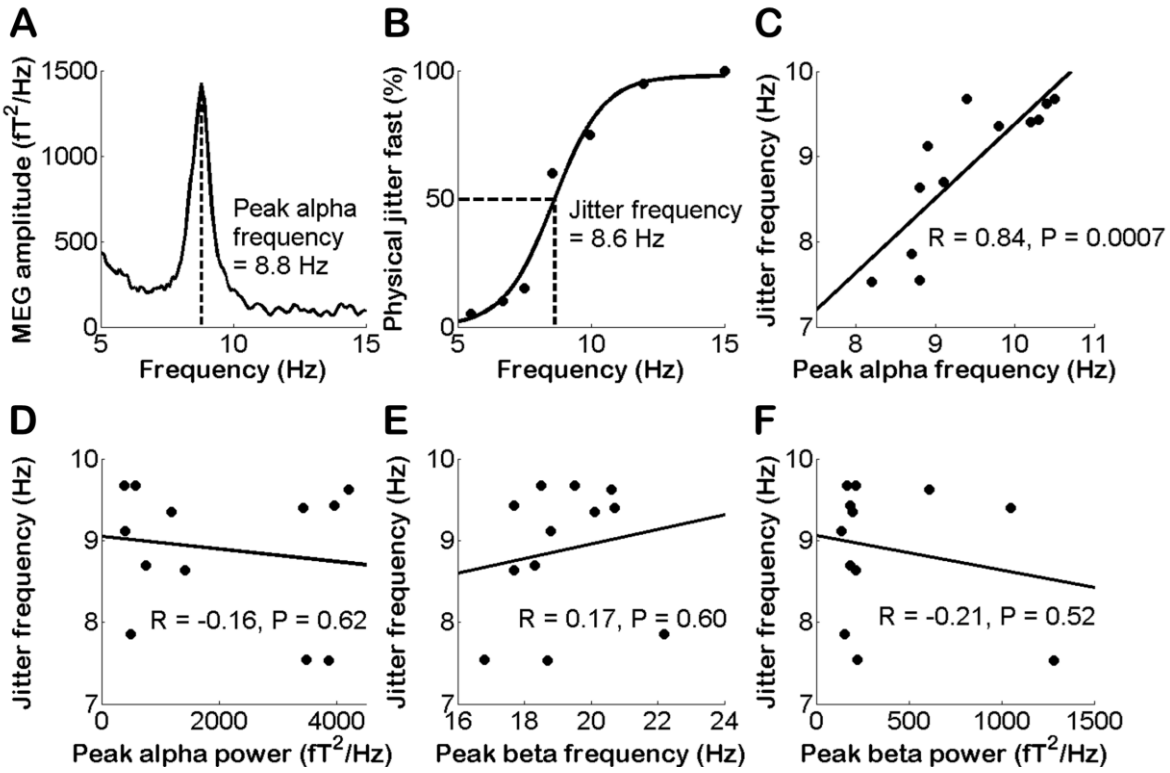

Figure 2.1.4：The correlation between the amplitude/frequency of the neural oscillations and the frequency of illusory jitter.

I show a typical power spectrum of MEG in the eye-closed resting condition in Figure 2.1.4A. A peak clearly appeared in the alpha band (8–13 Hz). Figure 2.1.4B shows the function of the physical jitter frequency for the same participant. The PAF in the eyes-closed resting condition (8.8 Hz) of this participant matched well with the perceived jitter frequency (8.6 Hz). Figure 2.1.3 shows the spectra of all participants. I then statistically compared the individual

resting alpha frequency with the illusory jitter frequency for all participants (n = 12, Figure 2.1.4C). I found there was a significant correlation between the illusory jitter frequency and PAF during the eyes-closed resting condition (r = 0.84, p = 0.0007). The perceived jitter frequency was also significantly correlated with PAF during the eyes-open resting condition (r = 0.87, p = 0.0002). Overall, PAFs in the eyes-closed condition were slightly lower than those in the eyes-open condition (9.5 ± 0.2 vs 10.0 ± 0.3 Hz, respectively; $t(11) = 2.34$, p = 0.039, two-tailed paired t-test) I think this tendency may reflect the decrease in PAF along drowsiness or decreased alertness [79, 80]. I confirmed that the PAF during illusory jitter perception, measured in the following experiment for source localization, was also significantly correlated with illusory jitter frequency (r = 0.80, p = 0.005). In contrast to PAF, the peak amplitude of the alpha oscillation was not correlated with the perceived jitter frequency (eyes-closed: $r = -0.16$, p = 0.62, Figure 2.1.4D; eyes-open: $r = -0.37$, p = 0.24). In addition, neither the PBF nor the PBP were correlated with perceived jitter frequency (BPF: r = 0.17, p = 0.60, Figure 2.1.4E; BPB: $r = -0.21$, p = 0.52, Figure 2.1.4F). These tendencies indicated that the illusory jitter frequency is associated only with the intrinsic PAF, rather than with the PAP, PBF or PBP.

2.1.3 Discussion

This experiment revealed that the the perceived frequency of the illusory jitter correlated with the inter-individual variation in the alpha frequency. The measurement of the alpha frequency at the resting state is conducted, separated from a session for estimating the illusory jitter frequency. Therefore, the frequency of the resting intrinsic alpha oscillation is not affected by the perception of illusory jitter. This finding implies that the illusory jitter perception is derived from the rhythm of the intrinsic alpha oscillation rather than that the perceived illusory jitter modulates the frequency of the intrinsic alpha oscillations.

As well as this experiment, there are several previous studies indicating the correlation between the illusory perception and the alpha oscillation. A study using a flickering wheel illusion [9] whose center at the periphery is perceived as flickering showed that the frequency of alpha amplitude most largely modulated by the flicker perception was significantly correlated with the individual PAF measured during the resting state. Although the study has not directly shown the correlation between the perceived flicker frequency and PAF during the resting state, partly because of relatively large variations (2–20 Hz) in the perceived flicker frequency, the phenomenon might be related to the current finding in the sense that the frequency of the intrinsic alpha oscillations is tightly related to the visual perception. The result

in my experiment is novel in the sense that the PAF during rest was correlated with illusory jitter frequency itself. Sound-induced double flash illusion is also a similar phenomenon with the motion-induced spatial conflict. In this illusion, an illusory double flash is perceived while one flash is simultaneously presented with two sounds [21]. A threshold of the sound interval for illusory flash perception is around 100 ms, and the threshold was negatively correlated with the individual alpha frequency in the task. Moreover, a threshold of the inter-stimulus interval at which two continuous flashes can be distinguished from a single flash was negatively correlated with the eye-closed resting PAF [10]. These findings are compatible with the finding in my study showing that the alpha frequency during the rest and during illusory jitter perception was correlated with perceived jitter frequency.

2.2 Effect of intra-participant variation of PAF on jitter frequency

2.2.1 Methods

Participants

Ten (all males; age range: 22–53 yr) took part in this experiment. All participants gave their written informed consent to participate and had normal or corrected-to-normal vision. The ethics committee of the National Institute of Information and Communications Technology (NICT) approved all experimental procedures.

MEG measurement

I used the same measurement parameters and conducted the same preprocessing of MEG data as in Section 2.1. However, this measurement was conducted with a sampling rate of 5000 Hz.

Apparatus and visual stimuli

Apparatus and parameters for visual stimulus presentation are the same as Chapter 2.1.

Procedure for experiment 2

In experiment 2 (Figure 2.2.1), I studied how spontaneous fluctuations in intrinsic alpha frequency within participants affected illusory jitter frequency. MEG was continuously measured during the experiment including each trial consisted of 8 s. After the blank period of 2

s (pre-stimulus period), visual stimuli for illusory jitter were presented in both the lower and upper visual fields for 2 s (stimulus period). After the blank period of 2 s (post-stimulus period), following the stimulus period, the color of a fixation point turned to red from white for 2 s (response period). At this time, the participants were instructed to judge whether the frequency of illusory jitter in the current trial was faster or slower than the pre-memorized mean frequency by pushing one of two buttons. At the first phase of this experiment, participants were instructed to go through a practice with the same stimulus and task. In total, participants completed one or two practice sessions (50 or 100 trials) until the average response rate within a session became 40%–60%. Once the practice was completed, participants engaged in 300 trials for the main experiment.

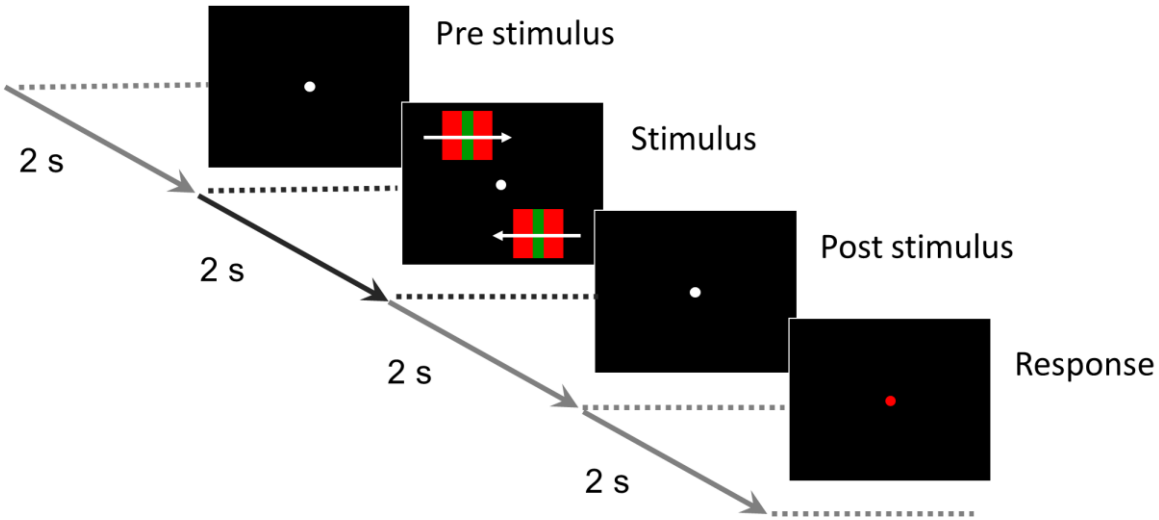

Figure 2.2.1：Time course of visual stimuli to estimate the perceived frequency of illusory jitter.

Analysis

I analyzed MEG data by using FieldTrip toolbox running on Matlab, ANOVA by using IBM SPSS. Data throughout the manuscript are presented by mean ± SEM. Details of n for each experiment indicate the number of participants. A significant *p*-value was 0.05.

Trials were divided into faster and slower perceived jitter trials based on behavioral response. To equate the number of trials between faster and slower jitter trials, and thus the signal-to-noise ratio of MEG data, 100 trials were randomly chosen from each group of trials. I selected 5 combined channels (10 planar gradiometers) which had the largest alpha amplitude from an averaged spectrum of data without using the response period of 200 (100

faster and slower) trials. I performed FFT analysis with a Hanning taper on the data of 4 periods (−2 to −1 s, −1–0 s, 0–1 s, 1–2 s, 5000 time-points each). Then the data were zero-padded to 10 s (50,000 time-points). I averaged the spectrum across 100 faster and slower trials separately. PAF of each group of trials was defined as the frequency of maximum amplitude in the alpha band. I performed paired *t*-test (n = 10) to compare the frequency of four periods between the faster and slower trials. Bonferroni correction was used to correct *p*-values.

To examine how the amplitude and phase of alpha oscillations affect illusory jitter frequency, I calculated the amplitude and phase at each time-frequency point by using wavelet analysis (−1.5–1.5 s from stimulus onset at 50 ms intervals, frequencies increasing logarithmically from 3 to 40 Hz while the number of cycles in each wavelet increases linearly from 3 to 12 cycles). Then I calculated the amplitude difference and phase opposition sum [81] between the faster and slower trials at each point in the time-frequency plane for each participant. For the statistical analysis, I utilized a method called "Permutation + z-score Test" [81]. Namely, the amplitude difference and phase opposition sum were recomputed after randomly permuting the faster and slower jitter trials. The permutation test was repeated for 1000 times. Subsequently, I expressed the difference between the original dataset and the mean of all permutations in units of standard deviation across all permutations. I obtained the time-frequency map of *p*-values by using means of the normal cumulative distribution function. To combine the time-frequency maps of *p*-values across participants, I converted the *p*-value into an equivalent z-score with the inverse normal cumulative distribution function. The z-scores are combined across observers and finally turned back into probabilities [82]. To correct for multiple comparisons, I analyzed the distributions of *p*-values with the false discovery rate (FDR) procedure [83] to compute a *p*-threshold that set the expected rate of falsely rejected null hypotheses to 5%.

2.2.2 Results

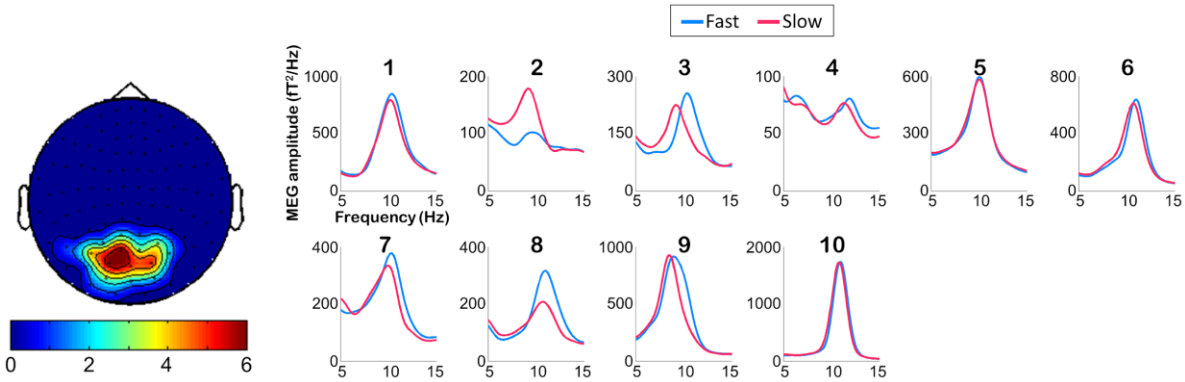

Figure 2.2.2: The distribution map of selected gradiometer channels and power spectra of all participants

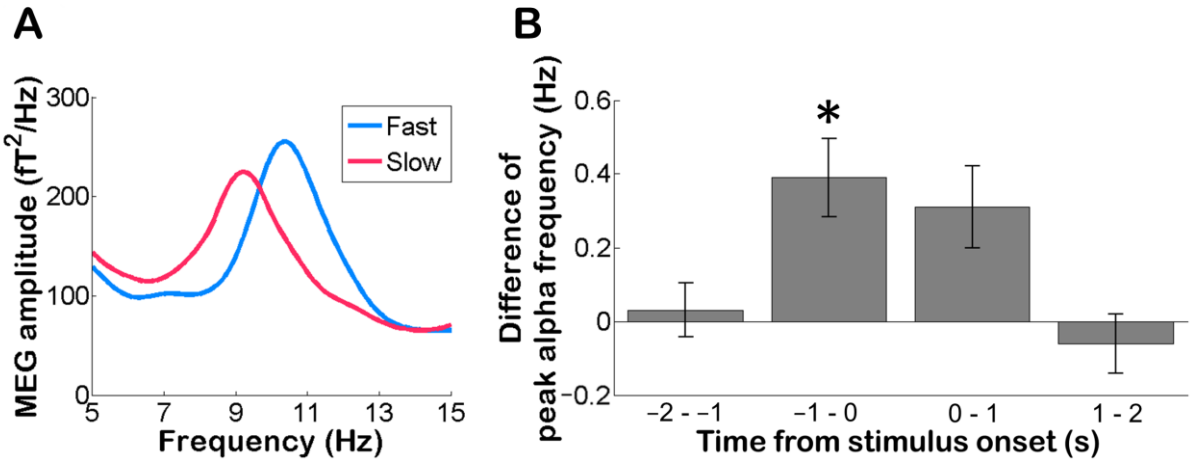

Figure 2.2.3: Dependence of perceived jitter frequency on the intra-participant variation of alpha frequency

Figure 2.2.3A shows a power spectrum showing a clear difference for the 1-s period just before stimulus onset. I found that PAF of slower trials was 1.2 Hz slower than that for faster trials [PAF for slower trials = 9.2 Hz, PAF for faster trials = 10.4 Hz]. Figure 2.2.3B shows the difference in PAF between the faster and slower trials. The difference was averaged across participants (n = 10, Figure 2.2.2 for the spectra of all participants). I found a significant difference in PAF for the 1-s period just before stimulus onset by applying the Bonferroni correction for multiple comparisons across four 1-s periods surrounding the stimulus onset [$t(9) = 3.68$, $p = 0.020$, Bonferroni-corrected two-tailed paired t-test]. I also found the marginally significant difference in PAF for the 1-s period during the stimulus presentation (0–1 s) [$t(9) = 2.79$, $p = 0.084$, Bonferroni-corrected two-tailed paired t-test].

To test how the power and phase of alpha oscillations affect perception of illusory jitter frequency, I calculated the power and phase at each time-frequency bin (from −1.5 s to 1.5 s from stimulus onset at 50 ms intervals, frequencies increasing logarithmically from 3 to 40 Hz while the number of cycles in each wavelet increases linearly from 3 to 12 cycles) by using the data in the experiment 2. Figure 2.2.4 shows the *p*-value distributions for the power difference and phase opposition sum between slow and fast PAF groups at around the stimulus onset computed by using permutation + *z*-score test. As a result, there was no time-frequency point with significant *p*-value about the power difference and phase opposition sum from *z*-score that satisfy a false discovery rate (FDR) of 5%. These results support the idea that illusory jitter specifically reflects the frequency of alpha oscillations.

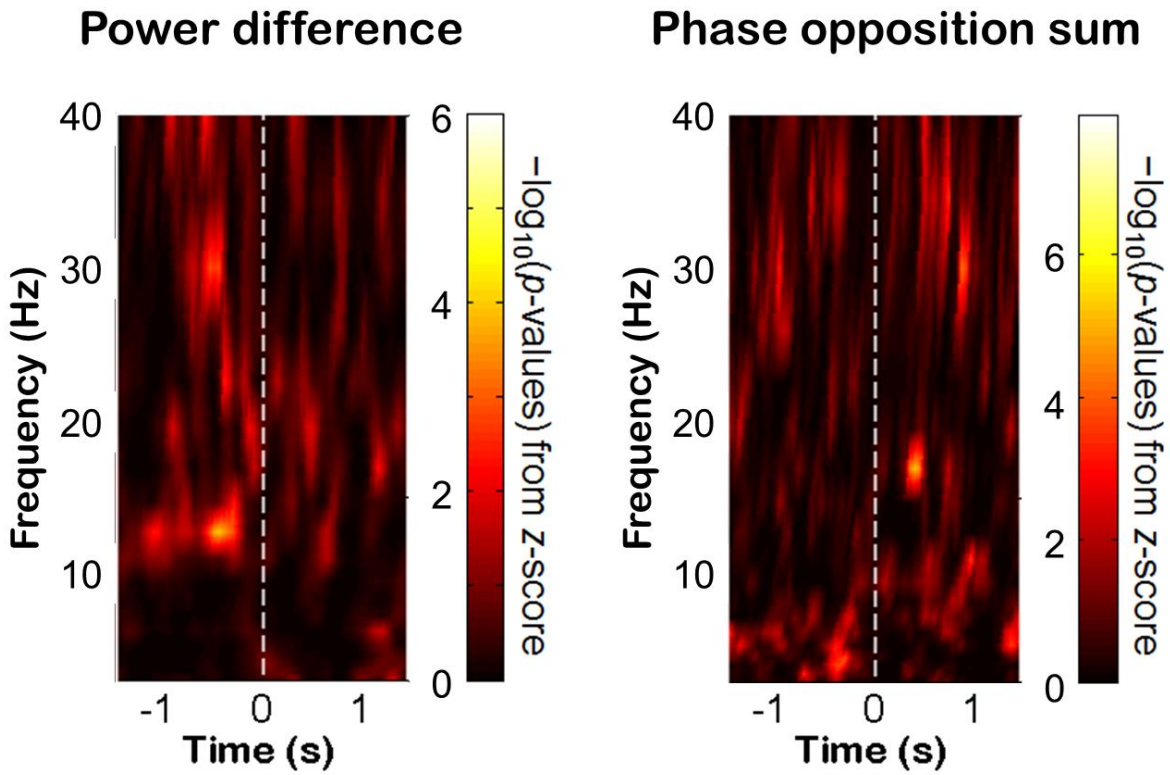

Figure 2.2.4: Time and frequency map of *p*-value for the power difference and phase opposition sum between slow and fast PAF groups at around the stimulus onset computed by using permutation + *z*-score test.

2.2.3 Discussion

The experiment 2 in my study indicated a change in PAF just before stimulus onset correlated with the perceived jitter frequency, which suggests that the illusory jitter frequency changed along the spontaneous fluctuation of PAF just before the stimulus presentation. While several studies [6, 14, 15, 84-88] have reported across-trial changes in visual perception correlated with the alpha phase at the stimulus onset, I think this is the first finding that has reported an association between the spontaneous fluctuation of alpha frequency and perception.

A significant point of this experiment is that the spontaneous fluctuation of the intrinsic alpha oscillations was utilized without modulating the alpha oscillations by external stimulation. In the case that alpha oscillation is modulated by an external stimulation, it is difficult to verify that the observed change is equal to the change in the intrinsic alpha oscillation due to the artifacts from external stimulation. Since the spontaneous fluctuation of the alpha oscillation is the intrinsic phenomenon, which enables us to more clearly elucidate the relationship between the alpha oscillations and the visual perception.

As the task in the current experiment was based on memorized mean of illusory jitter frequency, I cannot completely exclude the possibility that a fluctuation of the pre-stimulus PAF was associated with a non-perceptual process such as memory of the mean illusory jitter frequency. However, I think that the results of experiments 1 and 2 consistently suggest the tight coupling between PAF and illusory jitter frequency. I believe that the participantive response in this experiment (relatively fast or slow jitter) primarily reflects a perception instead of a non-perceptual process.

Experiments 1 and 2 in my study suggest that the illusory jitter frequency is correlated not only with inter-individual but with intra-participant variation in the alpha frequency. Nonetheless, it remains possible that a direct causal link between neural oscillation at the alpha frequency and jitter perception does not exist. To obtain more direct evidence for the involvement of neural oscillations in the illusory jitter perception, I performed experiment 3 to determine whether manipulation of PAF by current stimulation results in a change in the perceived jitter frequency.

2.3 Effect of the manipulation of PAF by AM-tACS on jitter frequency

2.3.1 Methods

Participants

Twelve participants (all males; age range: 22–53 yr) took part in the experiments 3. Three (all males; age range: 22–38 yr) and 8 (all males; age range: 20–53 yr) participants took part in the two control experiments to study the possible involvement of phosphine perception. Six participants (all males; age range: 22–38 yr) took part in the control experiment for eye movements. All participants gave their written informed consent to participate and had normal or corrected-to-normal vision. The ethics committee of the National Institute of Information and Communications Technology (NICT) approved all experimental procedures.

MEG measurement

I used the same measurement parameters of MEG data as in Section 2.2 (a sampling rate of 5000 Hz). In the analysis, I applied the temporal signal space separation (tSSS) [43] with bandpass filtering between 1 and 40 Hz. I then removed artifacts originating from blinks or heart beats by ICA before FFT analysis.

Apparatus and visual stimuli

Apparatus and parameters for visual stimulus presentation are the same as Chapter 2.1 and 2.2.

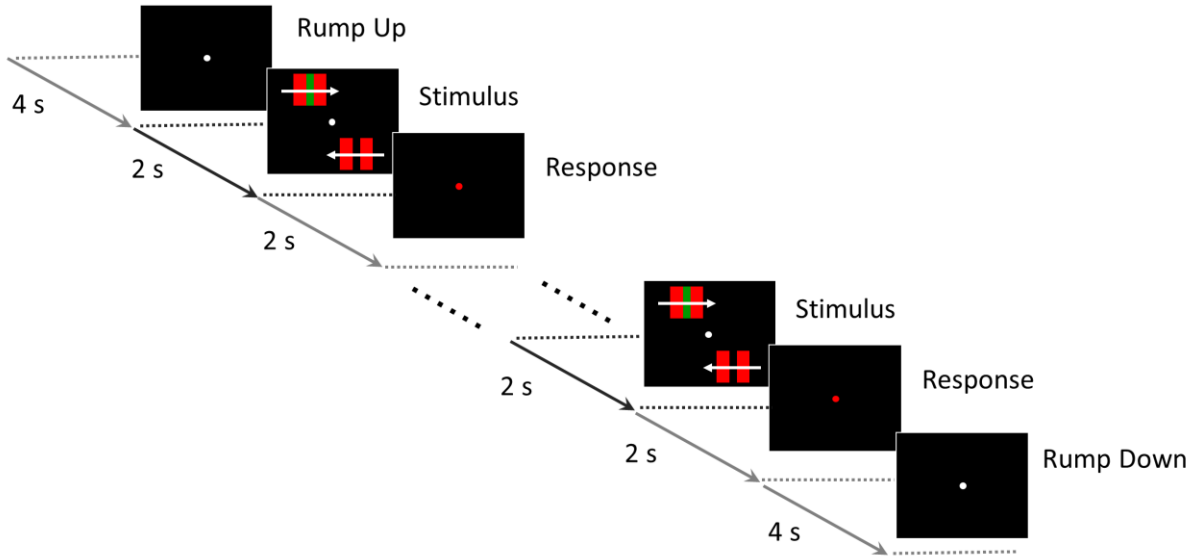

Figure 2.3.1：The time course of stimulus and task in experiment 3

Procedure for experiment 3

In experiment 3, I tried to modulate the individual PAF by current stimulation. During the current stimulation, I measured both PAF and the illusory jitter frequency. I used a commercial stimulator for controlling current stimulation (NeuroConn, DC-stimulator MR) in the magnetically shielded room. Two electrodes (5 × 7 cm^2) were placed at the parietal and occipital areas with saline solution. The positions roughly correspond to Pz and Oz in 10–20 Electroencephalography (EEG) system, respectively (Figure 2.3.2A). The DC-stimulator was connected to the battery-driven stimulator device located outside the magnetically shielded room. The outer stimulator delivered electrical currents via a twisted pair of wires with a peak-to-peak intensity of 2 mA. The current output of the DC-stimulator was proportional to the electric potential generated by a multifunction DAQ (USB-6211, National Instruments). The DAQ was controlled via a Data acquisition toolbox running on Matlab.

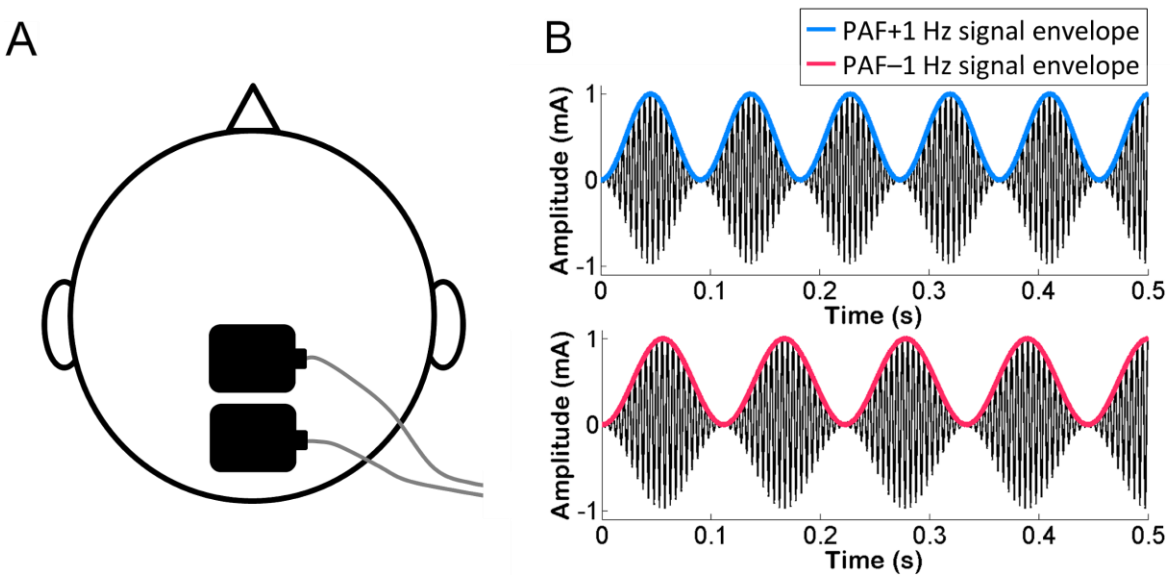

Figure 2.3.2: (A) The position of current stimulation for each participant. (B) The waveform of current stimulation from the DC-stimulator MR (Neuro Conn) controlled by the electric potential which is generated by a multifunction DAQ

In order to measure the MEG during current stimulation, I utilized amplitude

modulation (AM) of electric current [75]. The amplitude modulated (AM) waveforms can be described by a combination formula of trigonometric functions related to time and voltage, including in the carrier waveforms and modulated waveforms.

The voltage v_c of the carrier waveforms is 1-19, where the amplitude is V_c, and the angular frequency of signal waveforms is $\omega_c (= 2\pi f_c)$.

$$v_c = V_c \cos \omega_c t \qquad 1-19$$

Similarly, the voltage v_s of the signal waveforms can be expressed as 1-20, where the amplitude is $V_{s,}$ and the angular frequency of the signal waveforms is $\omega_s (= 2\pi f_s)$.

$$v_s = V_s \cos \omega_s t \qquad 1-20$$

At this time, the amplitude V_m of the modulated carrier waveforms is 1-21.

$$v_s = V_s \cos \omega_s t \qquad 1-20$$

The modulated waveform v_m is described as 1-22.

$$\begin{aligned} v_m &= V_m \cos \omega_c t \\ &= (V_c + V_s \cos \omega_s t) \cos \omega_c t \\ &= V_c (1 + mV_s \cos \omega_s t) \cos \omega_c t \\ &= V_c \cos \omega_c t + mV_s \cos \omega_s t \cos \omega_c t \\ &= V_c \cos \omega_c t + \frac{m}{2} \left[\cos(\omega_c + \omega_s)t + \cos(\omega_c - \omega_s)t \right] \end{aligned} \qquad 1-22$$

Here, $m = V_s / V_c$ is a modulation degree, which is defined as a ratio between the amplitude of the signal waveforms and the amplitude of the carrier waveforms. $\omega_c + \omega_s$ is called an upper waveforms, and $\omega_c - \omega_s$ is called a lower waveforms.

In the frequency spectrum of the AM waveforms, as can be seen from Figure 2.3.3, the peaks are only in three positions ω_c, $\omega_c + \omega_s$, $\omega_c - \omega_s$, ideally no noticeable peak appears at the modulation frequency ω_s. From the above points, AM-tACS has an advantage that MEG

measurement can be performed without generating current noises in the target frequency band while giving current stimulation of modulation frequency ω_s.

In this experiment, I will take this advantage and aim to manipulate the frequency of illusory jitter into the modulation frequency of AM-tACS and also try to observe the change in alpha oscillations during current stimulation.

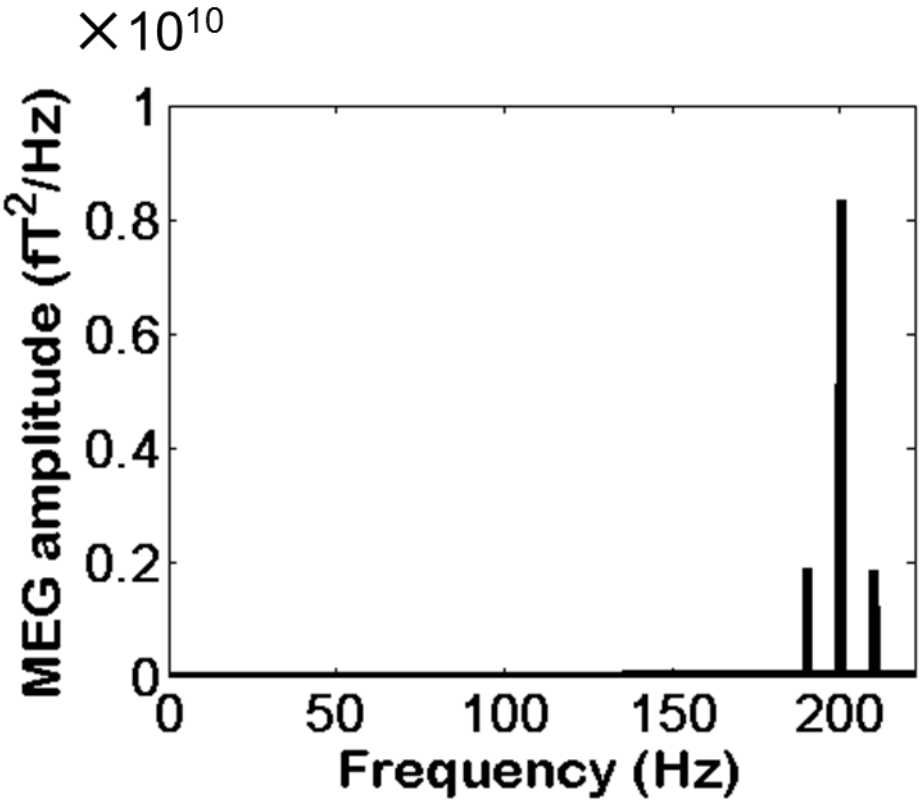

Figure 2.3.3: Frequency spectrum of AM-tACS with carrier frequency of 200 Hz and modulation frequency of 10 Hz

This waveform pattern reduces the artifact of current stimulation at the modulated frequency. In this experiment, the carrier frequency was set 200 Hz and its amplitude was modulated at PAF ± 1 Hz Figure 2.3.2B). I measured PAF in the eyes-open resting state for 1 min in a session before the main experiment for each participant. This frequency was used to set the frequency of current stimulation.

The current stimulation conditions were kept constant at either PAF + 1 Hz, no stimulation, or PAF − 1 Hz in each block of 64 s. The current amplitude was ramped up and ramped down at the first/last 4 s of the block, respectively. The average of current amplitude was kept constant for the middle 56-s when the psychophysical experiment was conducted.

During the no stimulation condition, no current stimulation was generated over the whole period of the block. The order of stimulation within each set of three blocks was either PAF + 1 Hz, no stimulation, and PAF − 1 Hz or PAF − 1 Hz, no stimulation, and PAF + 1 Hz. The set of three blocks was repeated 5 times in random order. There were 14 trials (4 s each) for the measurement of illusory jitter frequency in each block. Then participants were instructed to judge whether a physical jitter stimulus in the lower visual field was faster than an illusory jitter stimulus in the upper visual field. Seven physical jitter frequencies were repeated twice in random order within each block. In total, 20 trials were conducted of each physical jitter frequency in each of three current stimulation conditions. I continuously recorded MEG responses in this experiment.

Retinal stimulation control

To investigate a possible effect of the retinal stimulation [89-91] for illusory jitter perception, I asked participants whether they perceived phosphene after the experiment 3. Furthermore, to test whether participants can distinguish three current stimulation conditions, possibly with phosphene or a cutaneous sensation, I performed another experiment on 3 participants in experiment 3 (all males; age range: 22–38 yr). The participants conducted the same task as experiment 3 in a block of 64 s whose current stimulation conditions were selected either AM-tACS at PAF ± 1 Hz or no stimulation. Then participants were instructed to report which current stimulation was given by pushing one of three buttons. In total, there were 21 blocks in each of three current stimulation conditions.

Finally, to study the possible effect of subthreshold retinal stimulation by current stimulation on the perception of illusory jitter, I repeated experiment 3 with the central electrode (C3-C4) for 8 participants (all males; age range: 20–53 yr). This setting of electrode position was anticipated to have similar retinal effects (if any), without modulating the PAF.

Eye movement control

I also repeated experiment 3 for 6 participants (4 participants in the main experiment showing relatively large modulation in PAF and 2 new participants) during simultaneous measurement of eye movements using EyeLink 1000 Plus (SR Research). I measured only left-eye data. I then computed the standard deviation of eye position and velocity, blink rate,

and microsaccade rate. It is assumed that the standard deviation of the eye position and velocity correspond to fixation precision and drift amplitude [92], respectively. I used an unsupervised clustering method [93] for microsaccade detection.

Analyses

I analyzed MEG data by using FieldTrip toolbox running on Matlab, ANOVA by using IBM SPSS, and multinomial logistic regression by using SAS. Data throughout the manuscript are presented by mean ± SEM. Details of n for each experiment indicate the number of participants. A significant *p*-value was 0.05.

I analyzed the data of each block after excluding the ramp-up and ramp-down periods. I first applied a 40-Hz low-pass filter to the raw MEG data after applying the tSSS method [43]. Although an AM signal contains power only at around the carrier frequency in theory, the artifacts still exist because of the nonlinearity of the DAQ system generating the current stimulus. So I applied tSSS to remove AM-tACS artifacts at around the AM frequency. In the tSSS method, I reconstructed MEG data consisting of waveforms that were derived from neural activity inside the scalp. I removed the waveforms derived from the artifacts originating outside the scalp. After preprocessing, the data were divided into 10 × 56-s data for three conditions (AM-tACS at PAF ± 1 Hz, or no stimulation). I performed FFT analysis with a Hanning taper on the data of each block (5000 time-points) that were zero-padded to 10 s (50,000 time-points). FFT analysis were applied at 1-s time windows (5000 time-points) that were zero-padded to 10 s (50,000 time-points), shifted by 1 s. I averaged 560 spectra (56 spectra per each 56-s period). Finally, I selected 5 combined channels (10 planar gradiometers) which had the largest alpha amplitude and defined PAF as the frequency of maximum power in the alpha band (8–13 Hz).

To verify the removal of the electrical artifact from the MEG data, I computed a correlation of the topographic map of the alpha amplitude map (8–13 Hz) between the no stimulation and current stimulation conditions before and after the tSSS (n = 12, Figure 2.3.4).

As for the psychophysical data, I plotted the response rate as a function of physical jitter frequency and fitted a cumulative Gaussian function in each stimulation condition of each participant. I defined the individual illusory jitter frequency for each condition as the frequency corresponding to a 50% response rate.

Finally, I calculated the correlation between the change in the illusory jitter frequency

and the change in the PAF (either PAF + 1/PAF − 1 Hz vs no stimulation or PAF + 1 vs PAF − 1, n = 12).

Retinal stimulation control

As for the discrimination experiment, I tested whether participants can distinguish among current stimulation conditions. Therefore, I used a multinomial logistic regression analysis (n = 3) to test whether the response category (PAF + 1 Hz, PAF − 1 Hz, and no stimulation) can be predicted by the frequency of current stimulation (PAF + 1 Hz, PAF − 1 Hz, and no stimulation).

As for the experiment with the central electrodes, I used two-way repeated measures ANOVA (n = 12 and n = 8 for parieto-occipital and central electrodes, respectively) to test whether the frequency of current stimulation (PAF + 1 Hz, PAF − 1 Hz, and no stimulation) and electrode position (parieto-occipital and central) affect the PAF and illusory jitter frequency.

Eye movement control

I used one-way repeated measures ANOVA (n = 6) to test whether the frequency of current stimulation (PAF + 1 Hz, PAF − 1 Hz, no stimulation) affects the PAF, illusory jitter frequency, standard deviation of eye position and velocity, blink rate, and microsaccade rate.

2.3.2 Results

I recorded MEG responses to observe the change in PAF by AM-tACS at the parieto-occipital area. Simultaneously, I measured illusory jitter frequency during current stimulation. Similar to the psychophysical measurement during experiment 1, participants were instructed to judge whether a physical jitter in the lower visual field was faster than an illusory jitter in the upper visual field. There were three conditions of AM-tACS consisting of AM frequency of PAF + 1 or PAF − 1 Hz, and no stimulation.

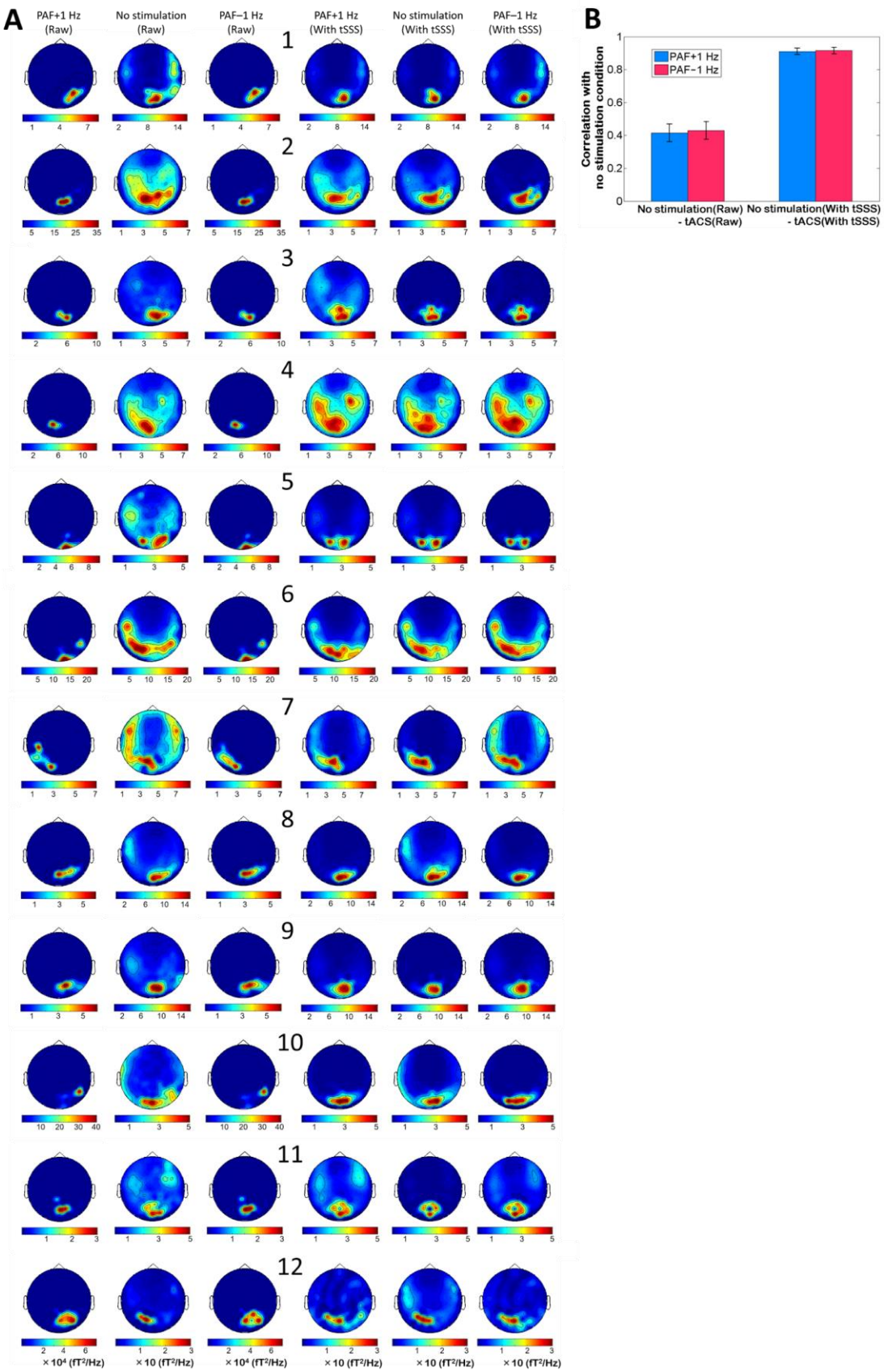

Figure 2.3.4: Topographic maps of the alpha power for each current stimulation condition of experiment 3 for all participants

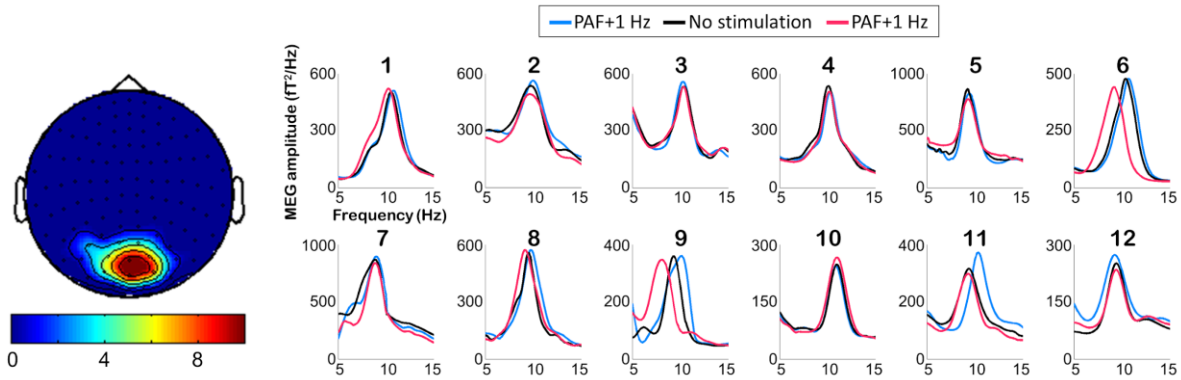

Figure 2.3.5: Distribution maps of selected channels and the power spectra of MEG data for all participants

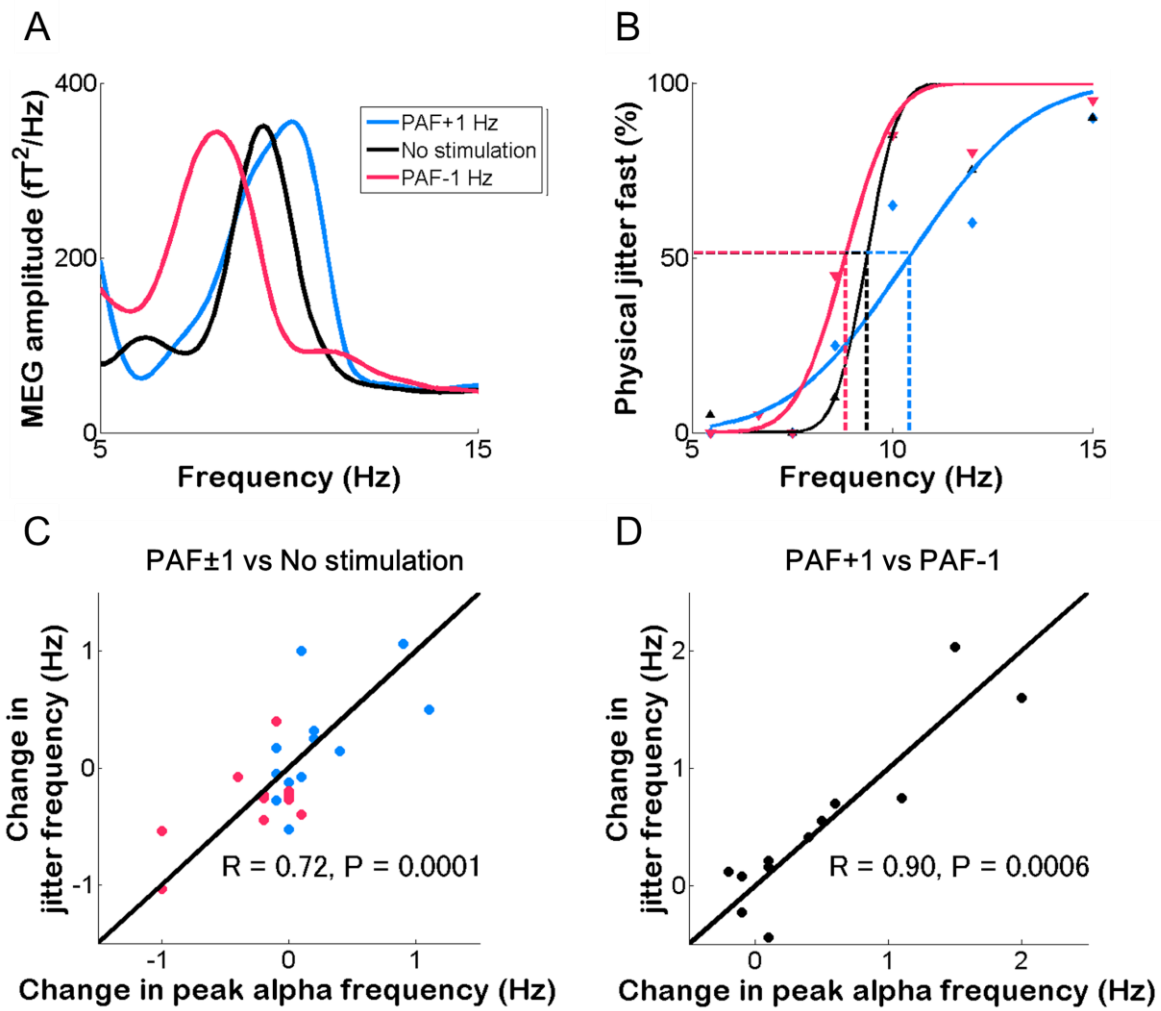

Figure 2.3.6: Manipulation of alpha frequency and illusory jitter by AM-tACS

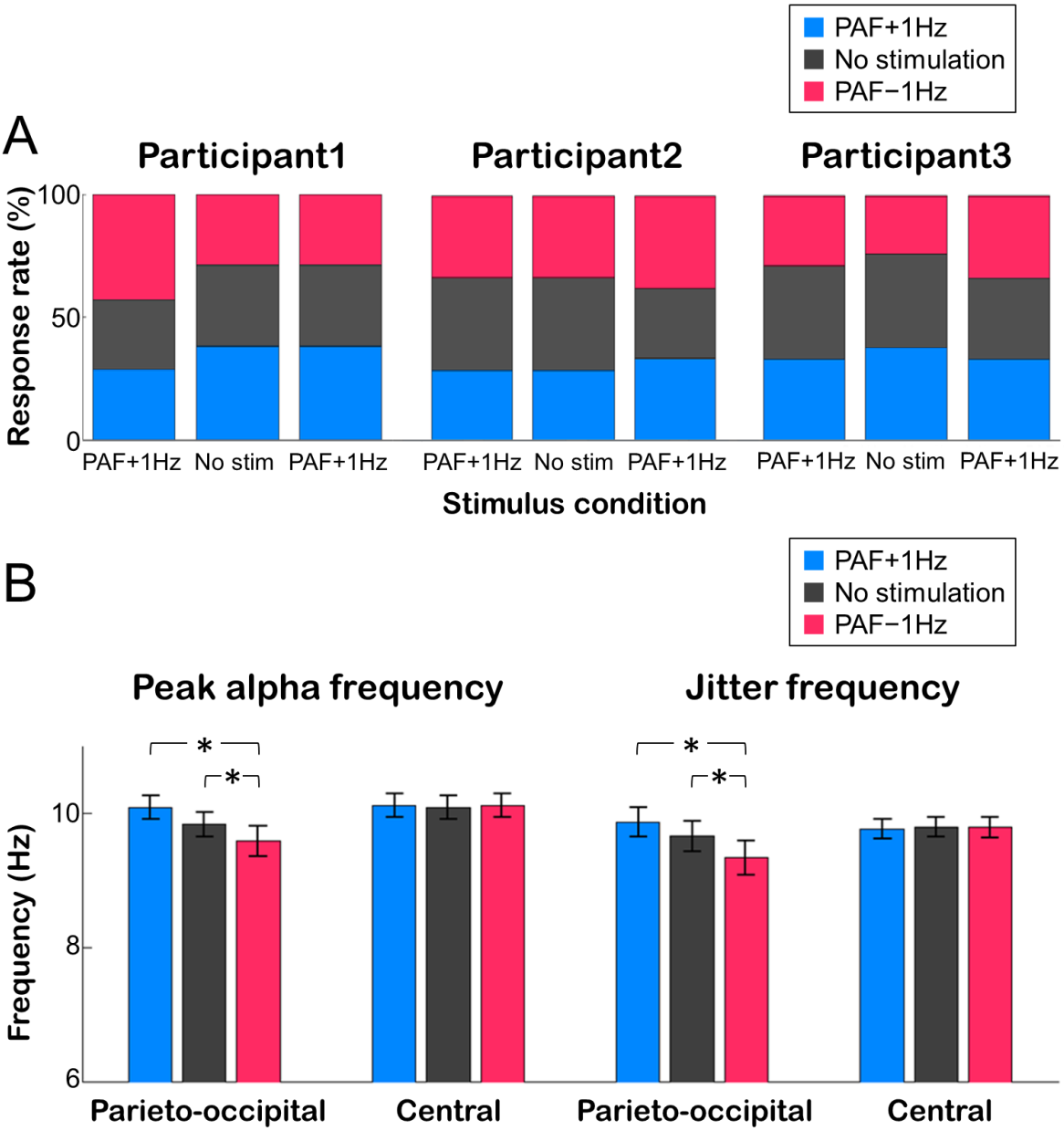

Figure 2.3.7: Control experiments to study the possible involvement of retinal stimulation by AM-tACS

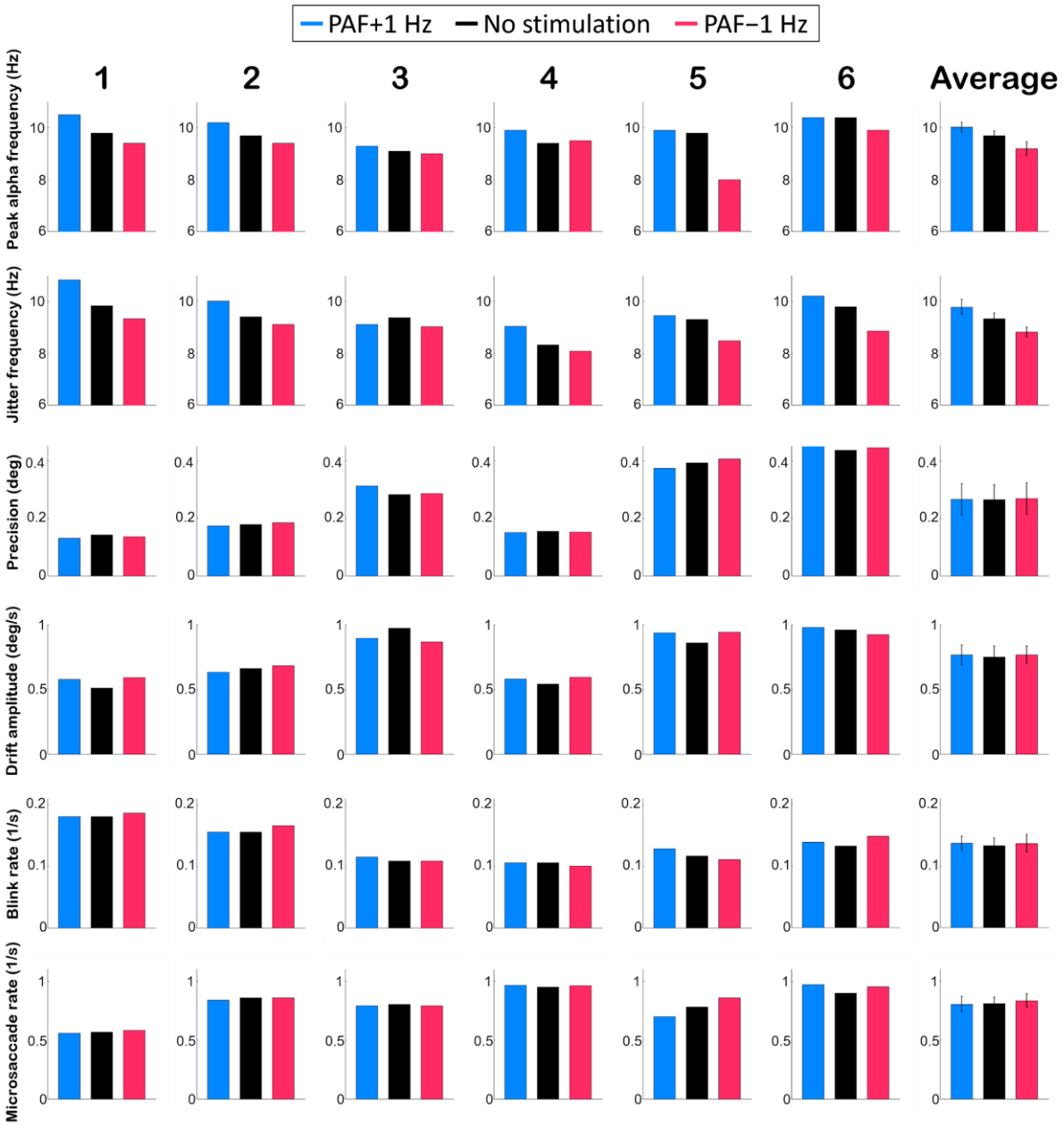

Figure 2.3.8: Difference in eye movements across different current stimulation conditions

After I confirmed that the MEG signals during current stimulation are free from its artifact (Figure 2.3.4), I analyzed the modulation in PAF by current stimulation. Figure 2.3.6A shows an example of the power spectrums for three current stimulation conditions after applying tSSS (Figure 2.3.5 for the averaged positions of the channels and the spectra of all participants). I found that the PAF during AM-tACS at PAF + 1 and PAF − 1 Hz was higher (10.1 Hz) and lower (8.1 Hz) than PAF in the no stimulation condition (9.3 Hz), respectively. Further, the illusory jitter frequency for the same participant during PAF + 1 or PAF − 1 Hz was faster (10.6 Hz) or slower (9.1 Hz) than the no stimulation condition (9.9 Hz), respectively (Figure 2.3.6B). Figure 2.3.6C shows a relationship between the change in PAF

and illusory jitter frequency, which was relative to the no stimulation condition for both PAF + 1 and PAF − 1 Hz conditions, for all participants (n = 12). Figure 2.3.6D shows a relationship between differences in PAF and illusory jitter frequency between PAF + 1 and PAF − 1 Hz stimulation conditions for all participants (n = 12). Each of these plots showed a strong correlation [$r = 0.72$, $p = 0.0001$; $r = 0.90$, $p = 0.0006$, respectively].

It is widely known that tACS at around the PAF induces phosphene due to direct stimulation of the retina [89-91]. People may wonder whether phosphene, or cutaneous perception originating from AM-tACS may have an effect on the measurement of illusory jitter frequency during current stimulation. However, I do not think this suggestion is plausible because no participant reported that they perceived phosphene in the experiment 3, and an additional experiment indicated that participants could not discriminate current stimulation conditions (Figure 2.3.7A).

To further verify the possible effect of subthreshold retinal current stimulation on illusory jitter frequency, I repeated experiment 3 (n = 8) with the central electrode (C3-C4), and anticipated that the experiment has similar or even larger retinal effects (if any), without changing the PAF. As a result, I found that the modulation in PAF and illusory jitter frequency was not significant for the central stimulation [$F(2, 14) = 0.64$, $p = 0.54$, $F(2, 14) = 0.23$, $p = 0.80$, respectively, two-way repeated measures ANOVA, the simple main effect of current frequency] (Figure 2.3.7B), while the change was significant for parieto-occipital stimulation [$F(2, 22) = 6.15$, $p = 0.008$, $F(2, 22) = 6.37$, $p = 0.007$, respectively, two-way repeated measures ANOVA, the simple main effect of current frequency]. These results suggest that the change in illusory jitter frequency correlated with the modulation in PAF by parieto-occipital stimulation didn't derive from a retinal artifact.

There is still another possibility that illusory jitter perception induces a small eye movement at the same frequency. In the case, the eye movement may be reflected as an increase in neural activity at the same frequency. Motion perception in the Enigma illusion is known to be driven by microsaccades [94]. I do not believe that the possibility is probable because the PAF in the resting state (experiment 1) and that before the stimulus onset (experiment 2), which cannot be affected by illusory jitter, showed a clear relationship with the perceived frequency of illusory jitter. However, I cannot fully eliminate the possibility that the differences in eye movements affected both the PAF and illusory jitter frequency, resulting in the correlation between them. To test this possibility, I repeated the experiment 3 (n = 6) while measuring eye

movements. While I replicated the change in the PAF and illusory jitter frequency by current stimulation [$F(2, 10) = 7.15$, $p = 0.012$; $F(2, 10) = 15.93$, $p = 0.001$, respectively, one-way repeated measures ANOVA], There was no variability among fixation precision, drift amplitude, blink rates, or microsaccade rates across current stimulation conditions [$F(2, 10) = 0.19$, $p = 0.83$; $F(2, 10) = 0.29$, $p = 0.76$; $F(2, 10) = 0.82$, $p = 0.47$; $F(2, 10) = 1.14$, $p = 0.36$, respectively, one-way repeated measures ANOVA]. This result excludes the possibility that the correlation between the PAF and illusory jitter frequency is mediated by the difference in eye movements or blinks Figure 2.3.8.

2.3.3 Discussion

The experiment 3 in my study indicated that the PAF during AM-tACS was modulated toward the target frequency, and simultaneously, the perceived jitter frequency was also changed. This finding suggested that the manipulation of PAF by AM-tACS resulted in the corresponding change in illusory jitter frequency. In this results, PAF was manipulated for only approximately half of the 12 participants so PAF was unchanged for the other half (Figure 2.3.5). Although the different effects of AM-tACS across participants may be related in part to the impedance of electrodes or skull thickness, I cannot identify the exact cause. Thus, in the future work, it will be necessary to elucidate the appropriate experimental condition to modulate the alpha frequency.

Consistent with my hypothesis that alpha oscillation is associated with the perception of illusory jitter, changes in illusory jitter frequency were only found for the participants whose PAF was modulated. These findings support the possibility that change of PAF induced by AM-tACS resulted in change in illusory jitter frequency. My pilot experiment suggested that modulation in PAF by current stimulation was not sustained after current stimulation offset. I think it is consistent with the fact that intrinsic alpha entrainment by tACS or transcranial magnetic stimulation (TMS) continues stable only for maximally a few oscillatory cycles after stimulation offset [95]. Therefore, I think that measurement of neural oscillation during the stimulation was crucial. Here, I succeeded in the simultaneous measurement by combining a AM-tACS and a noise reduction technique (tSSS). To the best of my knowledge, this result is the first time that manipulation of PAF has been demonstrated. My study also ascertains the validity of AM-tACS for inducing neural oscillations by its envelope, a technique that has rarely been tested [75].

2.4 Alpha activity during illusory jitter perception

2.4.1 Methods

Participants

Ten participants (2 females; age range: 22–53 yr) took part in the experiment for source localization. All participants gave their written informed consent to participate and had normal or corrected-to-normal vision. The ethics committee of the National Institute of Information and Communications Technology (NICT) approved all experimental procedures.

MEG measurement

I used the same measurement parameters of MEG data as in Section 2.1 (a sampling rate of 1000 Hz). In the analysis, I applied the temporal signal space separation (tSSS) with bandpass filtering between 1 and 40 Hz. I then removed artifacts originating from blinks or heart beats by ICA before FFT analysis.

Apparatus and visual stimuli

Apparatus and parameters for visual stimulus presentation are the same as Chapter 2.1

Source localization experiment

To research which brain areas are associated with illusory jitter perception, I performed a source localization experiment. The stimulus was the same as in experiment 2 (Figure 2.2.1) except that a luminance of the green bar was either isoluminant with (main condition in which participants perceive illusory jitter, 200 trials) or darker/brighter than (control conditions in which participants rarely perceive illusory jitter, 100 trials each) that of a surrounding red square.

Analysis

I performed a source localization using Dynamic Imaging of Coherent Sources (DICS) [47]. I applied the DICS on the Fourier spectra of a 2-s pre-stimulus period and a 2-s stimulus period at around the alpha band (8–13 Hz), and calculated the power at the stimulus period relative to the power during the pre-stimulus period.

I used one-way repeated measures ANOVA (n = 10) to test whether the stimulus condition (dark, isoluminant, and bright) affects the relative alpha amplitude in the left inferior parietal lobe (IPL), the coherence between the left IPL and left IT, and the coherence between the left IPL and left superior occipital area (SO). I anatomically defined all regions of interest

(ROI) based on the Automated Anatomical Labeling (AAL) atlas [96].

2.4.2 Results

First, I confirmed whether the illusory jitter was perceived only in the isoluminant condition as in the previous study [25]. As a result, as shown in Figure 2.4.1, the rate of illusory jitter perception was approximately 80% in the isoluminant condition, whereas that of illusory jitter perception was less than 10% in the dark and the bright conditions.

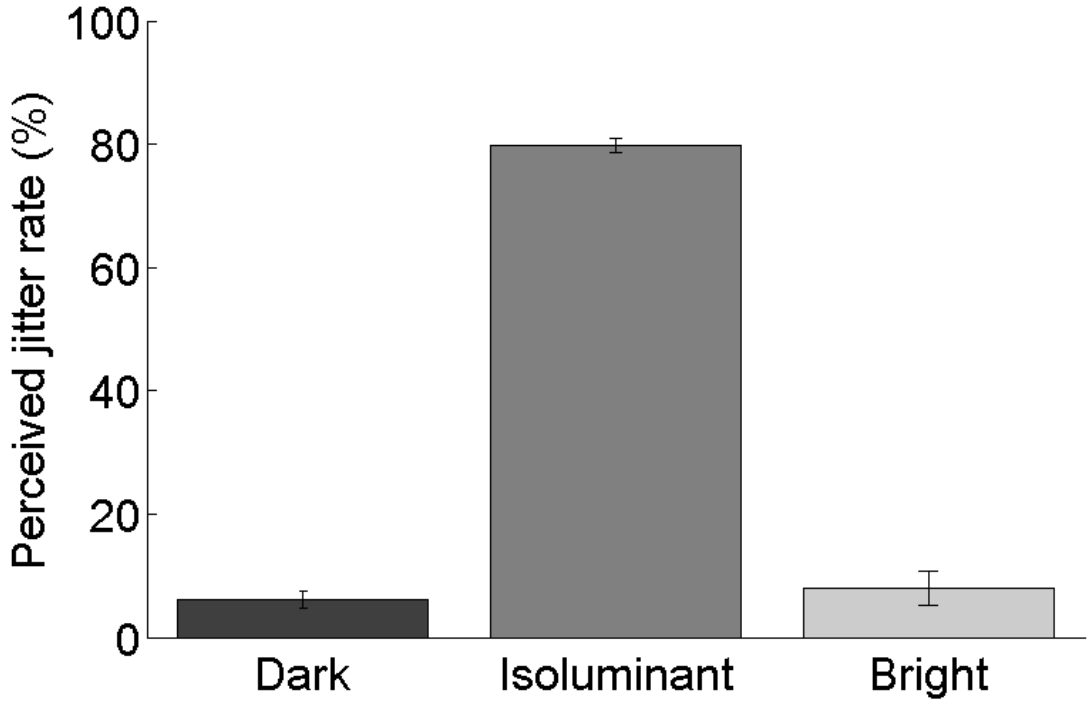

Figure 2.4.1: Perception rate of illusory jitter in the dark, isoluminant, and bright conditions

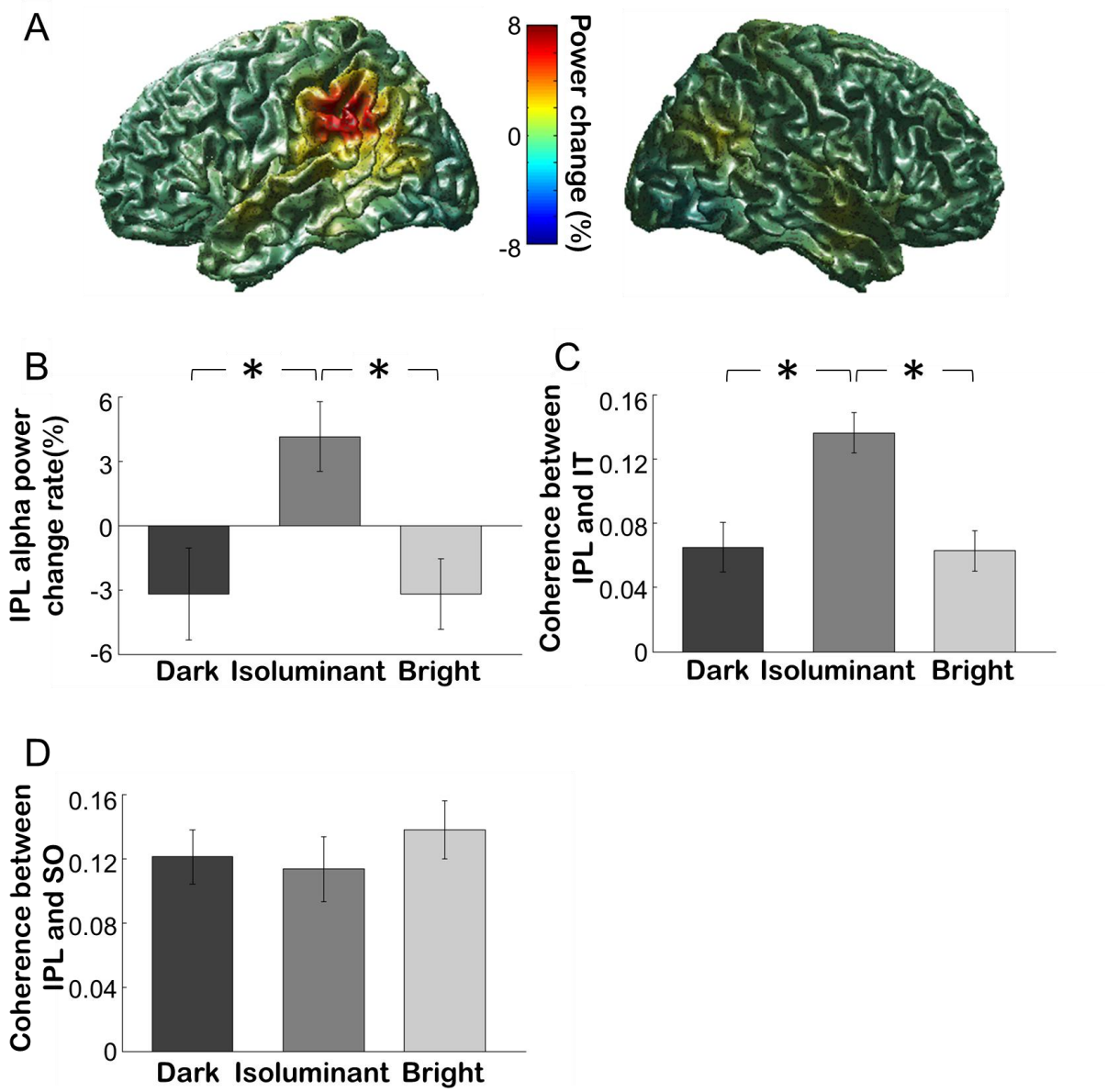

Figure 2.4.2: Source localization analysis of alpha oscillation during illusory jitter perception

I took the difference of the relative power between the isoluminant and dark conditions averaged across all participants (n = 10, Figure 2.4.2A). To equate the number of trials across conditions, I randomly selected 100 trials from the isoluminant condition. I observed enhanced alpha power around the left inferior parietal lobe (IPL) (Figure 2.4.2B). I confirmed a very similar spatial pattern of the contrast between the isoluminant and bright conditions. I found that relative alpha amplitude averaged within the anatomically-defined left IPL was significantly larger in the isoluminant condition than in the dark and bright conditions ($F(2, 18) = 4.65$, $p = 0.024$, one-way repeated-measures ANOVA, isoluminant vs bright; $t(9) = 3.45$, $p = 0.022$, isoluminant vs dark; $t(9) = 3.21$, $p = 0.032$, Bonferroni-corrected two-tailed paired t test).

I then calculated the difference in alpha coherence between conditions to further investigate the underlying mechanisms. I found that alpha coherence between the left IPL and the left inferior temporal area (IT) was significantly larger in the isoluminant condition than in the control two conditions (Figure 2.4.2C, $F(2, 18) = 6.74$, $p = 0.007$, one-way repeated-measures ANOVA, isoluminant vs bright: $t(9) = 3.19$, $p = 0.033$, isoluminant vs dark: $t(9) = 3.13$, $p = 0.036$, Bonferroni-corrected two-tailed paired t test). On the other hand, alpha coherence between the left IPL and the left superior occipital area (SO) did not show significant difference across conditions (Figure 2.4.2D, $F(2, 18) = 0.46$, $p = 0.64$, one-way repeated-measures ANOVA). I think that the increase of coherence between the left IPL and IT does not merely reflect that of alpha amplitude in the left IPL.

2.4.3 Discussion

In experiment 4, I found significantly higher alpha coherence between the IPL and IT in the isoluminant condition than in the control conditions. The IPL and IT can be generally regarded as the higher areas in the dorsal and ventral streams, respectively. Based on this finding, I propose a functional hypothesis of alpha oscillations in visual processing. In the motion-induced spatial conflict, moving borders defined by color contrast are perceived to be jittering when they are placed in close proximity with those defined by luminance contrast. I assume that there are two positional representations of visual stimuli; one in the dorsal and the other in the ventral visual pathway. The dorsal stream has high temporal and low spatial resolution, whereas the ventral stream has low temporal and high spatial resolution, and these two systems behave complementary to each other. In the dorsal pathway where positional information is calculated based on speed of motion, the position of a green bar is delayed relative to the surrounding red square because of the slower perceived speed of the green bar than the red square. In the ventral pathway where positional information is calculated based on object detection, the position of the green bar relative to the red square is correctly represented at each time point. Here, dissociation between motion-based delayed representation of color contrasts and shape-based correct representation is cyclically resolved, causing the color-defined edge to make a small, apparent jump, catching up to the luminance edge. I speculate that the conflict in positional representation between the dorsal and ventral visual areas is resolved at a specific phase of intrinsic alpha oscillation, which is why illusory jitter is perceived at the frequency of the intrinsic alpha oscillations. In other words, alpha oscillation may involve the interaction between motion and shape processing, which are generally

believed to be rather independent. My hypothesis that the illusory jitter is perceived at the frequency of intrinsic alpha oscillations suggest that alpha oscillations control the timing of interactions between motion-based and shape-based positional representations, which goes beyond previous studies suggesting that alpha oscillations are related to the timing of local processing [5].

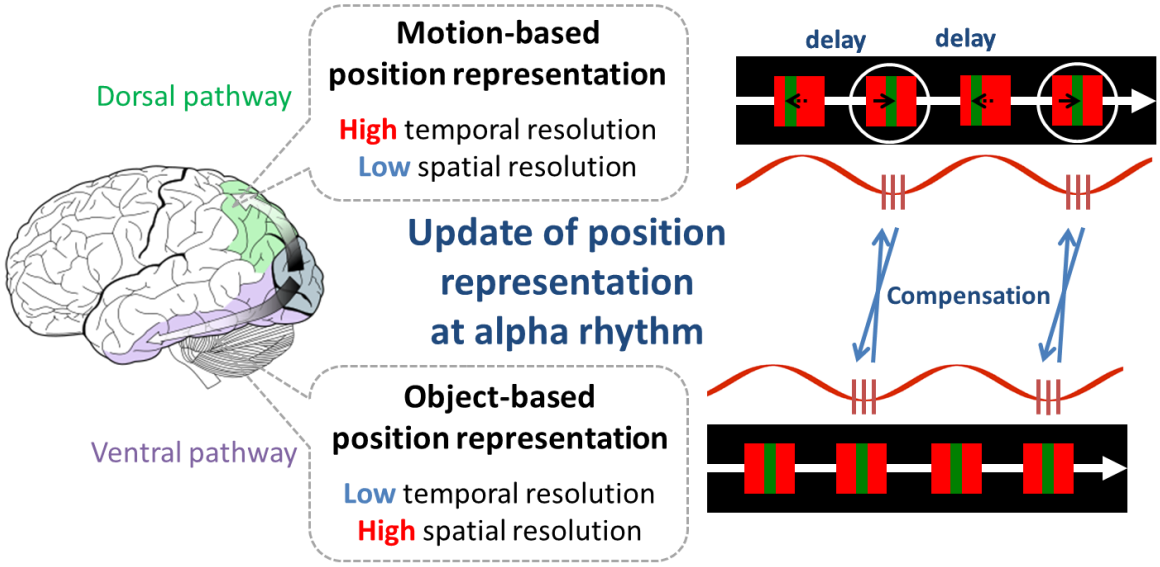

Figure 2.4.3: The functional role of alpha oscillation

The experiment 4 in my study also indicated that the alpha amplitude in the left IPL was significantly increased in the isoluminant condition, compared with the control conditions. One possible interpretation for this increase in alpha power is that alpha activities in the IPL are related to the generation of illusory jitter. In the motion-induced spatial conflict, as I mentioned in the previous paragraph, the position of a green bar in the IPL is delayed, which is compensated by the correct positional information in the IT. In Figure 2.4.4, if the compensation of the delayed positional representation is reflected in the burst of the spikes or gamma oscillations in the IPL at a specific phase of alpha oscillations, the activities of the IPL neurons on top of the intrinsic alpha oscillations might result in the increased alpha power, as shown in Figure 2.4.2B. Since the burst firing reflecting neuronal representations can be regarded as the gamma band activities [48, 56], the increase in alpha power might reflect the consequence of cross-frequency phase-amplitude coupling between alpha and gamma oscillations. According to these speculations, the alpha coherence between the IPL and IT, as well as the increased alpha power in the IPL, might be causally related to illusory jitter perception. In order to examine these possibilities in more detail, it is necessary to perform

additional experiments.

One possible approach for testing the causal contribution of the alpha coherence for illusory jitter perception is to investigate whether the suppression of alpha coherence between the left IPL and IT, possibly by applying focal tACS [43, 97] at the left IPL and IT with the opposite or randomly different phases, deteriorates the perception of illusory jitter. If the increases in alpha power and coherence during the illusory jitter perception reflect neural responses necessary for the perception, suppression of alpha coherence will affect the perception. The approach for testing the causal contribution of the burst spikes in the IPL and thus the increased alpha power for illusory jitter perception is to first identify neurons in the monkey parietal area showing the burst responses at a specific phase of alpha oscillations, and then investigate whether deactivation of these neurons, possibly by using muscimol, decreases the alpha power in the IPL and deteriorates illusory jitter perception (though I need to invent a method to measure illusory jitter perception of monkey).

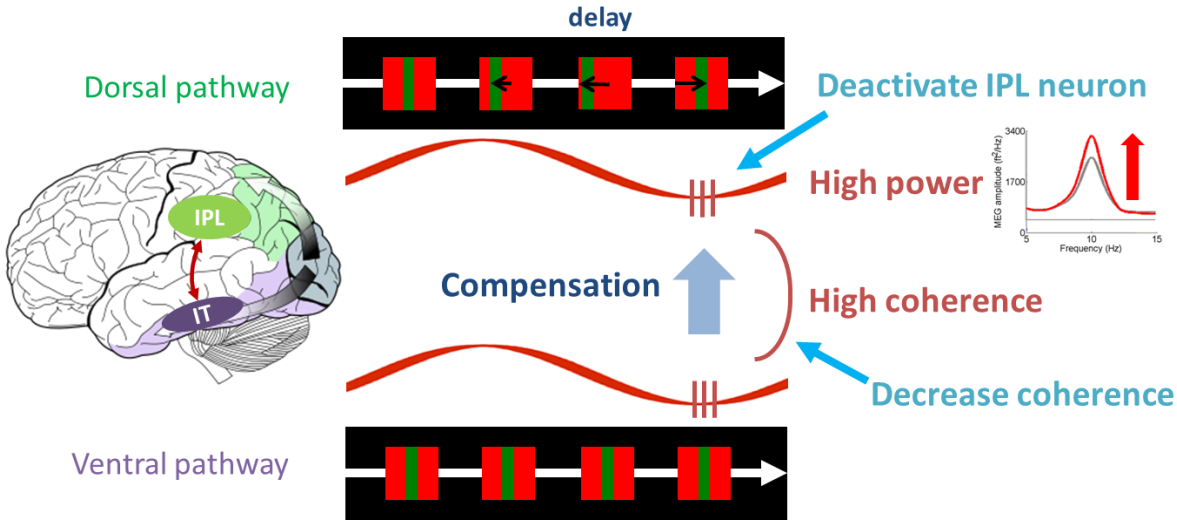

Figure 2.4.4：Two candidates for contributing to illusory jitter perception

3 Microstructural properties of visual white matter tracts correlated with the inter-individual differences in alpha oscillations

3.1 Methods

Participants

A total of 24 participants were recruited in the study (3 females; 22–53 years). All participants gave their written informed consent to participate and had normal or corrected-to-normal vision. The ethics committee of the National Institute of Information and Communications Technology (NICT) approved all experimental procedures.

The present study consisted of MEG and MRI experiments measuring occipital alpha oscillations and the tissue property of the visual white matter tracts, respectively. In each measurement, the inter-individual variations in (1) the peak power/frequency of alpha/beta oscillations during resting state; (2) the tissue properties of visual white tracts, were studied. MEG and MRI measurements were conducted on different days.

Quantification and Statistical Analysis

Analyses of MEG data were performed using FieldTrip toolbox running on MATLAB. Data throughout the manuscript are presented by mean ± SEM. Details of n for each experiment is the number of participants. A *p*-value of 0.05 was used to define significance.

MEG measurement

In a magnetically shielded room, I measured MEG data by using a 360-channel whole head MEG system (Neuromag® 360, Elekta) consisting of 204 planar gradiometers, 102 magnetometers, and 54 axial gradiometers. Magnetic signals were recorded at a sampling frequency of 1,000 Hz. Two hundred four planar gradiometers which have high signal-to-noise ratios were used for the analysis. The planar gradiometers consisted of two coils that measure spatial derivatives of magnetic fields along the surface. Pairs of planar gradiometers, which is located at 102 positions, measure the derivatives in orthogonal directions (x and y). I first performed a fast Fourier transform (FFT) analysis for each planar gradiometer. I then summed the power of the two gradient components at the same location, termed combined channels, before plotting a topographic map or selecting channels showing the maximum amplitude. I removed artifacts originating from blinks or heart beats using independent component analysis (ICA). I then applied bandpass filtering between 1 and 40 Hz before FFT analysis.

MEG data were measured during the resting state. Participants opened and closed their

eyes for 30 s in response to a sound cue in a dark room; this was repeated 6 times. Therefore, I obtained MEG data for 3 min in the eyes-open and closed resting conditions.

I first applied an FFT analysis on the data within 10-s time windows (10,000 time-points) shifted by 1 s and averaged 126 spectra (21 spectra per each 30-s period). I then selected 5 combined channels (10 planar gradiometers, refer above) with the largest alpha power for each participant. From these, I defined the peak alpha frequency (PAF) and the peak alpha power for each participant from the frequency showing the maximum power in the alpha band (8–13 Hz). As a control, I also estimated the peak beta frequency. Linear regression was applied to fit a linear model to the log-transformed spectrum in the beta range (13–30 Hz) [8], and the fitted linear trend (1/f component) was subtracted from the spectrum because this component obscures the smaller peaks in the beta range. I then defined the peak beta frequency and power from the frequency showing the maximum power in the beta band (15–25 Hz) for each participant. For the estimation of the peak beta power, the original spectrum before subtracting the linear trend was used.

Structural MRI data acquisition

All MRI data were acquired at CiNet, National Institute of Information and Communications Technology, and Osaka University.

Anatomical MRI data acquisition and tissue segmentation

T1-weighted MP-RAGE image (1 mm isotropic; TR, 1900 ms; TE, 2.48 ms) were measured from all participants (N = 24). An automated procedure in Freesurfer software (https://surfer.nmr.mgh.harvard.edu/) was used to determine white/gray matter border which was used for subsequent diffusion MRI (dMRI) analyses. The total scan time of acquisition of the anatomical MRI data was approximately 15 minutes for each participant.

Diffusion MRI data acquisition

dMRI data were measured from all participants (N = 24) using a 3T SIEMENS Prisma scanner with a 32-channel head coil. For data acquisition, dual-spin echo planar imaging (EPI; TR, 3300 ms; TE, 66.4 ms; multi-band factor, 3; partial Fourier, 5/8; voxel size, $2 \times 2 \times 2$ mm^3) were implemented in multi-band accelerated EPI pulse sequence provided by the Center for Magnetic Resonance Research, Department of Radiology, University of Minnesota (https://www.cmrr.umn.edu/multiband/).

Diffusion weighting with b = 300, 1000, 2000 s/mm^2 were carried out along 6, 30, 64

isotropically distributed directions respectively. Each data was acquired with a pair of reversed phase-encoding directions (A-P and P-A). In the dMRI session, non-diffusion-weighted with b = 0 images were acquired with eight pairs of A-P and P-A directions to minimize EPI distortion. The total scan time of dMRI was approximately 25 minutes for each participant.

Quantitative MRI data acquisition

Quantitative MRI (qMRI) data were measured from all participants (N = 24) using a 3T SIEMENS Trio Tim scanner with a 32-channel head coil. These measurements were followed for protocols described in a previous publication [98]. Four Fast Low Angle Shot (FLASH) images were measured with flip angles of 4°, 10°, 20°, and 30° (TR, 12 ms; TE, 2.41 ms), and a scan resolution of 1 mm isotropic. Five additional spin echo inversion recovery (SEIR) scans were also measured with an EPI readout (TR, 3 s; TE, 49 ms; 2× acceleration) to remove field inhomogeneities. The inversion times were 50, 200, 400, 1200, and 2400 ms. In-plane resolution and slice thickness of the additional scan was 2×2 mm^2 and 4 mm, respectively. The total scan time of qMRI was approximately 35 minutes for each participant.

Diffusion MRI data analysis

Preprocessing

DMRI images were corrected for susceptibility-induced distortions using FSL TOPUP tools [99]. Eddy current distortions and participant motion in the dMRI images were corrected using FSL EDDY tools [100]. Finally, dMRI images were aligned into T1-weighted MPRAGE image.

Estimation of ODI

After preprocessing, Neurite Orientation Dispersion and Density Imaging (NODDI) model was fitted to dMRI data by using NODDI MATLAB toolbox to obtain orientation dispersion index (ODI) maps in individual voxels [51].

Tractography on the optic radiation

The optic radiation (OR) was identified by using a dedicated method (ConTrack) [101], because there are known challenges to estimate human OR by using a standard tractography for a whole brain, in order to track the crossing fibers around Meyer's loop [102]. First, the approximate location of the lateral geniculate nucleus (LGN) was estimated on manual

inspection of T1-weighted image and deterministic tractography from the optic chiasm. Then a 8-mm radius sphere was placed, which covered the LGN endpoints of streamlines from the optic chiasm. Second, the location of the primary visual cortex (V1) was identified by using a probabilistic atlas of retinotopic visual areas [103]. Using ConTrack, Then 100,000 candidate streamlines connecting LGN and V1 (angle threshold, 90 deg; step size, 1 mm) were sampled. Tracking was restricted using the white matter mask generated by tissue segmentation. Top 50,000 streamlines with a higher score in ConTrack scoring process [104] were selected. Further details on the methods to identify the OR using ConTrack are described in previous papers [104, 105].

Tractography on the VOF and pArc

For identifying VOF and pArc, it is essential to use tractography algorithm with better sensitivity for resolving crossing fibers [106]. For this reason, a constrained spherical deconvolution (CSD; L_{max} = 8) [107] was used to estimate fiber orientation distribution in each voxel using MRTrix3 [108]. Then, a probabilistic tractography was implemented in MRTrix to generate 2 million streamlines for each dMRI dataset (step size = 0.2 mm; maximum angle between successive steps = 9 deg; minimum length = 10 mm; maximum length = 250 mm; FOD amplitude stopping criterion = 0.05). The seed voxels for tracking was randomly chosen from the gray-white matter interface region [109]. Finally, the VOF and pArc were identified from whole-brain streamlines using automated pipelines implemented as a part of AFQ toolbox (https://github.com/yeatmanlab/AFQ/tree/master/vof).

Across-session averaging and outlier exclusion

Each streamline of the identified white matter tracts (VOF, pArc, and OR) was merged from two dMRI sessions with reversed phase encoding directions. Then outlier streamlines were excluded based on criteria used in previous studies [106] for subsequent evaluation of tissue property.

Quantitative MRI data analysis

By using the mrQ software package (https://github.com/mezera/mrQ) in MATLAB, both the FLASH and SEIR scans were processed to produce the macromolecular tissue volume (MTV) maps [110]. After RF coil bias was corrected by the mrQ analysis pipeline with SEIR-EPI scans and accurate proton density (PD). T1 fits were then produced across the brain. The maps of MTV were produced by computing the fraction of one voxel that is non-water (cerebrospinal fluid (CSF) voxels were classed as approximately 100% water). Here CSF was

defined by voxels from within the ventricles. Finally, MTV maps are aligned to MPRAGE image in order to register them with dMRI data. The full analysis pipeline can be found in previous publications [110].

Evaluating the tissue property of white matter tracts

The tissue property (MTV) of each visual white matter tract was evaluated using the methods used in previous studies [33]. Briefly, each streamline to 100 equidistant nodes was resampled. The tissue property (MTV) was calculated at each node of each streamline. The property at each node was then summarized by taking a weighted average of microstructural measurement (MTV) on individual streamlines within that node. Based on the Mahalanobis distance from a tract core, the weight of each streamline was assigned. The first and last 10 nodes near gray or white matter interface in which the tract is likely to be heavily intersected with the superficial U-fiber system were excluded. The profile of each tract with a vector of remaining 80 nodes and averaged 80 values was summarized to estimate subject-specific single number summary on MTV for each tract. MTV along each tract was averaged across the left and right hemisphere.

Statistical comparisons

I calculated Pearson correlation coefficient between the amplitude and frequency of alpha/beta oscillations in the resting condition and the tissue properties in white matter tracts for each participant. When the correlation was computed, Bonferroni correction for multiple comparisons across two tract tissue properties (MTV and ODI) was applied for p-values because we do not have a strong hypothesis about which measure is more important for explaining the amplitude/frequency of alpha oscillations. A *p*-value of 0.05 was used to define significance.

3.2 Results

In order to investigate the relationship between characteristics of alpha oscillations and tissue structure property of white matter fibers in the visual area, I first measured MEG from 24 participants at the eye-open and closed resting states, and determined the occipital peak alpha power (PAP) and frequency (PAF). Figure 3.1 shows the spectra of MEG of all participants in the eye-open and closed resting conditions measured from 10 planar gradiometers showing the maximum amplitude.

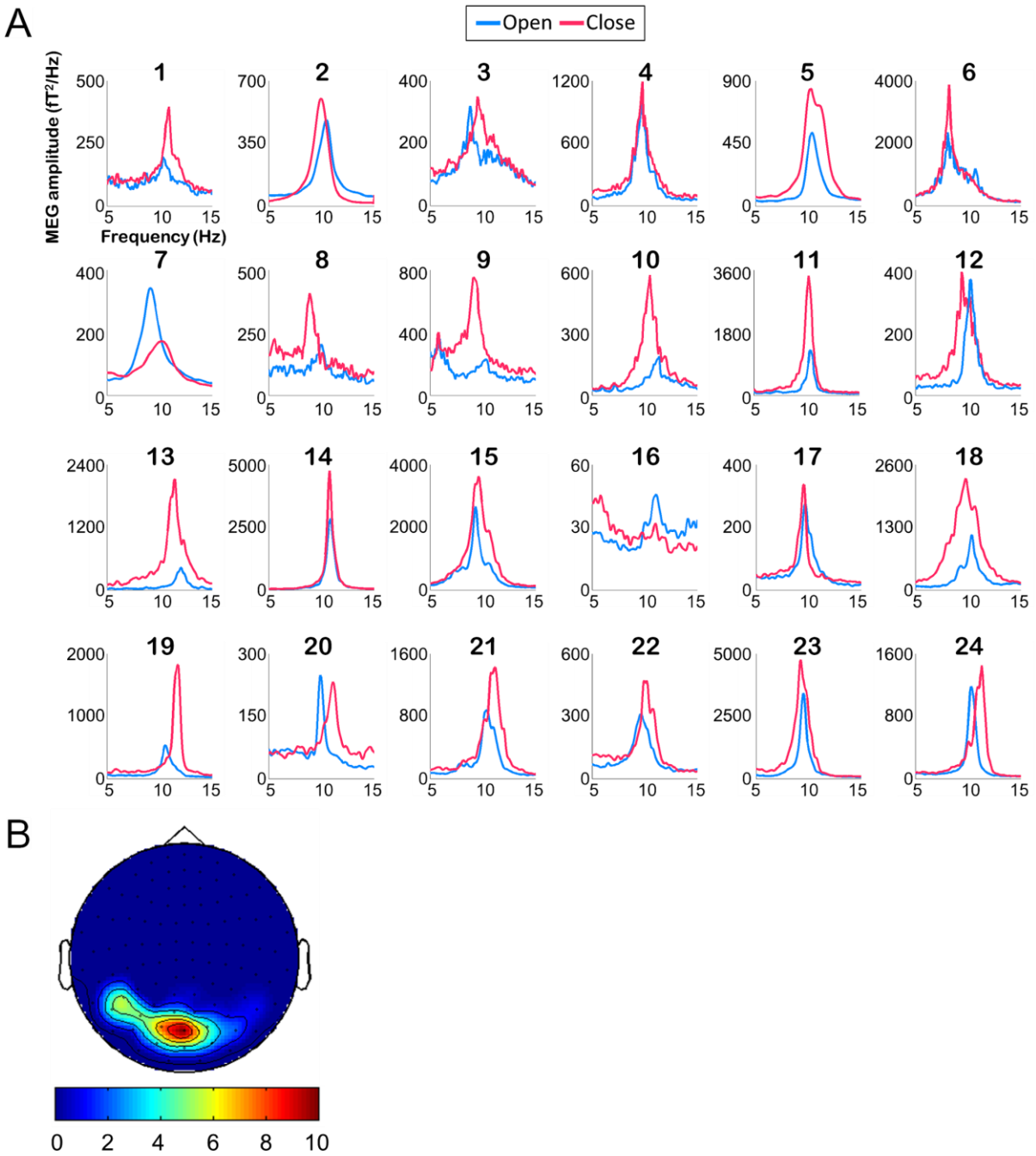

Figure 3.1: The power spectra of MEG data for all participants (A) and distribution maps of selected channels averaged across participants (B).

Second, dMRI and qMRI data were obtained from the same subject and performed probabilistic tractography on the dMRI dataset to identify the trajectory of focused visual white matter tracts (optic radiation, OR) following the anatomical prescriptions in previous studies (see *Methods*). The OR is the geniculo-cortical pathway carrying signals between the lateral

geniculate nucleus (LGN) and primary visual cortex [59]. The tissue property along these visual white matter tracts were evaluated using the qMRI-based microstructural measurement, Macromolecular Tissue Volume (MTV) that quantifies the non-proton neural tissue density [49], and the Orientation Dispersion Index (ODI) that indicates the spatial configuration of the neurite structures [51].

I then quantitatively compared the power of individual alpha oscillations in the resting condition with the MTV in the OR (n = 24; Figure 3.2). As a result, I found a significant correlation between PAP in the eyes-closed resting condition and the MTV in the OR ($r = 0.49$, $p = 0.031$, Figure 3.2A). The correlation between the resting state PAF in the eyes-open condition and the MTV in the OR was also found to be significant ($r = 0.52$, $p = 0.019$, Figure 3.2B). Thus, the tendency of the correlation between PAP and the MTV in the OR was consist across the eye-closed and open conditions.

Unlike MTV, the ODI in the OR was not significantly correlated with PAP in the eyes-closed resting condition ($r = 0.37$, $p = 0.16$, Figure 3.2C). On the other hand, the correlation between the resting state PAP in the eyes-open condition and the ODI in the OR was found to be significant ($r = 0.47$, $p = 0.039$, Figure 3.2D).

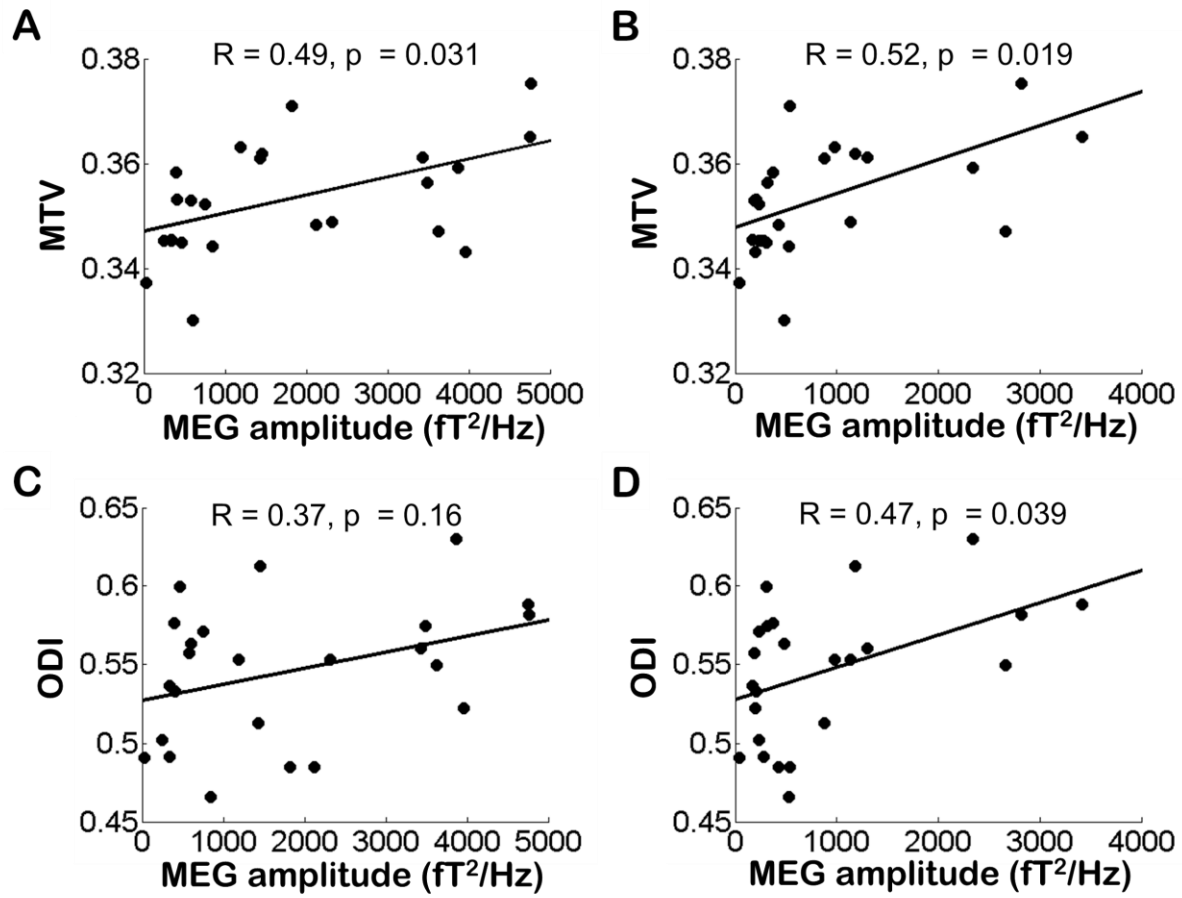

Figure 3.2: Dependence of peak alpha power on inter-individual variation in the tissue properties of the OR.

Next, I quantitatively compared the frequency of individual alpha oscillations in the resting condition with the MTV in the OR (n = 24; Figure 3.3). Unlike PAP, there was no significant correlation between PAF in the eyes-closed and eyes-open resting conditions and the MTV in the OR (eyes closed: r = 0.11, p = 1.0, Figure 3.3A; eyes open: r = −0.15, p = 0.98, Figure 3.3B). On the other hand, I found a significant negative correlation between PAF in the eyes-open resting condition and the ODI in the OR (r = −0.52, p = 0.018, Figure 3.3D). The PAF in the eyes-closed condition was also marginally significant (r = −0.44, p = 0.058, Figure 3.3C).

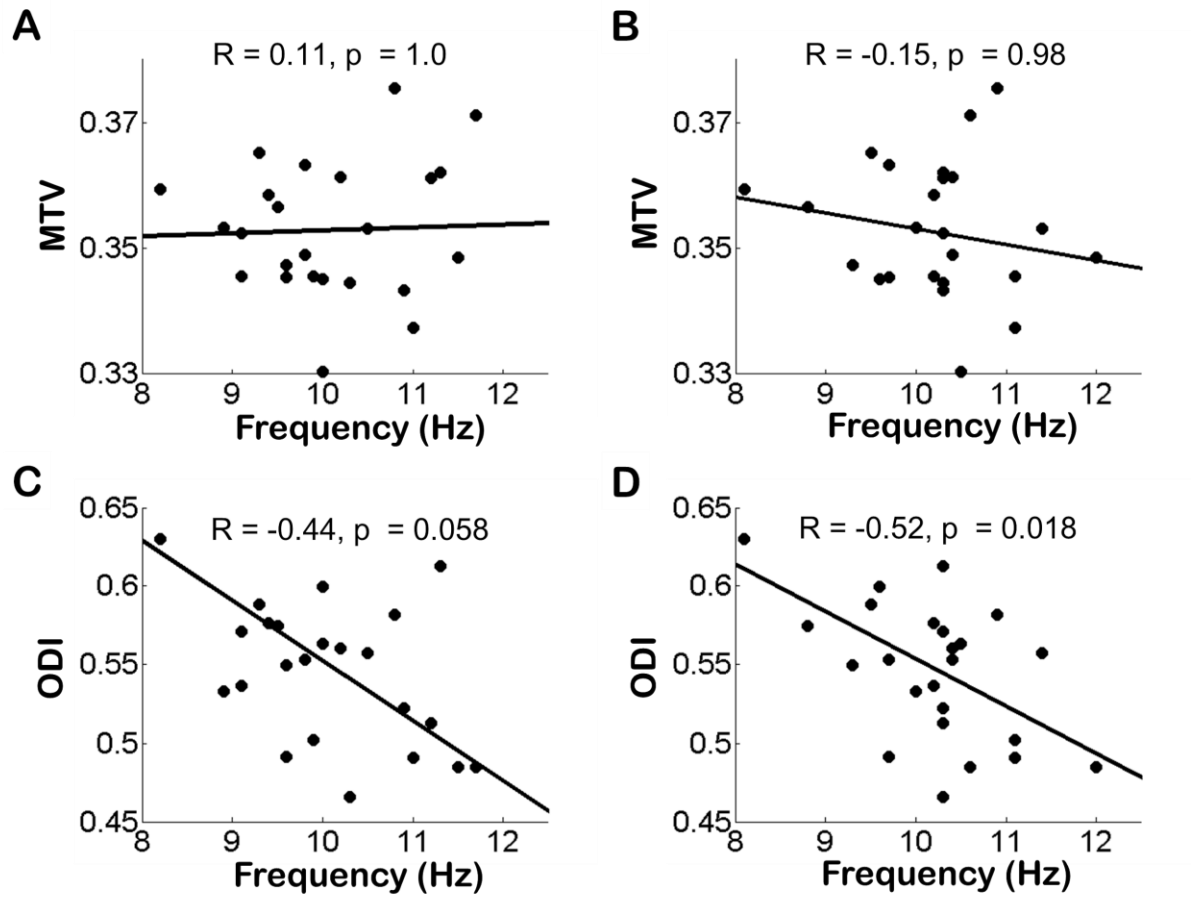

Figure 3.3: Dependence of peak alpha frequency on inter-individual variation in the tissue properties of the OR.

To confirm that the correlation between the characteristics of neural oscillations and the tissue properties in the OR is restricted to the alpha band, I next estimated the peak power and frequency of beta oscillations in the resting conditions. I then compared the power of individual beta oscillations in the resting condition with the MTV in the OR (n = 24; Figure 3.4). As a result, there was no significant correlation between the peak beta power in the resting conditions and MTV in the OR (eyes closed: $r = -0.06$, $p = 1.0$, Figure 3.4A; eyes open: $r = -0.17$, $p = 0.84$, Figure 3.4B). I also confirm that ODI in the OR was not significantly correlated with the peak beta power in the resting conditions (eyes closed: $r = -0.035$, $p = 1.0$, Figure 3.4C; eyes open: $r = -0.29$, $p = 0.34$, Figure 3.4D).

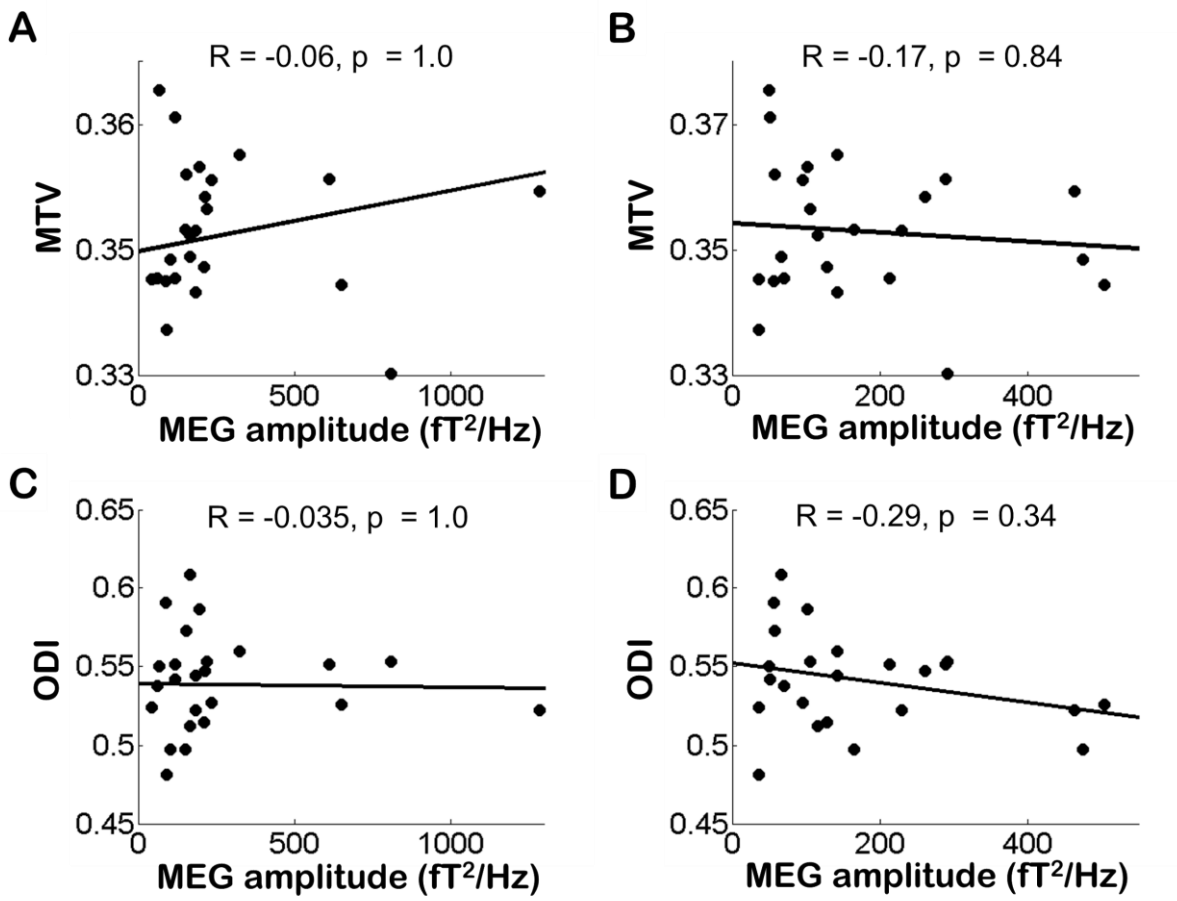

Figure 3.4: Dependence of peak beta power on inter-individual variation in the tissue properties of the OR.

Moreover, I compared the frequency of individual beta oscillations in the resting condition with the MTV/ODI in the OR (n = 24; Figure 3.5). As was found for the peak beta power, there was no significant correlation between the peak beta frequency in the resting conditions and MTV in the OR (eyes closed: r = 0.28, p = 0.37, Figure 3.5A; eyes open: r = 0.28, p = 0.36, Figure 3.5B). ODI in the OR was not also significantly correlated with the peak beta frequency in the resting conditions (eyes closed: r = 0.22, p = 0.60, Figure 3.5C; eyes open: r = 0.41, p = 0.092, Figure 3.5D). These results suggest that the tissue properties in the OR are associated with the intrinsic alpha oscillations, not with the beta oscillations.

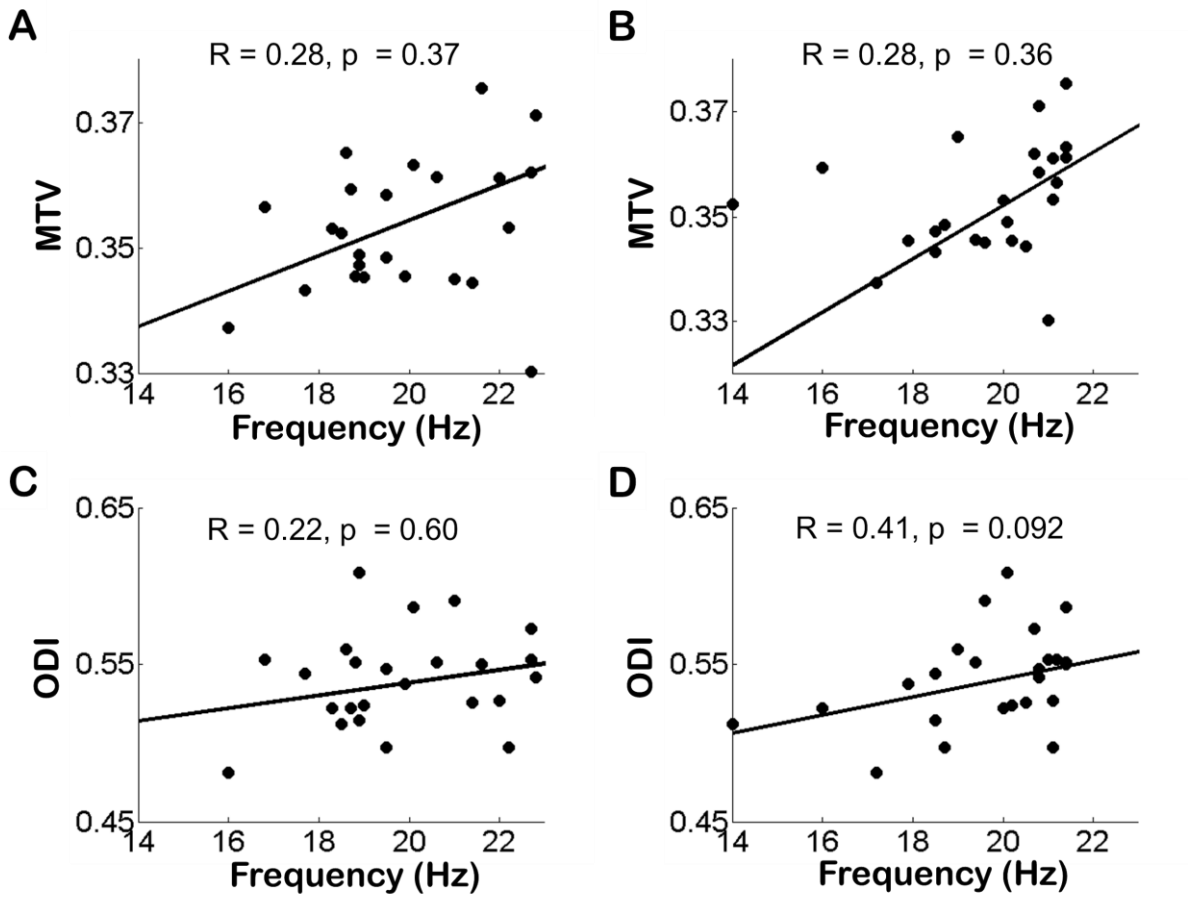

Figure 3.5: Dependence of peak beta frequency on inter-individual variation in the tissue properties of the OR.

Next, to examine whether the correlation between neuroanatomical properties and alpha oscillations is selective to the OR, I identified another major white matter tracts, which are the vertical occipital fasciculus (VOF) and posterior arcuate (pArc) (see *Methods*). The VOF is the association fiber across the visual ventral stream (hV4, LO, VO) and visual dorsal stream (Posterior IPS, V3A/B) [50, 106]. The pArc is an association fiber located posterior to the lateral sulcus and connecting the parietal cortex and the inferotemporal cortex [111]. I then quantitatively compared the power of individual alpha oscillations in the resting condition with the MTV in the VOF (n = 24; Figure 3.6). I confirmed that there was no significant correlation between PAP in the resting conditions and the MTV in the VOF (eyes closed: r = 0.43, p = 0.070, Figure 3.6A, eyes open: r = 0.37, p = 0.15, Figure 3.6B). ODI in the VOF was not also significantly correlated with the PAP in the resting conditions (eyes closed: r = −0.22, p = 0.60, Figure 3.6C; eyes open: r = −0.30, p = 0.31, Figure 3.6D).

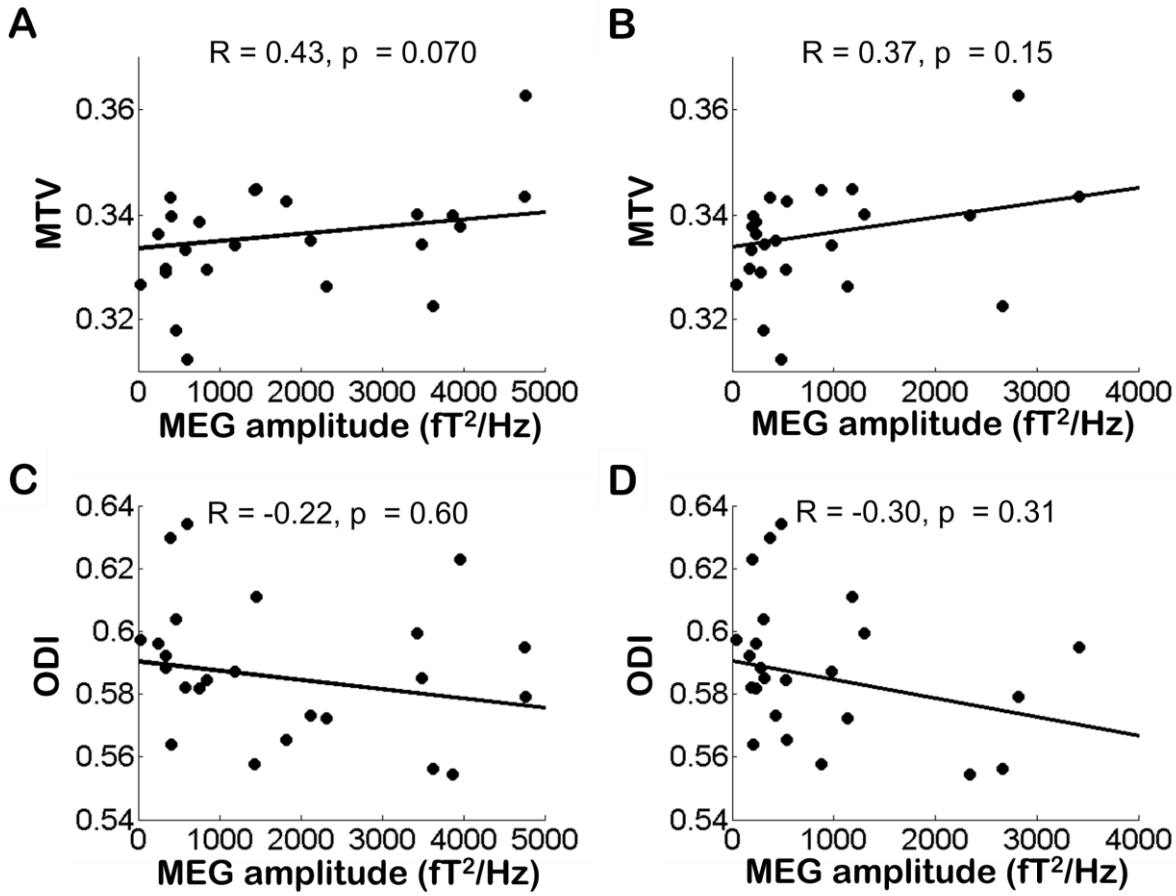

Figure 3.6: Dependence of peak alpha power on inter-individual variation in the tissue properties of the VOF.

Moreover, I compared the frequency of individual alpha oscillations in the resting condition with the MTV/ODI in the VOF (n = 24; Figure 3.7). Again, there was no significant

correlation between the PAF in the resting conditions and MTV in the VOF (eyes closed: r = 0.18, p = 0.80, Figure 3.7A; eyes open: r = 0.088, p = 1.0, Figure 3.7B). ODI in the VOF was not also significantly correlated with the PAF in the resting conditions (eyes closed: r = −0.089, p = 1.0, Figure 3.7C; eyes open: r = −0.18, p = 0.79, Figure 3.7D).

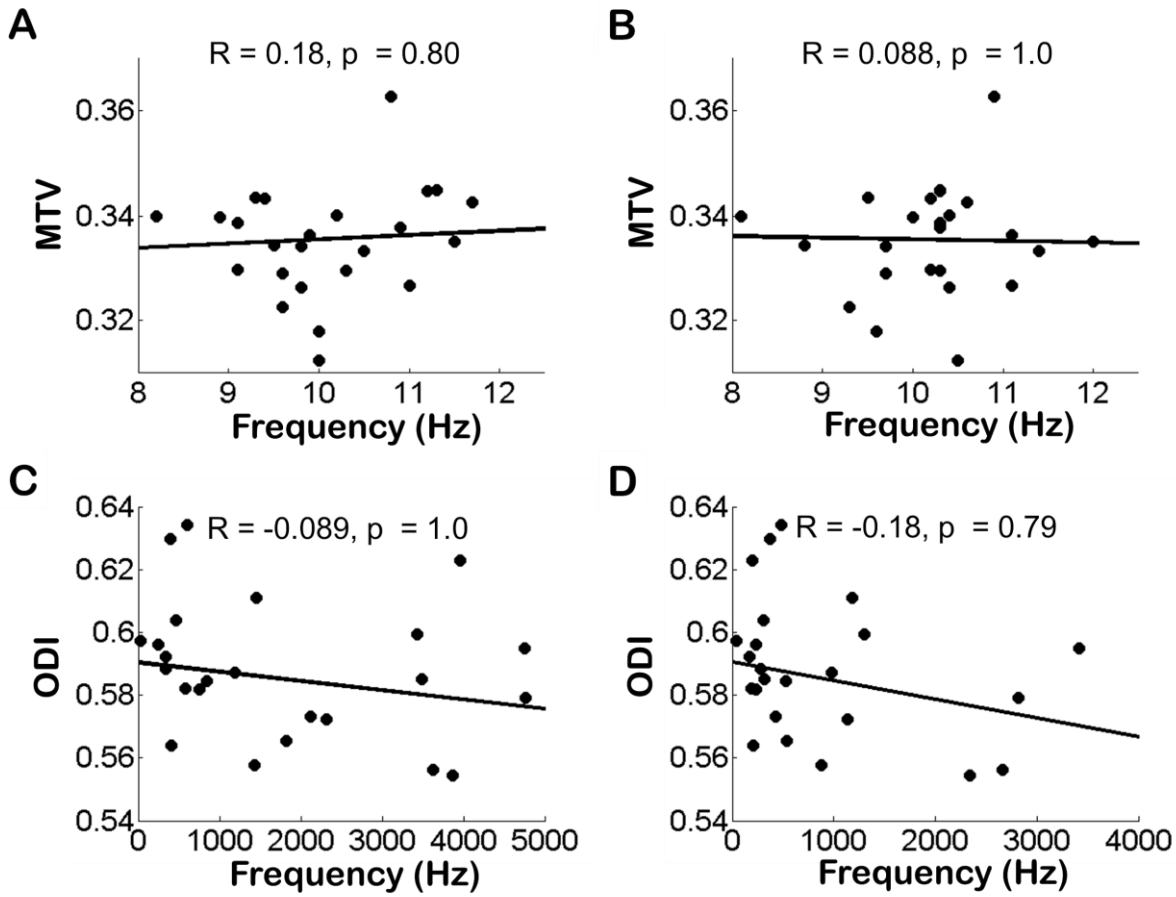

Figure 3.7: Dependence of peak alpha frequency on inter-individual variation in the tissue properties of the VOF.

I also quantitatively compared the power of individual alpha oscillations in the resting condition with the MTV in the pArc (n = 24; Figure 3.8). I confirmed that there was no significant correlation between PAP in the resting conditions and the MTV in the pArc (eyes closed: r = 0.43, p = 0.068, Figure 3.8A, eyes open: r = 0.42, p = 0.085, Figure 3.8B). ODI in the pArc was not also significantly correlated with the PAP in the resting conditions (eyes closed: r = −0.10, p = 1.0, Figure 3.8C; eyes open: r = −0.22, p = 0.60, Figure 3.8D).

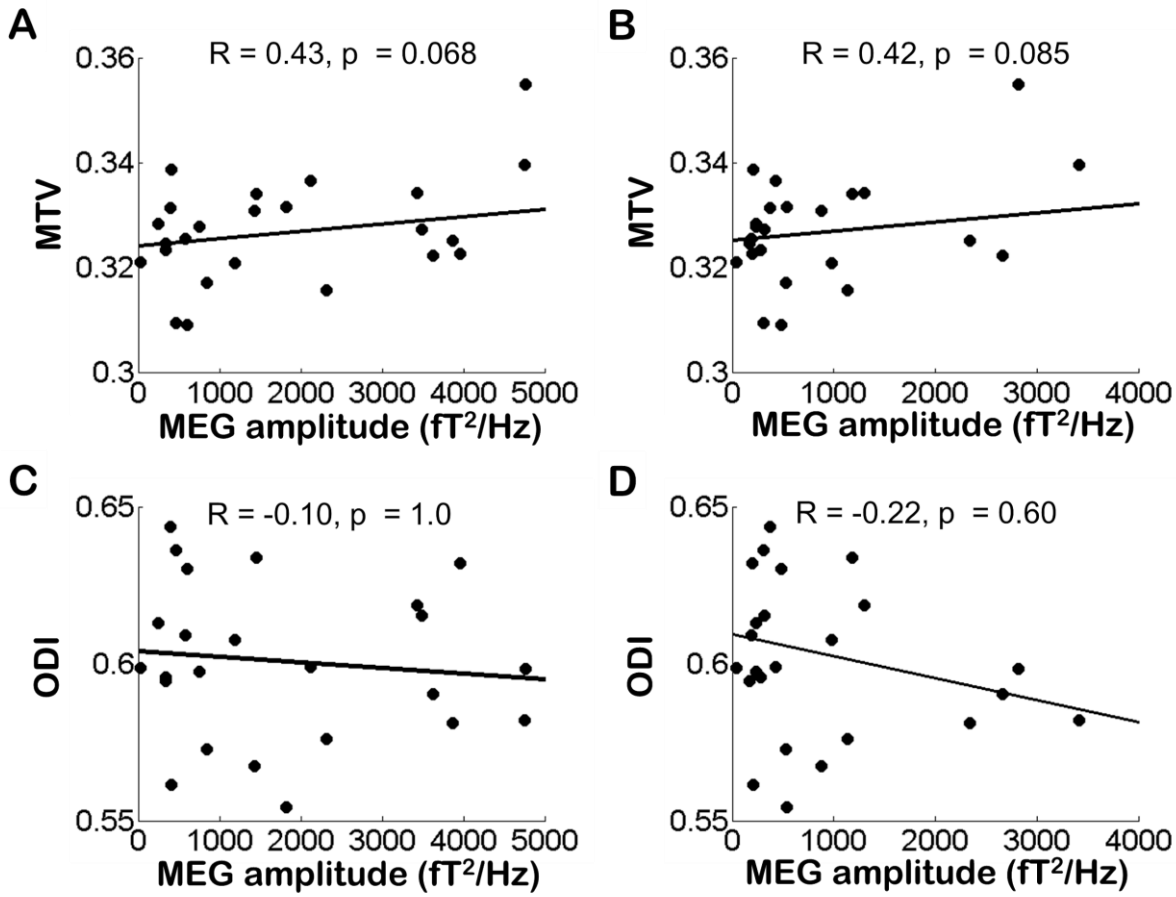

Figure 3.8: Dependence of peak alpha power on inter-individual variation in the tissue properties of the pArc.

Finally, I compared the frequency of individual alpha oscillations in the resting condition with the MTV/ODI in the pArc (n = 24; Figure 3.9). There was no significant correlation between the PAF in the resting conditions and MTV in the pArc (eyes closed: r = 0.16, p = 0.93, Figure 3.9A; eyes open: r = 0.20, p = 0.70, Figure 3.9B). ODI in the pArc was not also significantly correlated with the PAF in the resting conditions (eyes closed: r = 0.041, p = 1.0, Figure 3.9C; eyes open: r = 0.068, p = 1.0, Figure 3.9D). These results suggest that the characteristics of alpha oscillations are associated with the tissue properties in OR rather than with VOF and pArc.

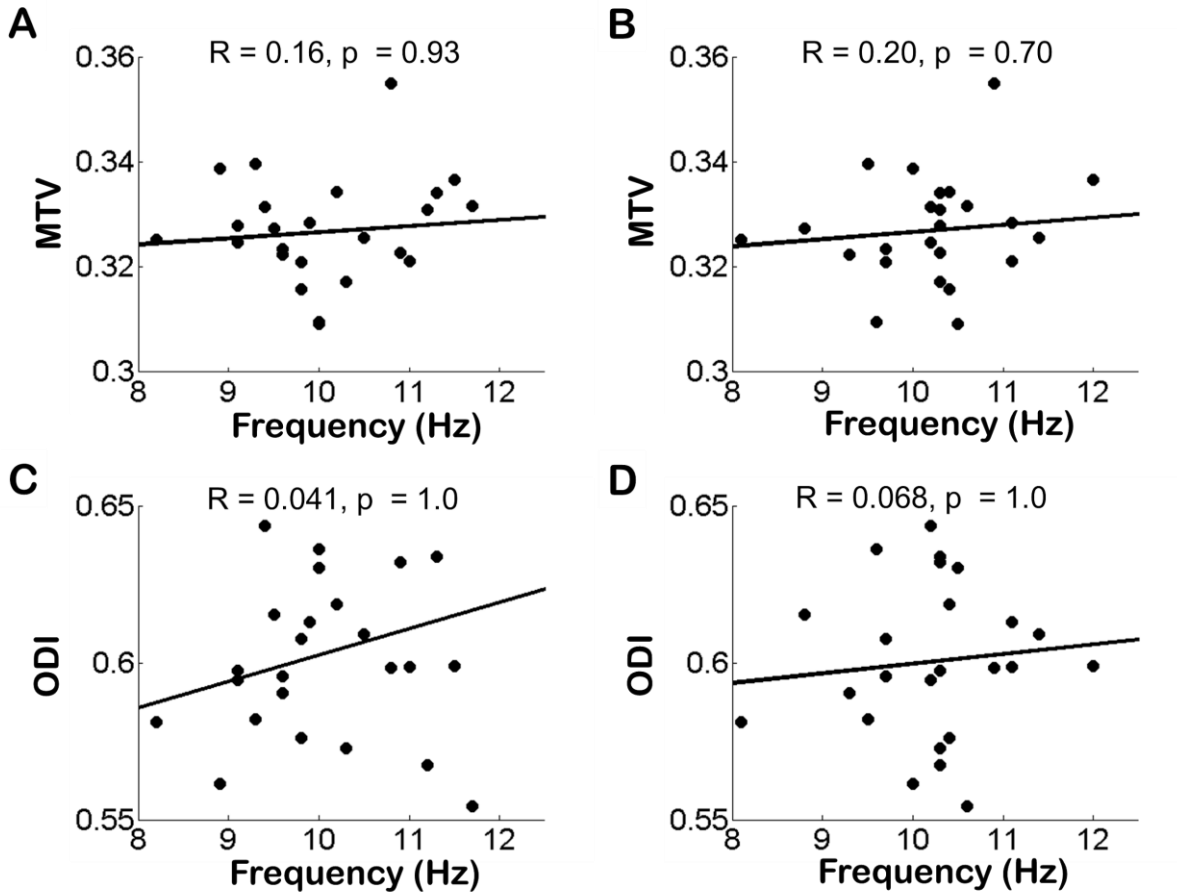

Figure 3.9: Dependence of peak alpha frequency on inter-individual variation in the tissue properties of the VOF.

3.3 Discussion

In this study, the peak power and frequency of the intrinsic alpha oscillations were correlated with MTV and ODI of the OR, respectively. In order to understand the selectivity on the relationship between alpha characteristics and tissue properties, it is necessary to elucidate how each MRI index reflects the microstructural properties. Macromolecular tissue volume (MTV) is an index derived from proton density (PD), which is a quantitative index obtained by qMRI. MTV represents the density of tissue macromolecules other than proton. By definition,

the formula (PD + MTV = 1) holds between MTV and PD. Therefore, quantitative MTV can be calculated from quantitative PD. The quantitativeness of MTV has also been confirmed in the phantom experiment and measurements using different coils and scanners by Mezer and colleagues [110]. Although these findings indicated reliable quantitativeness of MTV, there are some unclear points about its physiological interpretation. While the macromolecules qualified by MTV include myelin, cell membranes, proteins, and so on, it is unclear how each macromolecule affects MTV. Although recent studies have reported the relationships between the MTV of the white matter tracts and various biophysical properties, concrete physiological interpretation of MTV has not been shown yet. On the other hand, the phantom experiment by Mezer and colleagues indicated that the MTV reliably quantifies the lipid volume [110]. Since myelin has a much higher lipid content than the other brain components, it is expected that the MTV reflects the lipid volume of the myelin in the brain. Therefore, the current result suggests that the amplitude of the intrinsic alpha oscillations might be associated with the myelin density in the OR.

ODI is an index quantifying the spatial configuration of the neurite structures [51]. The ODI model has more spatial constraints than FA which quantifies the degree of anisotropy of a diffusion process in both the intra- and extra-cellular spaces in the same manner. Thus, the physiological interpretation of ODI is more complex model than FA. Moreover, since ODI is an index obtained by dMRI which measures dynamic diffusion of proton, it is difficult to verify the relationship between dMRI index and macromolecules (e.g. lipid) in phantom experiment. The value of ODI also depends greatly on the position in the brain. Since the microstructural properties such as the alignment of the axons differ across brain regions, the physiological interpretation of ODI optimized for the neurite structures of each brain region is required for each brain region. From these reasons, ODI also has some unclear points about the physiological interpretation. On the other hand, it is widely accepted that lower ODI value corresponds to more aligned directions of the neurite structures. Therefore, the negative correlation between the peak alpha frequency and the ODI in the OR (Figure 3.3) suggests that the more strictly the direction of the neurite structures is aligned, the higher the peak alpha frequency is.

In summary, the current findings that both the power and frequency of the intrinsic alpha oscillations were correlated with the microstructural properties of the OR suggests tight relationship between OR and intrinsic alpha oscillations. Currently, it is no clear interpretation why the alpha power was correlated with MTV, not ODI, of OR while the alpha frequency was

correlated with ODI, not MTV, of OR. For more detailed mechanism characterizing the intrinsic alpha oscillations, it is indispensable to investigate the physiological significance of MTV and ODI by a new framework such as simulating the proton in the white matter tracts.

Beta oscillations are also observed in the occipital area, although they are much weaker than alpha oscillations. The tissue property of OR was correlated neither with the amplitude of beta bands nor with the frequency. One possibility is that the neuroanatomical substrate characterizing beta oscillation is located in the white matter tracts connecting sensory areas other than visual areas. In fact, given that beta oscillations are also dominant in the motor cortex, the tissue properties of white matter tracts such as the superior longitudinal fasciculus (SLF), connecting motor and parietal areas, may be related to characteristics of beta oscillations. Another possibility is that signal-to-noise ratio of MEG signals in the beta band was not adequate. Generally, at the resting state, the amplitude of the beta oscillations tends to be much weaker than that of alpha oscillations. Therefore it was difficult to reliably estimate the peak power or frequency of beta oscillations. Given that beta activity is activated during a perceptually attentive state, compared with the resting state [112], it might be possible to find the correlation between the characteristics of beta oscillations during task and tissue properties of white matter tracts in the future.

4 General discussion

In 2.1, I found that the perceived illusory jitter correlated the inter-individual differences in the frequency of intrinsic alpha oscillations. Moreover, in chapter 3, it was suggested that the inter-individual differences in the frequency of the intrinsic alpha oscillations is correlated with the tissue properties of the OR. The OR connects the LGN and the primary visual cortex, and has bidirectional fibers, which are the tracts from LGN to V1 and those from V1 to LGN.

A previous study has shown that alpha activities were simultaneously observed in the V1 Layer 4C and Layer 6 [36]. Given that the V1 Layer 4C has the projection from LGN, and the V1 Layer 6 has the projection to LGN, the result is consistent with our results suggesting that the occipital alpha oscillation is derived from the thalamo-cortical interaction between LGN and V1. While the experiment 4 in chapter 2 implied the involvement of the alpha oscillation in the cortico-cortical network between dorsal and ventral areas, no significant correlation between the tissue properties in VOF/pArc and the characteristics of alpha oscillations was found. These findings suggest that the rhythms of the intrinsic alpha oscillations is generated by the network between thalamus and lower visual areas, and the rhythms are inherited to higher visual areas for further processing.

On the other hand, there are a lot of previous studies advocating the candidates of the alpha rhythm generators such as a cortico-cortical loop, thalamo-cortical loop other than the LGN - V1 loop. For example, it has been reported that the alpha power in V1 increased during the microstimulation at the gamma band in V4 [2], providing a possibility that alpha oscillations are generated by the interaction between the visual cortices, such as the feedback processing from V4 to V1. The feedback processing from V4 to V1 in the low frequency band (alpha/beta) suppresses the feedforward processing from V1 to V4 in gamma frequency for non-attended objects. Therefore, the feedback processing in alpha may preferentially route information for processing only salient object [113, 114]. In addition, Saalmann and colleagues [115] have reported that the alpha phase synchronizations between pulvinar and V4, pulvinar and TEO, or TEO and V4 were intensified during the attention to objects. Moreover, the granger causalities from pulvinar to V4/TEO were also increased during the attention to objects. If the pulvinar controls of processing of V4 and TEO, the pulvinar may have the top-down effect on the cortico-cortical system generating the intrinsic alpha oscillation. According to a study by Michael and colleagues, it is thought that the pulvinar has projections to various visual cortices including dorsal and ventral areas, and can also receive the input from each region

[116]. Perhaps, not only the top-down information processing from the pulvinar to the visual cortex, but also the mutual information exchange may contribute to the generation of the alpha oscillation. Given the spatial resolution of dMRI and qMRI, optic radiation defined in the current study may at least partly contain the tracts between the pulvinar and the lower visual cortices. Therefore it is possible that the interaction between pulvinar and lower visual regions may create the rhythm in the alpha band.

To further understand the mechanism underlying the generation of alpha oscillations, it is necessary to conduct an invasive physiological experiment using non-human primates. One possible approach is to measure how the activation or deactivation of pulvinar/LGN by external stimulation modulates the intrinsic alpha oscillations. For this purpose, measuring alpha oscillations from the entire visual areas of monkey by ECoG electrodes while the microstimulation is provided to the pulvinar/LGN would be a powerful approach.

Conclusion

In the first study, I investigated the relationship between the frequency of alpha oscillations and illusory jitter, and found that illusory jitter frequency is correlated with both inter- and intra-participant differences of PAF. Moreover, it has been shown that the manipulation of PAF by current stimulation resulted in the change in illusory jitter frequency. These findings that the intrinsic occipital alpha oscillations are consciously experienced as an illusory vibration at the same frequency suggests the direct contribution of alpha oscillation in creating temporal characteristics of human visual percept. The measurement of alpha activity during illusory jitter perception indicated that the alpha power in the left IPL and alpha coherence between the IPL and IT were increased during illusory jitter perception, which suggested that the illusory jitter may reflect the temporal dynamics of recurrent neural processes mediating the integration between motion-based spatial prediction and subsequent processing. In the second study, I compared the characteristics of the resting alpha oscillations with the tissue properties in the white matter tracts. I found that the power and frequency of alpha oscillations were significantly correlated with the tissue properties in optic radiation (OR) connecting the LGN and V1, which suggested that the characteristics of the occipital alpha oscillations reflect the tissue properties in OR. In summary, this study elucidated a functional role of alpha oscillations in visual perception and the neuroanatomical basis characterizing the alpha oscillations.

5 Reference

1. Herrmann, C.S., Munk, M.H. & Engel, A.K. Cognitive functions of gamma-band activity: memory match and utilization. Trends Cogn Sci 8, 347-355 (2004).
2. Fries, P. Rhythms for Cognition: Communication through Coherence. Neuron 88, 220-235 (2015).
3. Siegel, M., Donner, T.H. & Engel, A.K. Spectral fingerprints of large-scale neuronal interactions. Nat Rev Neurosci 13, 121-134 (2012).
4. Buzsaki, G. & Wang, X.J. Mechanisms of gamma oscillations. Annu Rev Neurosci 35, 203-225 (2012).
5. Jensen, O., Bonnefond, M. & VanRullen, R. An oscillatory mechanism for prioritizing salient unattended stimuli. Trends Cogn Sci 16, 200-206 (2012).
6. Mathewson, K.E., Gratton, G., Fabiani, M., Beck, D.M. & Ro, T. To see or not to see: prestimulus alpha phase predicts visual awareness. J Neurosci 29, 2725-2732 (2009).
7. van Driel, J., Knapen, T., van Es, D.M. & Cohen, M.X. Interregional alpha-band synchrony supports temporal cross-modal integration. Neuroimage 101, 404-415 (2014).
8. Haegens, S., Cousijn, H., Wallis, G., Harrison, P.J. & Nobre, A.C. Inter- and intra-individual variability in alpha peak frequency. Neuroimage 92, 46-55 (2014).
9. Sokoliuk, R. & VanRullen, R. The flickering wheel illusion: when alpha rhythms make a static wheel flicker. J Neurosci 33, 13498-13504 (2013).
10. Samaha, J. & Postle, B.R. The Speed of Alpha-Band Oscillations Predicts the Temporal Resolution of Visual Perception. Curr Biol 25, 2985-2990 (2015).
11. Scheeringa, R., Mazaheri, A., Bojak, I., Norris, D.G. & Kleinschmidt, A. Modulation of visually evoked cortical FMRI responses by phase of ongoing occipital alpha oscillations. J Neurosci 31, 3813-3820 (2011).
12. Haegens, S., Nacher, V., Luna, R., Romo, R. & Jensen, O. alpha-Oscillations in the monkey sensorimotor network influence discrimination performance by rhythmical inhibition of neuronal spiking. Proc Natl Acad Sci U S A 108, 19377-19382 (2011).
13. Bonnefond, M., Kastner, S. & Jensen, O. Communication between Brain Areas Based on Nested Oscillations. eNeuro 4 (2017).
14. Samaha, J., Bauer, P., Cimaroli, S. & Postle, B.R. Top-down control of the phase of alpha-band oscillations as a mechanism for temporal prediction. PNAS 112, 8439-8444 (2015).
15. Spaak, E., de Lange, F.P. & Jensen, O. Local entrainment of alpha oscillations by visual stimuli causes cyclic modulation of perception. J Neurosci 34, 3536-3544 (2014).
16. Bonnard, M., et al. Resting state brain dynamics and its transients: a combined TMS-EEG study. Scientific reports 6, 31220 (2016).
17. Romei, V., Thut, G. & Silvanto, J. Information-Based Approaches of Noninvasive Transcranial Brain Stimulation. Trends Neurosci 39, 782-795 (2016).
18. Thut, G., et al. Rhythmic TMS causes local entrainment of natural oscillatory signatures. Curr Biol 21, 1176-1185 (2011).
19. Romei, V., Gross, J. & Thut, G. On the role of prestimulus alpha rhythms over occipito-parietal areas in visual input regulation: correlation or causation? J Neurosci 30, 8692-8697 (2010).
20. Herring, J.D., Thut, G., Jensen, O. & Bergmann, T.O. Attention Modulates TMS-Locked Alpha Oscillations in the Visual Cortex. J Neurosci 35, 14435-14447 (2015).
21. Cecere, R., Rees, G. & Romei, V. Individual differences in alpha frequency drive crossmodal illusory perception. Curr Biol 25, 231-235 (2015).
22. Arnold, D.H. & Johnston, A. Motion-induced spatial conflict. Nature 425, 181-184 (2003).

23. Arnold, D.H. & Johnston, A. Motion induced spatial conflict following binocular integration. Vision Research 45, 2934-2942 (2005).
24. Lu, Z.L., Lesmes, L.A. & Sperling, G. Perceptual motion standstill in rapidly moving chromatic displays. PNAS 96, 15374–15379 (1999).
25. Amano, K., Arnold, D.H., Takeda, T. & Johnston, A. Alpha band amplification during illusory jitter perception. J Vis 8, 3 1-8 (2008).
26. Lanciego, J.L. & Wouterlood, F.G. A half century of experimental neuroanatomical tracing. Journal of chemical neuroanatomy 42, 157-183 (2011).
27. Hindriks, R., et al. Role of white-matter pathways in coordinating alpha oscillations in resting visual cortex. Neuroimage 106, 328-339 (2015).
28. Jones, D.K. & Cercignani, M. Twenty-five pitfalls in the analysis of diffusion MRI data. NMR in biomedicine 23, 803-820 (2010).
29. Jones, D.K., Knosche, T.R. & Turner, R. White matter integrity, fiber count, and other fallacies: the do's and don'ts of diffusion MRI. Neuroimage 73, 239-254 (2013).
30. Wandell, B.A. & Le, R.K. Diagnosing the Neural Circuitry of Reading. Neuron 96, 298-311 (2017).
31. Catani, M., Howard, R.J., Pajevic, S. & Jones, D.K. Virtual in vivo interactive dissection of white matter fasciculi in the human brain. Neuroimage 17, 77-94 (2002).
32. Wakana, S., Jiang, H., Nagae-Poetscher, L.M., van Zijl, P.C. & Mori, S. Fiber tract-based atlas of human white matter anatomy. Radiology 230, 77-87 (2004).
33. Yeatman, J.D., Dougherty, R.F., Ben-Shachar, M. & Wandell, B.A. Development of white matter and reading skills. Proceedings of the National Academy of Sciences 109, E3045-E3053 (2012).
34. Yeatman, J.D., Wandell, B.A. & Mezer, A.A. Lifespan maturation and degeneration of human brain white matter. Nature communications 5, 4932 (2014).
35. Yendiki, A., Koldewyn, K., Kakunoori, S., Kanwisher, N. & Fischl, B. Spurious group differences due to head motion in a diffusion MRI study. Neuroimage 88, 79-90 (2014).
36. Bollimunta, A., Mo, J., Schroeder, C.E. & Ding, M. Neuronal mechanisms and attentional modulation of corticothalamic alpha oscillations. J Neurosci 31, 4935-4943 (2011).
37. Cohen, D. Magnetoencephalography: evidence of magnetic fields produced by alpha-rhythm currents. Science (New York, N.Y.) 161, 784-786 (1968).
38. Jaklevic, R.C., Lambe, J., Silver, A.H. & Mercereau, J.E. Quantum Interference Effects in Josephson Tunneling. Physical Review Letters 12, 159-160 (1964).
39. Singleton, M.J. Functional Magnetic Resonance Imaging. The Yale Journal of Biology and Medicine 82, 233-233 (2009).
40. Berger, H. Uber das elektrenkephalogramm des menschen. Arch. Psychiatr. Nervenkr. 87, 527-570 (1929).
41. James, V.S. Independent component analysis: an introduction. Trends Cognitive Sciences 6, 59-64 (2002).
42. Taulu, S., Simola, J. & Kajola, M. Applications of the Signal Space Separation Method. IEEE Trans Signal Process 53, 3359-3372 (2005).
43. Taulu, S. & Hari, R. Removal of magnetoencephalographic artifacts with temporal signal-space separation: demonstration with single-trial auditory-evoked responses. Hum Brain Mapp 30, 1524-1534 (2009).
44. Hamalainen, M.S. & Ilmoniemi, R.J. Interpreting magnetic fields of the brain: minimum norm estimates. Medical & biological engineering & computing 32, 35-42 (1994).
45. Pascual-Marqui, R.D., et al. Low resolution brain electromagnetic tomography (LORETA) functional imaging in acute, neuroleptic-naive, first-episode, productive schizophrenia. Psychiatry research 90, 169-179 (1999).
46. Van Veen, B.D., van Drongelen, W., Yuchtman, M. & Suzuki, A. Localization of

brain electrical activity via linearly constrained minimum variance spatial filtering. IEEE transactions on bio-medical engineering 44, 867-880 (1997).
47. Gross, J., et al. Dynamic imaging of coherent sources: Studying neural interactions in the human brain. Proc Natl Acad Sci U S A 98, 694-699 (2001).
48. Mori, S. & Zhang, J. Principles of diffusion tensor imaging and its applications to basic neuroscience research. Neuron 51, 527-539 (2006).
49. Wandell, B.A. Clarifying Human White Matter. Annu Rev Neurosci 39, 103-128 (2016).
50. Basser, P.J. & Pierpaoli, C. Microstructural and physiological features of tissues elucidated by quantitative-diffusion-tensor MRI. 1996. Journal of magnetic resonance (San Diego, Calif. : 1997) 213, 560-570 (2011).
51. Zhang, H., Schneider, T., Wheeler-Kingshott, C.A. & Alexander, D.C. NODDI: practical in vivo neurite orientation dispersion and density imaging of the human brain. Neuroimage 61, 1000-1016 (2012).
52. Wandell, B.A. & Yeatman, J.D. Biological development of reading circuits. Curr Opin Neurobiol 23, 261-268 (2013).
53. Genc, E., et al. Diffusion markers of dendritic density and arborization in gray matter predict differences in intelligence. Nature communications 9, 1905 (2018).
54. Rae, C.L., et al. Deficits in Neurite Density Underlie White Matter Structure Abnormalities in First-Episode Psychosis. Biological psychiatry 82, 716-725 (2017).
55. Mori, S., Crain, B.J., Chacko, V.P. & van Zijl, P.C. Three-dimensional tracking of axonal projections in the brain by magnetic resonance imaging. Ann Neurol 45, 265-269 (1999).
56. Conturo, T.E., et al. Tracking neuronal fiber pathways in the living human brain. Proceedings of the National Academy of Sciences 96, 10422-10427 (1999).
57. Jbabdi, S. & Johansen-Berg, H. Tractography: where do we go from here? Brain connectivity 1, 169-183 (2011).
58. Ajina, S., Pestilli, F., Rokem, A., Kennard, C. & Bridge, H. Human blindsight is mediated by an intact geniculo-extrastriate pathway. eLife 4, e08935 (2015).
59. Sherbondy, A.J., Dougherty, R.F., Napel, S. & Wandell, B.A. Identifying the human optic radiation using diffusion imaging and fiber tractography. J Vis 8, 12.11-11 (2008).
60. Lebel, C., Walker, L., Leemans, A., Phillips, L. & Beaulieu, C. Microstructural maturation of the human brain from childhood to adulthood. Neuroimage 40, 1044-1055 (2008).
61. Thomason, M.E. & Thompson, P.M. Diffusion imaging, white matter, and psychopathology. Annual review of clinical psychology 7, 63-85 (2011).
62. Ogawa, S., et al. White matter consequences of retinal receptor and ganglion cell damage. Investigative ophthalmology & visual science 55, 6976-6986 (2014).
63. Thiebaut de Schotten, M., et al. A lateralized brain network for visuospatial attention. Nat Neurosci 14, 1245-1246 (2011).
64. Oishi, H., Takemura, H., Aoki, S.C., Fujita, I. & Amano, K. Microstructural properties of the vertical occipital fasciculus explain the variability in human stereoacuity. Proceedings of the National Academy of Sciences 115, 12289-12294 (2018).
65. Genc, E., Bergmann, J., Singer, W. & Kohler, A. Interhemispheric connections shape subjective experience of bistable motion. Curr Biol 21, 1494-1499 (2011).
66. Mollink, J., et al. Evaluating fibre orientation dispersion in white matter: Comparison of diffusion MRI, histology and polarized light imaging. NeuroImage 157, 561-574 (2017).
67. Fukutomi, H., et al. Neurite imaging reveals microstructural variations in human cerebral cortical gray matter. Neuroimage 182, 488-499 (2018).
68. Weiskopf, R.B. New inhaled anesthetics. Current Opinion in Anesthesiology 2,

421-424-424 (1989).
69. Sereno, M.I., Lutti, A., Weiskopf, N. & Dick, F. Mapping the human cortical surface by combining quantitative T(1) with retinotopy. Cereb Cortex 23, 2261-2268 (2013).
70. Stuber, G.D. Cortical operation of the ventral striatal switchboard. Neuron 78, 6-7 (2013).
71. Barker, A.T., Jalinous, R. & Freeston, I.L. Non-invasive magnetic stimulation of human motor cortex. Lancet (London, England) 1, 1106-1107 (1985).
72. Nitsche, M.A. & Paulus, W. Sustained excitability elevations induced by transcranial DC motor cortex stimulation in humans. Neurology 57, 1899-1901 (2001).
73. Kanai, R., Chaieb, L., Antal, A., Walsh, V. & Paulus, W. Frequency-dependent electrical stimulation of the visual cortex. Curr Biol 18, 1839-1843 (2008).
74. Marshall, L., Helgadottir, H., Molle, M. & Born, J. Boosting slow oscillations during sleep potentiates memory. Nature 444, 610-613 (2006).
75. Witkowski, M., et al. Mapping entrained brain oscillations during transcranial alternating current stimulation (tACS). Neuroimage 140, 89-98 (2015).
76. Ives, H.E. Studies in the photometry of lights of different colours. I. Spectral luminosity curves obtained by the equality of brightness photometer and flicker photometer under similar conditions. Philosophical Magazine 24, 149-188 (1912).
77. Brainard, D.H. The Psychophysics Toolbox. Spatial vision 10, 433-436 (1997).
78. Oostenveld, R., Fries, P., Maris, E. & Schoffelen, J.-M. FieldTrip: open source software for advanced analysis of MEG, EEG, and invasive electrophysiological data. Intell. Neuroscience 2011, 1-9 (2011).
79. Niedermeyer, E. & Silva, F.L.d. eds. Magnetoencephalography in Clinical Neurophysiological Assessment of Human Cortical Functions (Lippincott Williams & Wilkins, Philadelphia, PA, 2004).
80. Santamaria, J. & Chiappa, K.H. The EEG of drowsiness in normal adults. Journal of clinical neurophysiology : official publication of the American Electroencephalographic Society 4, 327-382 (1987).
81. VanRullen, R. How to Evaluate Phase Differences between Trial Groups in Ongoing Electrophysiological Signals. Frontiers in Neuroscience 10 (2016).
82. Stouffer, S., Suchman, E., Devinney, L., Star, S. & Williams, R. Studies in Social Psychology in World War II: The American Soldier. Vol. 1, Adjustment During Army Life. (Princeton, NJ: Princeton University Press, 1949).
83. Benjamini, Y. & Hochberg, Y. Controlling the False Discovery Rate: A Practical and Powerful Approach to Multiple Testing. Journal of the Royal Statistical Society. Series B (Methodological) 57, 289-300 (1995).
84. Dugue, L., Marque, P. & VanRullen, R. The phase of ongoing oscillations mediates the causal relation between brain excitation and visual perception. J Neurosci 31, 11889-11893 (2011).
85. Busch, N.A., Dubois, J. & VanRullen, R. The phase of ongoing EEG oscillations predicts visual perception. J Neurosci 29, 7869-7876 (2009).
86. Romei, V., Gross, J. & Thut, G. Sounds reset rhythms of visual cortex and corresponding human visual perception. Curr Biol 22, 807-813 (2012).
87. de Graaf, T.A., et al. Alpha-band rhythms in visual task performance: phase-locking by rhythmic sensory stimulation. PLoS One 8, e60035 (2013).
88. Busch, N.A. & VanRullen, R. Spontaneous EEG oscillations reveal periodic sampling of visual attention. Proc Natl Acad Sci U S A 107, 16048-16053 (2010).
89. Schutter, D.J. & Hortensius, R. Retinal origin of phosphenes to transcranial alternating current stimulation. Clin Neurophysiol 121, 1080-1084 (2010).
90. Kar, K. & Krekelberg, B. Transcranial electrical stimulation over visual cortex evokes

phosphenes with a retinal origin. J Neurophysiol 108, 2173-2178 (2012).
91. Laakso, I. & Hirata, A. Computational analysis shows why transcranial alternating current stimulation induces retinal phosphenes. Journal of neural engineering 10, 046009 (2013).
92. Murakami, I. Correlations between fixation stability and visual motion sensitivity. Vision Research 44, 751-761 (2004).
93. Otero-Millan, J., Castro, J.L.A., Macknik, S.L. & Martinez-Conde, S. Unsupervised clustering method to detect microsaccades. Journal of Vision 14, 18-18 (2014).
94. Troncoso, X.G., Macknik, S.L., Otero-Millan, J. & Martinez-Conde, S. Microsaccades drive illusory motion in the Enigma illusion. Proc Natl Acad Sci U S A 105, 16033-16038 (2008).
95. Veniero, D., Vossen, A., Gross, J. & Thut, G. Lasting EEG/MEG Aftereffects of Rhythmic Transcranial Brain Stimulation: Level of Control Over Oscillatory Network Activity. Frontiers in Cellular Neuroscience 9 (2015).
96. Tzourio-Mazoyer, N., et al. Automated anatomical labeling of activations in SPM using a macroscopic anatomical parcellation of the MNI MRI single-subject brain. Neuroimage 15, 273-289 (2002).
97. Grossman, N., et al. Noninvasive Deep Brain Stimulation via Temporally Interfering Electric Fields. Cell 169, 1029-1041.e1016 (2017).
98. Mezer, A., Rokem, A., Berman, S., Hastie, T. & Wandell, B.A. Evaluating quantitative proton-density-mapping methods. Hum Brain Mapp 37, 3623-3635 (2016).
99. Andersson, J.L., Skare, S. & Ashburner, J. How to correct susceptibility distortions in spin-echo echo-planar images: application to diffusion tensor imaging. Neuroimage 20, 870-888 (2003).
100. Andersson, J.L.R. & Sotiropoulos, S.N. An integrated approach to correction for off-resonance effects and subject movement in diffusion MR imaging. Neuroimage 125, 1063-1078 (2016).
101. Sherbondy, A.J., Dougherty, R.F., Ben-Shachar, M., Napel, S. & Wandell, B.A. ConTrack: finding the most likely pathways between brain regions using diffusion tractography. Journal of vision 8, 1-16 (2008).
102. Chamberland, S., et al. Fast two-photon imaging of subcellular voltage dynamics in neuronal tissue with genetically encoded indicators. Elife 6 (2017).
103. Wang, L., Mruczek, R.E.B., Arcaro, M.J. & Kastner, S. Probabilistic Maps of Visual Topography in Human Cortex. Cerebral cortex (New York, N.Y. : 1991) 25, 3911-3931 (2015).
104. Sherbondy, A.J., Dougherty, R.F., Ben-Shachar, M., Napel, S. & Wandell, B.A. ConTrack: finding the most likely pathways between brain regions using diffusion tractography. J Vis 8, 15.11-16 (2008).
105. Takemura, H., et al. Occipital White Matter Tracts in Human and Macaque. Cereb Cortex 27, 3346-3359 (2017).
106. Takemura, H., Caiafa, C.F., Wandell, B.A. & Pestilli, F. Ensemble Tractography. PLoS computational biology 12, e1004692-e1004692 (2016).
107. Tournier, J.D., Calamante, F. & Connelly, A. Robust determination of the fibre orientation distribution in diffusion MRI: non-negativity constrained super-resolved spherical deconvolution. Neuroimage 35, 1459-1472 (2007).
108. Tournier, J.-D., Calamante, F. & Connelly, A. MRtrix: Diffusion tractography in crossing fiber regions. International Journal of Imaging Systems and Technology 22, 53-66 (2012).
109. Smith, R.E., Tournier, J.D., Calamante, F. & Connelly, A. Anatomically-constrained tractography: improved diffusion MRI streamlines tractography through effective use of anatomical information. Neuroimage 62, 1924-1938 (2012).

110. Mezer, A., et al. Quantifying the local tissue volume and composition in individual brains with magnetic resonance imaging. Nature medicine 19, 1667-1672 (2013).
111. Weiner, K.S., Yeatman, J.D. & Wandell, B.A. The posterior arcuate fasciculus and the vertical occipital fasciculus. Cortex; a journal devoted to the study of the nervous system and behavior 97, 274-276 (2017).
112. Wrobel, A. Beta activity: a carrier for visual attention. Acta neurobiologiae experimentalis 60, 247-260 (2000).
113. Bastos, A.M., et al. Visual areas exert feedforward and feedback influences through distinct frequency channels. Neuron 85, 390-401 (2015).
114. Jensen, O., Bonnefond, M., Marshall, T.R. & Tiesinga, P. Oscillatory mechanisms of feedforward and feedback visual processing. Trends in Neurosciences 38, 192-194 (2015).
115. Saalmann, Y.B., Pinsk, M.A., Wang, L., Li, X. & Kastner, S. The pulvinar regulates information transmission between cortical areas based on attention demands. Science (New York, N.Y.) 337, 753-756 (2012).
116. Arcaro, M.J., Pinsk, M.A. & Kastner, S. The Anatomical and Functional Organization of the Human Visual Pulvinar. The Journal of neuroscience : the official journal of the Society for Neuroscience 35, 9848-9871 (2015).

6 Acknowledgement

I would like to show my sincere gratefulness to my supervisors, Assoc. Prof. Kaoru Amano and Prof. Toshio Yanagida for their continuous support throughout my Master, and Ph.D. course. Assoc. Prof. Amano enthusiastically guided me on conducting my research, writing my thesis, and giving my presentation. I would like to thank Prof. Shigeru Kitazawa, Prof. Ichiro Fujita, and Prof. Takufumi Yanagisawa for serving on my thesis committee members.

I would like to thank Dr. Hiromasa Takemura and Hiroki Oishi for providing and analyzing dMRI/qMRI data in Chapter 3. I would like to thank Kazuhiro Okahashi for technical advice and continuous encouragement. I would like to thank Dr. Asuka Otsuka for technical support on MEG measurement. I would like to thank Dr. Kenichi Yuasa, Dr. Ai Koizumi, Dr. Nobuhiro Hagura, Dr. Hiroshi Ban and Dr. Masamichi Hayashi, Shuka Shibusawa for the scientific discussions and criticism.

I’m supported by the Program for Leading Graduate Schools of the Ministry of Education, Culture, Sports, Science and Technology, Japan (K03).

Finally, I thank all my colleagues for the collaboration and warm atmosphere during all these years.

7 Achievements

PEER-REVIEWED JOURNAL ARTICLES FOR THIS THESIS

Minami S, Amano K. (2017) Illusory Jitter Perceived at the Frequency of Alpha Oscillations. Current Biology 27(15):2344-51.
学位申請者の寄与：実験、解析、論文執筆

Minami S, Kawamura H. (2015) Low-temperature magnetic properties of the Kondo lattice model in one dimension, Journal of the Physical Society of Japan, Vol.84, No.4, Article ID: 044702
学位申請者の寄与：実験、解析、論文執筆

NON PEER-REVIEWED JOURNAL ARTICLES

南 宇人, 天野 薫, 視覚情報処理におけるアルファ波のクロック機能 ―アルファ周波数とジター周波数の関係―, VISION Vol. 27, No. 3, p. 103–106, (2015)
学位申請者の寄与：実験、解析、論文執筆

INTERNATIONAL CONFERENCES AND MEETINGS

Minami S, Amano K. Illusory jitter perceived at the frequency of intrinsic alpha oscillation, Vision Sciences Society 2016, 16:1127.
学位申請者の寄与：実験、解析、口頭発表

Minami S, Oishi H, Takemura H, Amano K. Functional roles of alpha oscillations underlying the communication between dorsal and ventral visual areas, Vision Sciences Society 2017, 17(10):1138.
学位申請者の寄与：実験、解析、ポスター発表

Minami S, Amano K. Alpha oscillation as a clock for visual processing -Illusory jitter frequency correlated with individual alpha frequency-, Society for Neuroscience, 2015, 79.19/V28.
学位申請者の寄与：実験、解析、ポスター発表

DOMESTIC CONFERENCES

南 宇人，天野 薫. ジター錯視の知覚におけるアルファ波の機能的役割 Functional role of alpha oscillations in illusory jitter perception, 日本神経科学大会，2016, P1-132
学位申請者の寄与：実験、解析、ポスター発表

南 宇人，天野 薫. 視覚情報処理におけるアルファ波のクロック機能 ―アルファ周波数とジター周波数の関係―, VISION Vol. 27, No. 3, p. 103-106, (2015)
学位申請者の寄与：実験、解析、口頭発表

南 宇人，天野 薫. ジター錯視におけるアルファ波の機能の解明，VISION Vol. 27, No. 3, p. 118, (2015)
学位申請者の寄与：実験、解析、ポスター発表

南 宇人，川村 光. 1 次元近藤格子モデルの低温磁気秩序，日本物理学会 2015 年秋季大会，18pDC-1 (2015)

学位申請者の寄与：実験、解析

南宇人，大石浩輝，竹村浩昌，天野薫.（2018），ヒト視放線の組織構造特性とアルファ波の関連．日本視覚学会 2018 年夏季大会
学位申請者の寄与：実験、解析

ACADEMIC AWARDS
日本視覚学会 2015 年冬季大会 ベストプレゼンテーション賞

Vision Sciences Society 2016 Student Travel Awards